UNIVERSITÀ DEGLI STUDI DI ROMA "TOR VERGATA"
Dipartimento di Ingegneria Civile e Informatica

XXVII-Cycle of Geoinformation Doctorate

Batteryless UHF RFID Technology for IoT-based Ambient Sensing

Sabina Manzari

A.A. 2014/2015

ADVISOR:
Prof. Gaetano Marrocco

COORDINATOR:
Prof. Giovanni Schiavon

Summary

The Internet of Things (IOT) is the logical further development of today's internet and envisions a future on billions of smart connected devices. Devices that senses their surroundings and which when combined into the cloud will provide informations on the environment from microscopic to global scaling. Therefore, the IOT will require enabling sensor hardware in addition to the cloud computing services: smart connected devices that have on-board sensors in order to provide metrics for ambient intelligence. It is predicted that smart mobile devices in the future will be equipped with a limited range of physical sensors but will be able to read a wide range of new sensors as separated accessories. Wireless sensors are widely developed in order to remotely detect, measure, monitor and control several entities in logistics, food quality and agriculture, environment, healthcare, homeland security, and process monitoring and control.

The selection of a particular sensor technology or radio-architecture has to account for the physical/chemical process to be measured, the location of the measurement site, the sensor size, the read range, the power consumption, the type of network and the cost. Among the different short-range radio technologies that potentially converge to this scenario, Radio Frequency Identification (RFID) systems may represent a strategic enabling component for the true pervasive diffusion of IOT-based Ambient Sensing. RFID is particularly attractive for the energy autonomy of battery-less (passive) tags, for the low-cost, the inter-operability and the relatively low-complexity. A passive RFID system is composed of a digital device called tag, embedding an antenna and an IC-chip with a unique identification code (ID), and a radio scanner device, called reader. Despite the RFID technology is currently mostly applied to logistics of goods, the very recent research is exploring other paths with the common goal of extracting physical information about

tagged objects and nearby environment through low-level processing of electromagnetic signals received and backscattered by the tags. RFID tags can be equipped with a large variety of passive digital and analog sensors for measuring environmental parameters such as temperature, pressure, light intensity, strain, accelerations and humidity or gases and thus performing the sensing activity without any local power supply. Body area networks (Bans) and wearable sensors are also an attractive area for smart tags applications, e.g. for motion recognition monitoring.

RFID systems could therefore permit to implement, in a simple and efficient way, the *last few meters of the Internet of Things* concerning the pervasive quantification of environmental parameters of interest. Ambient sensors, in particular, could permit to quantify the wellness of the environment itself and to analyze its correlation with the people health-state. The application of the RFID technology to the Pervasive ambient sensing is a rather new topic.

The subject of this Ph.D thesis deals with the study of RFID ambient sensing feasibility through of a multidisciplinary vision, which merges together Electromagnetics, Wireless Communication, Electronics, Sensors and Chemical Materials. From the perspective of IoT the research will cover passive (i.e. battery-less) devices in the UHF band (860-960MHz) which are capable to provide services and enough read-ranges to implement a network of sensors for monitoring the quality of the local environment. Each sensor-tag can be processed individually or together with those from the other distributed nodes in order to extract information in the most comprehensive way. Theoretical aspects will be addressed by studying the communication links of RFID devices for sensing purposes and validated by an extensive and targeted campaign of measurements for temperature and gas sensing.

Principles of Passive UHF RFIDs for Ambient Sensing

The first part of the thesis is devoted to the detailed analysis of RFID passive sensors and sensing paradigms for ambient monitor-

ing. The introduced sensing parameters are power-related measurements which highly depend on the set-up and external environment and impedance related measurements, which with appropriate measurement methods can be related to the variation of the only input impedance. Power-related parameters include the turn-on power, i.e. the lowest input power emitted by the reader required to activate the tag, and the backscattered power collected by the reader. Impedance-related parameters are the Analog Identifier (AID), a non-dimensional and set-up independent parameter and the phase of the backscattered signal whose variations are highly dependent on the change of antenna impedance and chip modulation.

The basic sensing mechanisms achievable by RFID sensor devices will be then described, by analyzing them with a theoretical approach to understand the physics of the phenomena, up to introduce and investigate in detail the particular case of Sensitive Material (SM) -loaded tags. General purpose antenna layouts, able to enhance the sensing transduction phenomena by hosting specialized distributed or lumped SM, will be proposed and analytically studied with the aim to control, enhance and optimize both sensing and communication performances.

Temperature Sensing

The second part of the thesis will cover different solutions for RFID sensing of ambient temperature. Three classes of passive UHF RFID Temperature sensors are proposed and experimented.

1) A threshold temperature sensor: An RFID "thermal switch" or fuse based on a threshold physical phenomenon, such that a sensitive material (a substrate of paraffin) changes its state when the external temperature overcomes a given threshold, and the event is permanently written into a physical memory. The paraffin substrate is a distributed SM all along the antenna and its melting enables the change of state of the tag. These devices could have application to the assessment of food and drugs integrity as well as to the detection of fire and over-heating of domestic devices.

2) A continuous temperature sensor: an instantaneous RFID sensor of temperature involving instead a sensitive material load, i.e. a

lumped element whose resistance and/or capacitance change with temperature. The sensor, in this case loaded by a thermistor, is capable to continuously react to the change of temperature and accordingly modify the tag's features detectable by the reader, up to temperatures of over 200°C. A minimum sensitivity of about 1°C may be achieved, by proper sensor design.

3) Digital data loggers: RFID temperature information is given by a new family of RFID microchips equipped with an integrated temperature sensor and with a local Analog to Digital Converter. Accordingly, the temperature information is read, in a range usually confined between -40°C and 85°C, from the tag straight away in a digital form. These kind of sensors will be just mentioned in this part referring to some more in-depth examples in the Appendix. Applications can range from generic ambient sensors up to sensors for civil infrastructures application, such as for the temperature monitoring of ashlars during the so called "curing concrete".

Volatile Compounds Sensing

The third part of the thesis is devoted to the extensive experimentation of chemically doped sensor tags in comparison with the models proposed in the first part. Volatile compounds, such as humidity or other gases, can be sensed by properly shaped tag antennas hosting specialized distributed or lumped SM coatings, capable to selectively change their electromagnetic properties according to gas exposure and convert the external phenomena into a change of the antenna's features. It was demonstrated that the the dynamic range of the sensed data can be easily controlled by simple geometry tuning and by the amount of chemical loading, while at the same time reducing the degradation of energy scavenging, and hence of the read distance. It was moreover proved that not only signal amplitude-related parameters, but even the phase response of a chemically coated passive RFID tag may be engineered to carry information about the change of the external environment. Several chemical SM species were experimented for applications to RFID sensors, aimed at detecting humidity and other gas species. Remarkable performance were obtained in hu-

midity sensing by loading different sensitive antenna layouts with PEDOT:PSS (poly (3,4-ethylenedioxythiophene):poly (styrenesulfonic acid)) that is a hygroscopic chemical compound. A minimum resolution of about 2%RH was achieved by passive RFID layouts. Finally four chemical SM (Pedot:PSS, Doped PSS, SWCNT and PDAC) were also combined into a wireless "RFID nose", e.g. a matrix of doped tags capable to respond in a selective way to the presence of different vapors. The selected materials revealed significantly sensitive, at different extent, to the tested volatile compounds: water, ethanol, ammonia and octane. The achieved responses show a clear selectivity of the set of sensor tags, suggesting the full feasibility of compounds classification by RFID sensor tags.

Chemical sensors still require to be mastered at the purpose to gain a full reproducibility of deposition, stability of performance and resistance over time. So far, no sensitive material has been characterized within the UHF band, hence a dedicated research activity described in this part and involving a strong interactions with chemical engineers, was produced to set-up procedures to characterize the SM at radiofrequency, in order to provide a more extensive database of useful chemical receptors and their sensitivity to a meaningful set of volatile compounds.

Nomenclature

4G-LTE	4th Generation Long Term Evolution
AID	Analog Identifier
Bans	Body Area Networks
BLE	Bluetooth Low Energy
COTS	Off-the-Shelf component
DC	Direct Current
Doped PSS	Doped poly(styrenesulfonate)
EPDM	Ethylene-Propylene-Diene Monomer
FDTD	Finite Difference Time Domain
Forex	expanded polyvinyl chloride
GSM	Global System for Mobile Communications
IC	Integrated Circuit
IOT	Internet of Things
MLA	Meander Line Antenna
MnTPPS	Manganese-Tetra-(sulfonatophenyl)porphyrin
NTC	Negative Temperature Coefficient
o.p.	operating point
PDAC	poly diallyldimethylammonium chloride
Pedot:PSS	poly (3,4-ethylenedioxythiophene):poly (styrene-sulfonic acid)

POM	Polyoxymethylene
RF	Radio Frequency
RFID	Radio Frequency Identification
RSSI	Received Signal Strength Indicator
SM	Sensitive Material
SWCNT	Single Wall Carbon Nanotubes
UHF	Ultra High Frequency
VNA	Vector Network Analyzer
WSN	Wireless Sensor Networks
ZnO Nanorods	Monocarboxytetraphenylporphyrin functionalized ZnO nanorods

Contents

1. The Internet of Things for Smart Environment Monitoring

The Internet of Things (IoT) is the interconnection of uniquely identifiable embedded computing devices within the existing Internet infrastructure. In principle, it allows people to be connected Anytime, Anyplace, with Anything and Anyone, ideally using Any path/network and Any service. In this context, the emerging trend of augmenting physical objects and devices with sensing, computing, and communication capabilities, could be applied to countless applications (Fig. 1.1) [1, 2, 3, 4]. With the growing presence everywhere of Wi-Fi and 4G-LTE wireless Internet access, the evolution towards ubiquitous information and communication networks is already evident. However, for the Internet of Things vision to successfully emerge, the computing paradigm will need to go beyond traditional mobile scenarios that use smart phones, laptops or tablets, and evolve into connecting everyday existing objects and embedding intelligence into our environment.

One of the major IoT application areas that is already drawing attention is the Smart Environment IoT. It can be defined as "Interconnection of sensing and actuating devices providing the ability to share information across platforms through a unified framework, developing a common operating picture for enabling innovative applications. This is achieved by seamless ubiquitous sensing, data analytics and information representation with Cloud computing as the unifying framework".

The quantity of devices connected to the Internet to date exceeds the population of people on Earth. Different sources predict that by 2020 [5], wireless sensors and other types of wireless network nodes

will account for the majority (60 percent) of the total installed base of IoT devices. Such devices range from simple detectors that trigger an alarm signal if the sensor passes a measurement threshold, to monitoring systems that collect data regarding different products or processes.

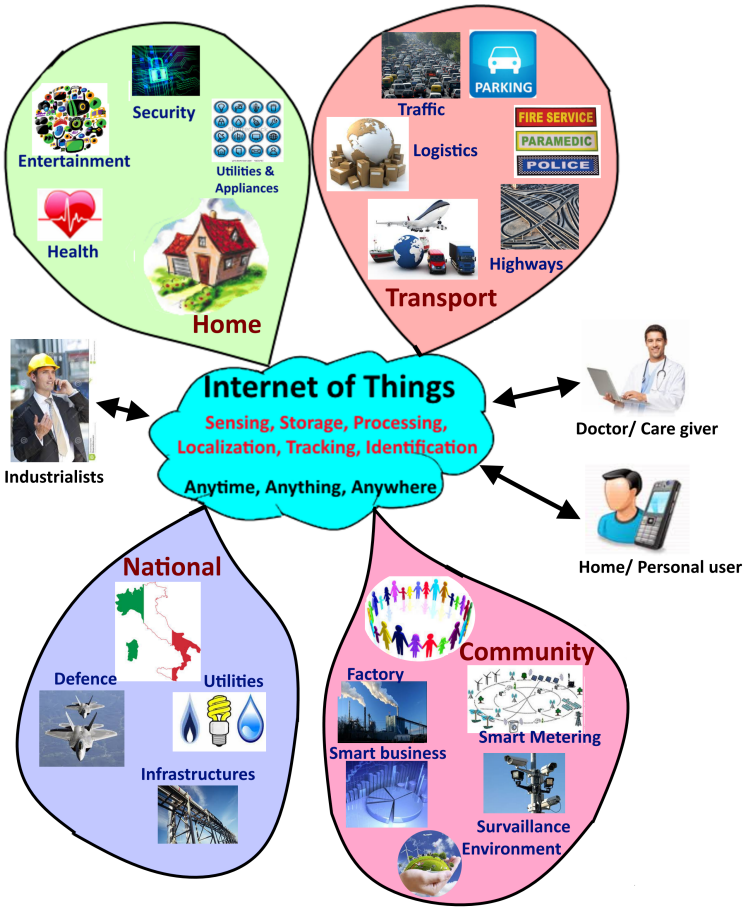

Figure 1.1.: Internet of Things schematic showing the end users and application areas based on data.

1.1. Enabling Technologies

Wireless Sensor Networks' (WSN) recent technological advances in low power integrated circuits and wireless communications have made available efficient, low cost, low power miniaturized devices for use in remote sensing applications. These factors allowed the diffusion of a large number of intelligent sensors, enabling the collection, processing, analysis and dissemination of valuable information, gathered in a variety of environments. Autonomous sensors can potentially be deployed everywhere, though there are usually constraints on the power supply of such devices, so the communication technology must be carefully selected.

Most of these sensors employ low-power-consumption wireless protocols, such as ZigBee or (BLE+). ZigBee is a protocol specifically developed for mesh communication, each sensing device can transmit data either directly to the acquisition module, or to another nearly ZigBee-based sensing device, which in turn will transmit both devices' data to the acquisition module. When they are deployed in urban areas, it is also typical to implement Wi-Fi-based devices, taking advantage of the Wi-Fi coverage associated with these places. A new, interesting trend with sensor devices connected to the IoT involves the use of smartphones to serve as a bridge between the sensors and the cloud. A force still to be reckoned with is that many people (the so called "citizen scientists") are eager to help their communities by installing smartphone applications that provide such a bridge to data, as long as the information is to be used for something they believe in.

1.1.1. Power Supplied COTS Sensors

The power supply of sensors is the key for the true pervasive diffusion of these devices. Even if research is continuously decreasing the power requirements of wireless sensors, the energy levels required are still a too large burden for the energy-harvesting technologies at hand. Power requirements from different communication protocols generally range from tens of milliamps to hundreds of milliamps. However, in most applications, there is no need to have the device continuously transmitting data, so the average power

consumption is lower. Tab. 1.1 shows some general data comparing power requirements of the three wireless protocols which are nowadays widely used: Wi-Fi, ZigBee and Bluetooth Low Energy.

	Wi-Fi	Zigbee	Bluetooth Low Energy
Sleep	10 µW	4 µW	8 µW
Receive (Rx) Power	90 mW	84 mW	28.5 mW
Transmit (Tx) Power	350 mW	72 mW	26.5 mW
Average Power for 10 Messages Per Day	500 µW	414 µW	50 µW

Table 1.1.: Power consumption of three widely used wireless protocols

In addition to wireless data transmission power consumption, it has to be considered the power consumption of the sensor itself. It is worth pointing out that this comparison of power requirements is intended for the purpose of analyzing the impact on the power supply of autonomous sensor devices, not considering other variables to compare, such as communication range (Wi-Fi and ZigBee are much longer than Bluetooth), data rate (Wi-Fi and ZigBee are significantly better) and others.

However, lifetime is extremely critical for many applications, and its primary limiting factor is the energy consumption of the active nodes during sensing and even stand-by modes, which need to be self-powered. The ideal case would be that the sensor devices are able to operate on their own by capturing energy from the environment, with a virtually infinite life.

The most-used natural power sources include photovoltaic, vibration, thermal and radio frequency (RF):

1. *Photovoltaic energy*: Typically known as photovoltaic or solar cells, this power source can be a feasible solution, since the energy level harvested can be quite high, depending on the amount of space available. However, these devices require continuous exposure to sunlight, greatly decreasing their performance as the intensity of the sunlight is reduced.
2. *Vibration energy*: There are multiple solutions for retrieving

energy from environments in which continuous vibration is guaranteed. Vibrational energy harvesting systems are designed for relatively stable conditions. For a selected frequency, the energy is correctly stored. However, for small frequency variations, efficiency dramatically decreases, thus reducing the amount of energy harvested over time.

3. *Thermal energy*: The concept of taking advantage of a temperature gradient is not new. A thermoelectric device creates a voltage when there is a temperature gradient between the two ends of it. It is a very efficient system when the temperature difference is significant (the exterior and interior temperatures of an airplane in flight, for example).
4. *Radio frequency energy* (RF): Signals from a variety of RF sources (television and radio transmissions, GSM signals from mobile phones and cell towers, Wi-Fi systems and so forth) can be captured by a sensor's antenna. The signals are then converted and conditioned to the desired output. RF is a constant energy source in every city of well-developed countries, but the amount of energy harvested is very limited.

Photovoltaic and thermal energy harvesting are very interesting in terms of the amount of energy that can be harvested, but the source must be very powerful in order for a sensor to draw a large level of energy, which is unlikely in most real-world applications. An RF-harvesting device can be suitable for sensors located near an RF source.

However, a number of applications require a more reliable energy source before they can be implemented in the real world.

1.1.2. RFID Technology

RadioFrequency Identification (RFID) systems [6] at UHF frequencies may represent a strategic enabling component for Smart ambient sensing, thanks to the energy autonomy of battery-less (passive) tags and their reliable read ranges (up to 10-15 meters). A passive RFID system is composed of a digital device called tag, embedding an antenna and an IC-chip with a unique identification code (ID), and a radio scanner device, called reader. The low-cost of the ele-

mental unit, the tag, is compatible with a widespread distribution and disposable applications. RFID technology is currently mostly applied to logistics of goods, particularly in retail and supply chain management [7]. Applications can be found in transportation (replacement of tickets, registration stickers) and access control as well. Passive tags are currently being used in many bank cards and road toll tags which are among the first global deployments.

Although it is not a natural source of energy, an RFID transmitter is a very interesting source to take into account for wireless sensors in the IoT scheme. A sensor that requires an RFID reader cannot be considered autonomous. However, this kind of device can be embedded at any place, and will always be ready to measure and transmit. As an example, passive RFID sensor tags can be embedded in concrete, inside piping systems and at many relatively inaccessible locations, and they will never require battery change or generic maintenance. The disadvantage is that they cannot measure or transmit when there is no nearby RFID reader to send RF power. Still, the advantages over natural sources harvesting are important: a passive RFID sensor has an "on-demand" reliable source of energy. There is usually no dependency on environment conditions for the transmission of the required data. It is also in general not affected by dark or hazardous locations, or by natural temperature changes. In this way battery-free RFID sensors could offer a different way to collect reliable sensor data in the IoT scheme, without being affected by unpredictable sources as sun, wind or temperature.

Very recently research is exploring new paths with the common goal of extracting physical information about tagged objects and nearby environment through low-level processing of electromagnetic signals received and backscattered by the tags [8, 9]. RFID systems could be the enabling technology to implement, in a simple and efficient way, the *last few meters of the Internet of Things*.

By displacing wireless sensors inside homes, objects, clothes or other personal items, and in the external environment, it becomes possible to monitor the macroscopic behavior and the health of people, as well as the state of perishable goods and of the environment itself. Possible applications are of interest to the most diverse fields, such as agri-food, chemical process monitoring, surveil-

lance and homeland security [10, 11]. Sensing volatile compounds through a non-invasive and direct way may indeed support clinical diagnosis [12] and human wellness by keeping the air quality under control in operating theaters, within manufacturing industrial facilities as well as inside hazardous working places characterized by the presence of harmful gases. An interesting application to civil engineering is the idea of Smart Buildings: wireless sensors integrated within buildings could allow distributed monitoring and control, improving living conditions and reducing the energy consumption, for instance controlling the temperature and air flow.

All the data collected by RFID sensors could be shared among different nodes and sent to a distributed or centralized system (cloud) for analytic computing and statistics (Fig. 1.2). The pervasive nature of RFID technology could improve the transparency, the reliability, the lifetime and the scalability, while minimizing the overall cost of the platforms.

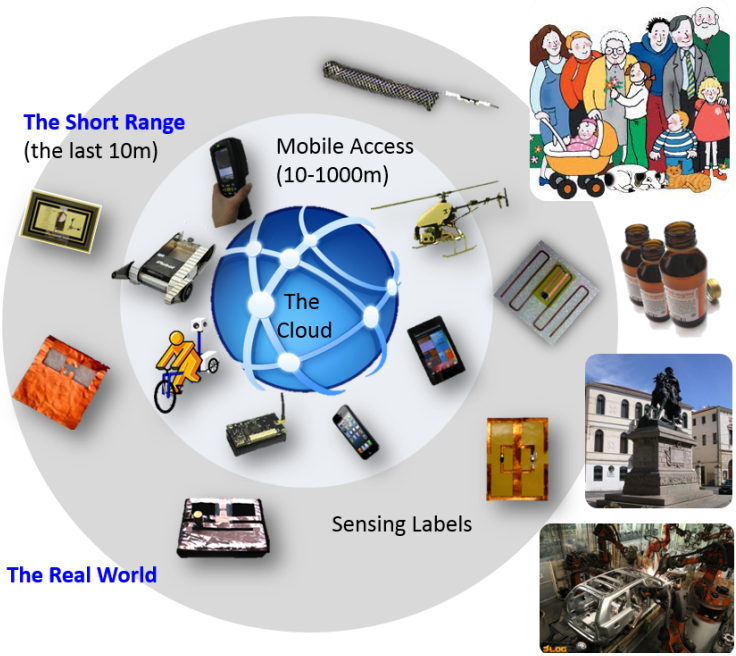

Figure 1.2.: RFID technology applications enabling the last few meters of the IoT.

1.1.2.1. Environmental Passive RFID Sensors

Fast and reliable detection of volatile compounds in the air and temperature are key issues in many daily and industrial applications [13]. The application

A passive RFID tag becomes capable to detect changes of the chemical/physical parameters of the environment when it is functionalized with special chemical compounds or interconnected to microchips integrating sensing features.

Volatile compound sensors Volatile compounds can be sensed by properly shaped tag's antenna hosting specialized Sensitive Mate-

rials capable to selectively change their electromagnetic properties and, accordingly, the tag response during gas exposure. Changes in turn-on power[1] or backscattered power can be hence monitored and decoded by the reader, obtaining information about the presence and the concentration of specific gases.

Some early experiments with augmented UHF RFID passive tags demonstrated in the last years the possibility to detect the level of humidity and other gases in air. In 2011 a loop-driven flat dipole doped with carbon nano structures (CNT), [14] was designed to sense the presence of ammonia in the environment (Fig. 1.3A). Changes in the CNT properties affect the matching and gain of the antenna, detectable through turn-on and backscattered power measurements. More papers addressed the sensing of humidity grade by UHF RFID tags. In [15] (2009) the sensitive material is simply a blotting paper, eventually doped with NaCl (salt), covering a patch-like RFID tag (Fig. 1.3B). The radiation performance of the tag sensibly degrades according to the water adsorption, producing appreciable variations of the tag response. An inkjet printed tag over a Kapton substrate loaded by distributed capacitors was described in [16] (2011). The capacitors convert the permittivity variation of the substrate into a change in the antenna's impedance, remotely detectable through the frequency shift of the turn-on power measurements (Fig. 1.3C). Humidity sensing has been considered even with a chipless approach in [17] (2013), where a cascaded set of group of transmission-line sections was doped by Silicon Nanowires. The radar cross section (RCS), the phase, and the group delay of the tag were related to the humidity adsorption. The humidity sensor in [18] (2014) was based on planar stepped-impedance resonator structures, wherein the dielectric change of Kapton tape attached on the resonator causes a frequency shift and a variation of the minimum power level.

First experiments involving the use of UHF RFID tags with several sensitive materials exposed to different vapours are presented in [19] (2013). Each commercial tag is functionalized with carbon black as the conducting element and a polymer as the sensing element. The different gas–solid partition coefficients for the polymers in

[1] the minimum power emitted by the reader to remotely activate the tag.

the sensor array produce a unique pattern of signal changes that can be used to classify different vapours. This sensor array was experimented with vapors of water, ammonia, ethanol and toluene.

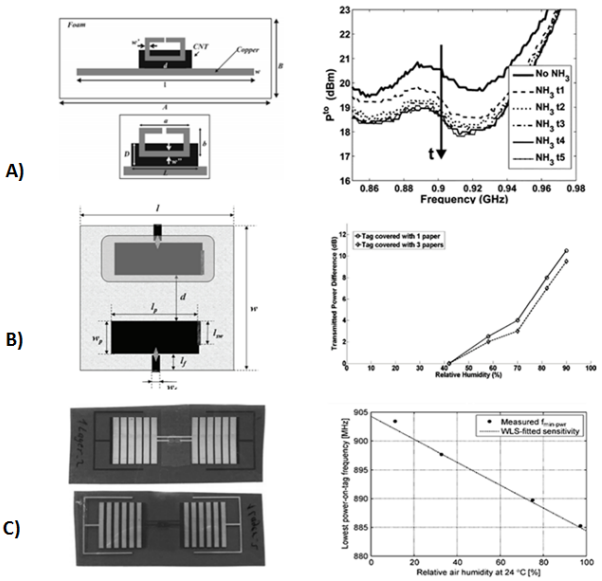

Figure 1.3.: Examples of RFID chemical loaded RFID tags and dynamic responses during gas exposures. A) Gas sensor integrating carbon nanotubes exposed to ammonia [14]; B) moisture sensor integrating blotting paper exposed to humidity [15]; C) moisture sensor with sensitive dielectrics exposed to humidity [16].

Temperature Sensors

Three classes of passive UHF RFID Temperature sensors have been experimented in the last few years ranging from threshold sensors, continuous sensors up to better performing digital data-loggers.

- Threshold Temperature Sensors: An RFID "thermal switch" or *fuse* is based on a threshold physical phenomenon, such that a material changes its state when the external tem-

perature overcomes a given threshold, and the event is permanently written into a physical memory. For instance the thermal-controlled event could be the melting of a ice region (low-temperature threshold) loading the tag's antenna [20] (2010), the change of properties of a polymer [21] (2010), or the geometric changes of Shape Memory Alloys such as the Nitinol [22] (2011). In these cases the temperature change induces an abrupt variation of the antenna response so that the microchip is activated or not depending on the temperature violation of a pre-defined level. For instance, Fig. 1.4 shows a two-chips threshold sensor integrating a temperature-controlled Nitinol switch [22]. The normal condition corresponds to the transmission of the only ID1 (label of the product) while an occurred overheating is revealed through and additional ID2 code (thermal event).

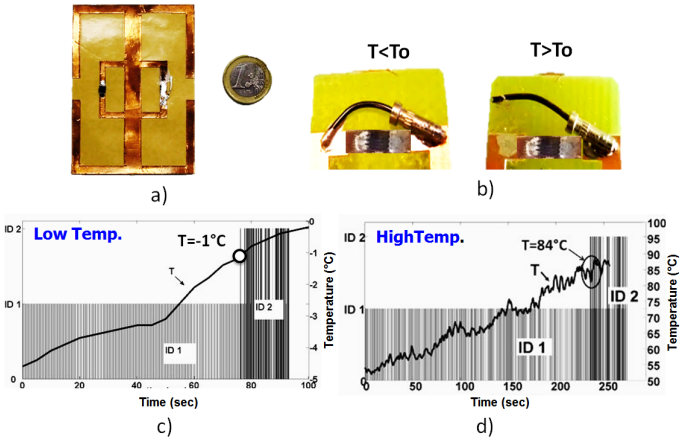

Figure 1.4.: a) Two-chip (with ID1 and ID2) temperature threshold sensor integrating a Nitinol switch [22]; b) Switch closed (chip is inactive, only ID1 is transmitted) and open (chip is active depending on the temperature, ID2 is transmitted in addition to ID1). c) chips' responses versus temperature for 0°C-threshold Nitinol and d) for 80°C-threshold Nitinol.

- Continous Temperature Sensors: An instantaneous RFID sensor of temperature involves instead a sensitive material capable to continuously react to the change of temperature. [23] and [24] (2012) consider (distilled) water region incased close to the tag whose conductivity and permittivity change with the temperature and accordingly modify the tag's resonant frequency detectable by the reader.
- Digital Data Loggers: The real revolution in the autonomous RFID temperature sensing will be probably boosted by a new family of RFID microchips equipped with an integrated temperature sensor and with a local Analog to Digital Converter. Accordingly, the temperature information is read from the tag straight away in a digital form. These chips [25]-[26] can be used in both passive and battery-assisted mode, and in the latter case the tag may trigger a temperature measurement and store the data inside the microchip's user memory. The price to pay for this very special capability is a higher cost of the chip (1-3$ versus a few cents for conventional RFID chips) and a rather poor power sensitivity when used in fully passive mode (10dB less than conventional chips), and therefore the read distance is currently limited to a couple of meters.

1.2. Outline and Open Challenges

From the perspective of IoT Smart Environment monitoring, this thesis will cover passive (i.e. batteryless) devices in the UHF band (860-960MHz) which are capable to provide services and enough read-ranges to implement a network of sensors for monitoring the quality of the local environment. Theoretical aspects will be addressed by studying the communication links of RFID devices for sensing purposes. Theory will be validated by an extensive and targeted campaign of measurements for the particular cases of temperature and gas sensing.

Several key and challenging issues regarding RFID passive sensing are still open:

1. The design of tag antennas suited to work as sensors in different environmental conditions. The tag may be consid-

ered as an analog component whose strength of received and backscattered power is sensibly affected by the electrical feature of the antenna, which is in turn dependent on the tagged object change. Since there is usually no decoupling from the operative point of view between antenna and sensor, both perspectives need to be taken into account in order to reach a trade-off between sensing and communication performance.

2. The full characterization of the tag as a sensor, such as the sensitivity, the recovery capabilities during cyclic exposures, the hysteresis, the robustness, the reproducibility, and not last the methodologies to master the sensing performance.
3. A reliable procedure to characterize at radiofrequency the electrical features of different kind of Sensitive Materials (SM) able to influence the reader-tag communication according to their state. These SM could be a chemical painting integrated with the RFID device to monitor volatile compounds variations, as well as a thermal fuse or a thermistor for temperature detection. Most of them are characterized only in DC and hence the design of RFID sensing antennas suffers from the lack of information about the sensor electromagnetic parameters in the UHF RFID band.
4. The RFID sensors cross-sensitivity to different environmental parameters should be taken into account. It is recommendable to study the performance of such sensors in real environment where mixtures of gases and variation of several parameters (temperature, pressure...) are present. A possible solution in these cases is the multiplication of sensors elements in order to form an array for the quantification and the identification of each measurand.

The proposed Thesis will carefully examine and address the open challenges, with the main goal to investigate, from a theoretical and experimental point of view, the feasibility of a Pervasive Ambient Sensing System entirely based on the passive UHF RFID technology. The Thesis is organized as follows:

The first part is devoted to the detailed analysis of RFID passive sensors and the sensing paradigms for ambient monitoring. The basic mechanisms achievable by RFID sensor devices will be de-

scribed with a theoretical approach to understand the physics of the phenomena, up to introduce and investigate in detail the particular case of SM-loaded tags. General purpose antenna layouts, able to enhance the sensing transduction phenomena by hosting specialized distributed or lumped SM, will be proposed and analytically studied with the aim to control and optimize both sensing and communication performances.

The second part of the thesis will cover different solutions for RFID sensing of ambient temperature considering threshold and instantaneous sensors. A distributed loaded and a lumped loaded sensor will be presented for the two applications.

The third part of the thesis is finally devoted to the extensive experimentation of chemically doped sensor tags in comparison with the models proposed in the first part. A dedicated research activity is produced to set-up procedures to characterize the SM at radiofrequency, in order to provide a more extensive database of useful chemical receptors and their sensitivity to a meaningful set of volatile compounds. Several chemical SM species are experimented for applications to RFID sensors, aimed at detecting humidity and other gas species. Finally a set of chemical SM is also combined into a wireless "RFID nose", e.g. a matrix of doped tags capable to respond in a selective way to the presence of different vapors.

Part I.

Principles and Tools of Passive UHF RFIDs for Ambient Sensing

The role of the tag antenna in UHF RFID systems and its impact on the global performance is very important [27]. Indeed, for any antenna there are two operating regions: near-field and far-field depending on the communication distance between reader and tags. In practice, the UHF RFID tags must operate regardless of the distance reader-tags, the environment in the vicinity which is different for each application and for any item they are tagging. So, designing compact and low-profile antennas exhibiting low cost, but at the same time relatively broad band and reconfigurability features for different applications is, at the present time, a real challenge in the field of UHF RFID technology [28]. A major objective for reader-tag communication is to develop compact and robust tags able to reply to reader's quaery regardless the place it is attached on, the specific application and the frequency bands [29, 30]. On the other hand, any tag is inherently sensitive to the close environment. This effect may be exploited to transform the tag into a sensor, able to detect changes of the tagged object or the nearby environment.

This part theoretically examines both the communication and sensing perspectives of RFID passive tags. The RFID antenna and the basic sensing mechanisms achievable by RFID sensor devices are introduced. In particular a theoretical approach to understand the physics of the phenomena, is investigated in detail for the particular case of Sensitive Material (SM) -loaded tags. Finally general purpose antenna layouts are proposed with the aim to enhance the sensing transduction phenomena by hosting specialized distributed or lumped SM, and to keep reliable communication performances.

2. Rationale and Theory of RFID Sensing

This chapter addresses the fundamental antenna design requirements of general UHF RFID sensor tags for ambient monitoring, focusing on communication and sensing performance parameters.

The sensitivity of the antenna to the external environment is certainly one of the major weaknesses of UHF tags utilized for logistics. However, this characteristic can be exploited to transform a simple tag into a sensing device. Indeed, it has been very recently demonstrated that under some specific design, the RFID tag can acquire interesting sensing capabilities [8]. Such an evolution is rapidly transforming RFID from a powerful identification technology (just as an optical barcode) to a more attractive and versatile technique that opens the door to the paradigm of the Internet of Things [31, 32]. From the previous discussion it appears that both antenna and sensor design for RFID tags are very specific and challenging topic to be faced from a theoretical and practical perspective.

2.1. RFID Principle of Operation

The principle of operation of a passive RFID system is illustrated in Fig. 2.1. It usually contains two parts: a base station, also called the RFID reader and an RFID passive transponder (tag). The tag consists of an antenna and an Integrated Circuit (IC) chip having its own identification code (ID).

In a conventional RFID link, the reader remotely activates and query the tag by means of radio-frequency electromagnetic signals.

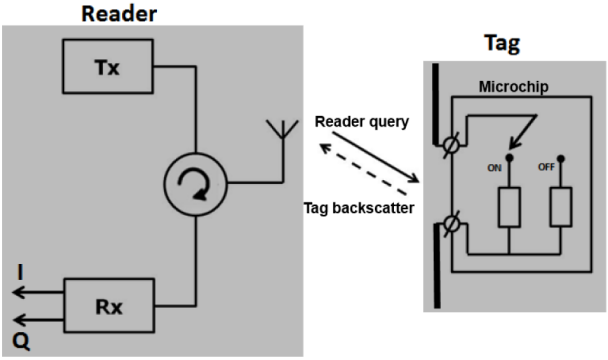

Figure 2.1.: Sketch of a passive RFID system which comprises a digital device called tag, embedding an antenna and an IC-chip with a unique identification code (ID), and the reader that acts as a transmitter and receiver.

The tag can operate in the interrogation zone of the reader, where the ID and other data in the memory can be wirelessly transferred to the reader. An RFID tag can be represented by its Thevenin circuit as shown in Fig. 2.2.

The input impedance of the tag is hereafter denoted with $Z_A = R_A + jX_A$ and its gain with G_T. The equivalent input impedance of the chip in the scavenging mode, e.g. when the tag is harvesting power from the reader, is referred to as $Z_C = R_C + jX_C$, with X_C capacitive reactance. The architecture of most UHF RFID readers is based on a direct-conversion by I/Q demodulator (homodyne receiver) [6]. Upon interrogation, the tag sends back the data contained in the chip memory by switching its input impedance between two states $\{Z_C^{ON}, Z_C^{OFF}\}$ and thus modulating the backscattered signal [33]. The energy harvesting capability of a tag is generally described by the power transfer coefficient

$$\tau = \frac{4R_C R_A}{|Z_C + Z_A|^2} \leq 1 \tag{2.1}$$

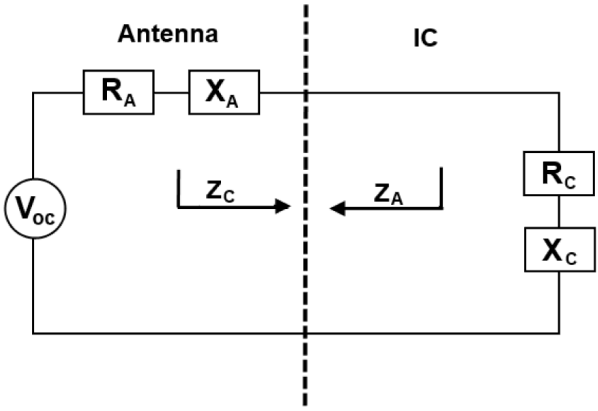

Figure 2.2.: Thevenin equivalent circuit of an RFID tag.

that it is maximum in case of conjugate impedance condition $Z_A = Z_C^*$. If the matching condition is realized, the chip can use the entire power available at the tag antenna. Hence, proper impedance matching is an important factor while considering an RFID system.

2.1.1. Forward and Backward Links

The first step of the reader-tag communication protocol consists of the forward link from the reader to the tag. In the hypothesis of free space, the fraction of power $P_{R\to T}$ emitted by the reader and collected by the tag is given by the *Friis* formula [6] valid in the free space:

$$P_{R\to T} = \left(\frac{\lambda_0}{4\pi d}\right)^2 P_{in} \cdot G_R(\theta,\phi) \cdot \hat{G}_T(\theta,\phi) \cdot \chi(\theta,\phi) \qquad (2.2)$$

where λ_0 is the free-space wavelength of the carrier tone emitted by the reader; ϕ and θ are the angles of a spherical coordinate system centered at the tag; P_{in} is the power entering the reader's antenna; $G_R(\phi,\theta)$ is the gain of the reader antenna; χ is the polarization

factor accounting for the mutual orientation reader-tag; $\hat{G}_T(\phi,\theta) = G_T(\phi,\theta)\cdot\tau$ is the *realized gain* of the tag, e.g. the radiation gain $G_T(\phi,\theta)$ of the antenna corrected by the power transfer coefficient τ between tag's antenna and microchip.

The *radar* equation defines instead the backward link; the power backscattered by the tag and collected by the reader, assuming perfect impedance matching ($\tau = 1$), is equal to:

$$P_{R\leftarrow T} = \frac{1}{4\pi}\left(\frac{\lambda_0}{4\pi d^2}\right)^2 P_{in}\cdot G_R^2(\phi,\theta)\cdot\chi^2(\theta,\phi)\cdot\sigma(\theta,\phi) \quad (2.3)$$

where $\sigma(\phi,\theta)$ is the tag's radar cross-section, related to the modulation impedance Z_{mod} of the microchip to encode the low and high digital state:

$$\sigma(\phi,\theta) = \frac{\lambda_0^2}{4\pi}\cdot G_T^2(\theta,\phi)\cdot\left(\frac{2R_A}{|Z_{mod}+Z_A|}\right)^2 \quad (2.4)$$

The backscattered power $P_{R\leftarrow T}$ is directly measurable by the reader in terms of the Received Signal Strength Indicator (RSSI) [34], here assumed to correspond to the binary modulating state having $Z_{mod} = Z_C$.

Let V_L^i denote the voltage collected at the reader's load after carrier suppression, when the chip is in $i = ON/OFF$ state, and $Z_0 = 50\Omega$ is the input impedance of the receiver, the amplitude (RSSI) and phase (φ) of the signal backscattered by the tag are directly retrieved [35] by the reader as

$$RSSI \propto \frac{1}{2}\frac{\left|V_L^{OFF} - V_L^{ON}\right|^2}{Z_0}. \quad (2.5)$$

$$\varphi = arg(V_L^{OFF} - V_L^{ON}). \quad (2.6)$$

The maximum distance at which a tag can be detected by the reader is a practical tag communication performance indicator. Normally, the reading range of passive tags is limited by the forward-link operation, i.e., the efficiency of the wireless power transfer from the reader to the tag's IC. Assuming free-space conditions for site-independent comparison, from (2.2) the tag reading range at the spatial observation angles ϕ and θ of a spherical coordinate system centered at the tag is given by [29]:

$$d_{max}(\phi,\theta) = \frac{\lambda_0}{4\pi}\sqrt{\frac{EIRP \cdot \hat{G}_T(\theta,\phi) \cdot \chi(\theta,\phi)}{P_{chip}}} \tag{2.7}$$

where $EIRP$ is the equivalent isotropic radiated power by the reader and $P_{R\to T} = P_{chip}$ is the power required to activate the IC. A challenging issue in the design of the RFID tag is to reduce the effect of impedance and gain variations caused by the physical environment changes which can affect the read distance of the tag.

2.2. RFID as a Sensor

In several practical implementations, the sensitivity of the tags to the external environment changes is observed and usually considered as a negative effect and as one of the major weaknesses of UHF RFIDs. The antenna behavior is sensitive to the environment, i.e. the physical phenomena surrounding it and located in its near-field region. However, this phenomena may be potentially exploited to see variations of humidity or other vapours [14, 36, 37], the proximity of dielectric materials, metal [30], or even the effect of coupling (due to near-field interaction with other resonant tags) observed when multiple tags are close to each other [38, 39]. For identification, logistics and tracking applications, these effects are negative, thus, a strategy to develop tags able at the same time to robustly communicate with the reader and sense the environment variation is a challenging but extremely attractive reasearch field.

Let suppose that the tag is exposed to some generic physical, chemical or geometrical external agent $\Psi(t)$ (such as temperature, humid-

ity, vapors, pressure) producing a modification of the antenna input impedance, $Z_A[\Psi]$, and gain, $G_T[\Psi]$, and accordingly of the amplitude and phase of the received backscattered signal, throughout any kind of chemical-electromagnetic or mechanical - electromagnetic transduction mechanism (Fig. 2.3). The aim of RFID sensing is to extract information about the change of external agent Ψ through RFID signals measurements.

It is possible to easily define some sensing indicators carrying information about the external agent change and directly derivable from the reader's measurements. At this purpose, the equations (2.2) and (2.3) of a two-way reader-tag link [33] need to be rewritten, making explicit the dependence on the variation of local parameters.

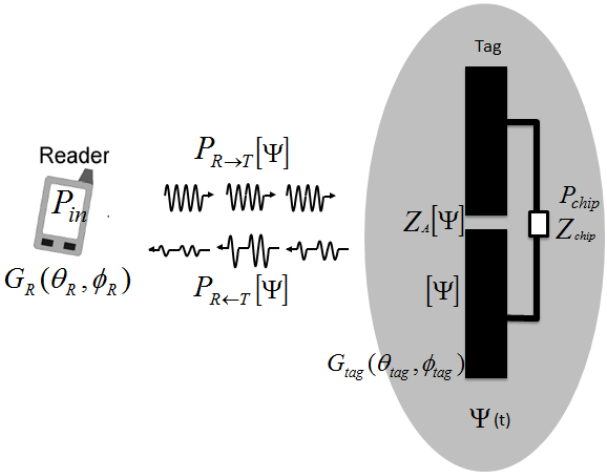

Figure 2.3.: A sketch of the RFID sensing system. A reader interrogates the tag, whose behavior is influenced by a changing external phenomena Ψ.

2.2.1. Power-related Measurable Data

Turn-on power: Under the simplifying hypothesis of free-space interactions, a first parameter obtainable from the forward link is the *turn-on power* $P_{in}^{to}[\Psi]$, e.g. the minimum input power P_{in} through the reader's antenna required to activate the tag's integrated circuit:

$$P_{in}^{to}(\theta,\phi)[\Psi] = (\frac{4\pi d}{\lambda_0})^2 \frac{P_{chip}}{G_R(\theta,\phi)\cdot\chi[\Psi]\cdot G_T(\theta,\phi)[\Psi]\cdot\tau\,[\Psi]} \quad (2.8)$$

where d is the reader-tag distance; $G_R(\theta,\phi)$ is the gain of the reader antenna, $G_T(\theta,\phi)[\Psi]$ is the gain of the tag's antenna; $\chi[\Psi]$ is the polarization mismatch between the reader and the tag; P_{chip} is the IC's sensitivity and finally $\tau[\Psi]$ is the power transmission coefficient of the tag defined as in (2.1).

From turn-on measurement it is possible to extract the *realized gain* of the tag $G_\tau[\Psi]$, as follows:

$$G_\tau(\theta,\phi)[\Psi] = (\frac{4\pi d}{\lambda_o})^2 \frac{P_{chip}}{G_R(\theta_R,\phi_R)\cdot\chi[\Psi]\cdot P_{in}^{to}(\theta,\phi)[\Psi]} \quad (2.9)$$

Backscattered power: By considering the backward link, an another sensing metric directly measurable by the reader in terms of the RSSI, is the normalized backscattered power $p_{BS}[\Psi]$, e.g the ratio between the backscattered power $P_{R\leftarrow T}[\Psi]$ collected by the reader and the input power $P_{in}[\Psi]$ to the reader's antenna:

$$p_{BS}(\theta,\phi)[\Psi] = \frac{P_{R\leftarrow T}(\theta,\phi)[\Psi]}{P_{in}(\theta,\phi)[\Psi]} \quad (2.10)$$

2.2.2. Impedance-related Measurable Data

Analog Identifier (AID): Combining above powers from measurements, the Analog Identifier (AID), a parameter which permits an-

gle and distance-independent measurements, is computed as [38, 9]

$$AID[\Psi] = \frac{P_{chip}}{\sqrt{P_{in}^{to}[\Psi] P_{R \leftarrow T}[\Psi]}} = \frac{2R_C}{|Z_C + Z_A[\Psi]|}. \tag{2.11}$$

The AID only depends on the antenna's impedance. It thus appears useful when the interrogation setup changes (position and orientation) in successive measurements, since it is immune to the interrogation modalities.

Phase:

Nowadays many RFID readers are capable to provide power information in a fully coherent way and extract the phase of the demodulated signals backscattered by the tag, thus the phase can be used as sensing carrier. Its dependence on the tag antenna impedance can be formalized as follows. Using the formalism in [38], and under free-space conditions, the port voltage $V_L^{ON/OFF}$ can be expressed in terms of the tag's and reader's parameters, so that

$$V_L^{ON/OFF}[\Psi] = V_{L,OC}[\Psi] +$$

$$+ \frac{\eta_0}{k_0^2} G_R \sqrt{\frac{P_{in} R_R^{in}}{2}} g^2[\Psi] \frac{1}{\left(Z_A[\Psi] + Z_C^{ON/OFF}\right)} \frac{e^{-2jk_0 r}}{r^2} \tag{2.12}$$

where $V_{L,OC}[\Psi]$ is the open-circuit voltage that is independent on the tag loading impedance, while it is instead potentially affected by the external agent; $g = \sqrt{\frac{R_A G_T(\hat{\underline{r}}) \chi[\Psi]}{\eta_0}} e^{j\Phi[\Psi](\hat{\underline{r}})}$ is the normalized gain of the tag; $\eta_0 = 120\pi\,\Omega$; k_0 is the propagation constant; G_R is the gain of the reader antenna; P_{in} is the power injected by the reader into its antenna; R_R^{in} is the input resistance of that antenna; r is the reader-tag distance. Finally polarization-dependent parameters $\{\chi,\Phi\}$, are such that $\chi[\Psi] = |\hat{\underline{h}}_T[\Psi] \cdot \hat{\underline{h}}_R|^2$

and $\Phi[\Psi](\hat{\underline{r}}) = angle(\hat{\underline{h}}_T[\Psi] \cdot \hat{\underline{h}}_R)$ with $\hat{\underline{h}}_R(\hat{\underline{r}})$ and $\hat{\underline{h}}_T[\Psi](\hat{\underline{r}})$ are the effective length of reader's and tag's antennas, respectively, the last one being in principle dependent on the external agent.

By application of (2.6) and after simple algebraic manipulations, the backscattering phase can be rewritten as

$$\varphi[\Psi] = -2k_0 r + 2\Phi[\Psi](\hat{\underline{r}}) +$$

$$+arg\left(\frac{1}{Z_A[\Psi] + Z_C^{OFF}} - \frac{1}{Z_A[\Psi] + Z_C^{ON}}\right). \tag{2.13}$$

The $-2k_0 r$ contribute accounts for propagation delay along distance r, $2\Phi[\Psi](\hat{\underline{r}})$ embeds the phase variation of polarization mismatch between reader and tag and the last term includes the dependence of the phase on the only input impedance of the tag's antenna.

2.3. Sensor Properties

An overview of a few definitions related to sensors are here considered, which will be most frequently used from now on. These are: *sensor response curve*, *sensitivity*, *noise*, *resolution, accuracy and precision, cross-sensitivity, drift*, and *specificity.* These quantities represent the basic knowledge that should be known and utilized on behalf of the sensor community [40].

Sensor response curve: The *sensor response curve* or *calibration curve* is the representation of the sensor output as a function of the measurand applied to its input. All the previously defined sensing indicators may correctly represent the RFID sensor response curve:

$$\left\{AID, \varphi, P_{in}^{to}, P_{bs}\right\} \leftrightarrow \Psi(t). \tag{2.14}$$

The sensor response curve represented in Fig. 2.4(a), as an example, tells us that in presence of high values, the output tends to remain constant, which means that the sensors, in this condition, do not react to the input variations, i.e it reaches saturation. The difference $\xi_{sat} - \xi_{min}$ is the dynamic range of the sensor.

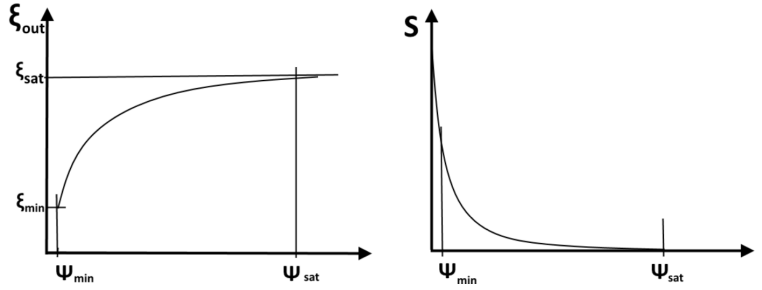

Figure 2.4.: (a) Response curve and (b) sensitivity of a generic sensor.

Sensitivity: The *sensitivity* (Fig. 2.4b) can be obtained by a derivative procedure from the response curve, as

$$S[\xi] = \frac{\delta\xi[\Psi]}{\delta\Psi} \tag{2.15}$$

The definitions based on the output/input derivative, always valid simply because sensors are, generally speaking, nonlinear in character, can be simplified in those cases where the degree of nonlinearity can be neglected. If, on the other hand, the sensor response curve can be piecewise linearized, then many sensitivities can be defined one for each linear piece, as

$$S[\xi] = \frac{\Delta\xi}{\Psi_{high} - \Psi_{low}} \tag{2.16}$$

but the interval to which the linearity applies should be specified.

Noise: Sensors, whatever their complexity may manifest *noise,* i.e. the unavoidable fluctuations of chemical, physical, biological and electrical quantities, at their output with a given signal to noise ratio. This noise is one of the reasons that the resolution cannot approach the zero value. Another direct reason is the sensitivity value limitation. Certainly, without the knowledge of the noise level, it is not possible to estimate the resolution.

Resolution: The *resolution* is obtained through a limit procedure in its general form

$$resolution = \lim_{\xi \to V_{noise}} \frac{\xi}{S} = \frac{V_{noise}}{S} \tag{2.17}$$

where V_{noise} is the amplitude of the noise fluctuations. It is worth pointing out that, in a nonlinear transfer function, the sensitivity and the noise level are functions of the operating point (o.p.) and so is the resolution.

Accuracy: *Accuracy* can be defined as the amount of uncertainty in a measurement with respect to an absolute standard and is measured as a ratio of the highest deviation of a value represented by the sensor to the ideal value.

Precision: *Precision* describes the reproducibility of the measurement. If the measured values are close together then the sensor has a high degree of precision or repeatability.

Drift: Concerning the *drift*, it can be defined as a slow unpredictable change of the sensor output, undefined from the statistical point of view, which is superimposed to both the signal and noise levels. Its origin may be correlated to the aging of the sensing material and of the electronic components that interact with chemical, physical and biological quantities present in the environment. Its presence can be detected usually through a long time observation and can be considered another reason of the loss of accuracy of the sensor.

Cross-sensitivity: Almost always, sensors designed to be sensitive to a given measurand show undesired internal sensitivities to other measurands whose nature can be physical, chemical, or even biological in character. There is one case (the use of sensor arrays for the so-called electronic noses and tongue applications) where the presence of different sensitivities plays the key role for the working principle of the overall sensor system. It is possible to define, for a given sensor or sensor system, the term *cross-sensitivity*, i.e. the sensitivity of the sensor to different measurands $\Psi_1, \Psi_2, ...\Psi_{n,}$.

Specificity: In the case of *specificity* (namely when among the quantities occurring in an environment the sensitivity toward one is dominant), a sensor may be fruitfully utilized to get information about a single measurand. In the case of independent sensitivities, selectivity can be estimated, at calibration level, by a one-by-one technique, determining the response to one measurand per time in a given domain of values. In other cases, being the response of the sensor, due to more than one quantity, the information provided by the sensor is ambiguous, and no straightforward information about the environment can be achieved. The way to overcome this situation is the use of arrays of sensors. In the general case of nonlinear sensors, given n measurands and m sensors (with $m \geq n$) the response of the sensors can be represented as

$$\begin{cases} \xi_1 = f_1(\Psi_1, \dots \Psi_n) \\ ... \\ \xi_m = f_m(\Psi_1, \dots \Psi_n) \end{cases} \tag{2.18}$$

It is possible to define a local sensitivity through the Jacobian matrix of the previous system of equations. It defines the sensitivities of the sensors toward all the involved quantities [40].

$$S = \begin{pmatrix} \frac{\delta \xi_1}{\delta \Psi_1} & \dots & \frac{\delta \xi_1}{\delta \Psi_n} \\ \vdots & & \vdots \\ \frac{\delta \xi_m}{\delta \Psi_1} & \dots & \frac{\delta \xi_m}{\delta \Psi_n} \end{pmatrix}. \tag{2.19}$$

Extending the concept of selectivity previously given, the selectivity of the array may be defined as the capability of the array to retrieve the n values of the quantities at which the m sensors are sensitive to. Around the o.p., the measure of $\xi_1, \xi_2, ...\xi_n$ is obtained inverting the linearized system. This is possible if the condition $det(S) \neq 0$ is met. The maximum selectivity is achieved when the Jacobian matrix is diagonal; this corresponds to the case of an array composed of fully specific sensors.

3. Functionalized RFID Sensors

In this chapter the different kinds of RFID sensors are introduced and the theory presented in chapter 2 is specialized for a particular case, where the portion of the antenna that senses the change of the external phenomena is concentrated within a very small region, at limit a dedicated lumped sensor in series or parallel to the IC.

Several papers in the last years have studied the sensing performance of "bare" sensor tags where the sensor is the antenna and the antenna is the sensor [9, 41, 42, 43, 44]. The main drawbacks of this case are the non-specificity and the limited range of parameters that can be monitored, mainly related to permittivity or shape changes. A second way to perform sensing with RFIDs is to equip the tag with a real passive sensor which could be either considered as a lumped load, connected in some part of the tag's antenna, or instead distributed all over the antenna surface as a chemical receptor painting. Such a sensing mechanism may be hence considered as a lumped or distributed impedance, loading the tag's antenna.

A passive RFID tag becomes capable to detect critical parameters such as the temperature and the presence/level of humidity or other gases in the environment, only if it is functionalized with special sensitive materials or interconnected to microchips integrating sensing features. Volatile compounds can be sensed by properly shaped tag antennas hosting specialized chemical sensitive materials capable to selectively change their electromagnetic properties and, accordingly, the tag response during humidity/gas exposures. Loaded RFID temperature sensors can range from threshold sensors [22], continuous sensors [24] up to better performing digital

data-logger [25].

A theoretical analysis is here introduced to address the changes inducted to the tag's features by the presence of a lumped SM interconnected in series or parallel to the IC.

3.1. Lumped Element Model of a Sensor Tag

A possible approach to RFID sensing engineering is to describe the complex interactions between SM antenna and agent under test as simple lumped-element circuits, that is possible when the loading SM is in a very localized displacement.

Let Ψ denote the generic physical, chemical or geometrical external agent that has to be monitored by the radio-sensor. The electromagnetic effect of the interaction between such an agent and the SM can be considered as a perturbation to the gain and to the input impedance of the tag antenna.

The sensing-oriented equations presented in sec. 2.2 are now rewritten for a particular case, where the portion of the antenna that senses the change of the external phenomena is concentrated within a very small region, at limit a dedicated lumped sensor. Such *Sensitive Material (SM)*, on reacting to an external stimulus, will produce a change of its equivalent RF impedance

$$Z_{SM}[\Psi] \equiv R_{SM}[\Psi] \parallel C_{SM}[\Psi] \tag{3.1}$$

that accounts for both permittivity and conductivity variations. Let moreover assume that the variable impedance of the Sensitive Material is directly connected in series or in parallel with the microchip (Fig. 3.1). Accordingly, the *unloaded* antenna of the tag can be now assumed to be unaffected by the change of the external process.

Since the RFID communication involves a direct (energy harvesting) and a reverse (backscattering modulation) links, two different

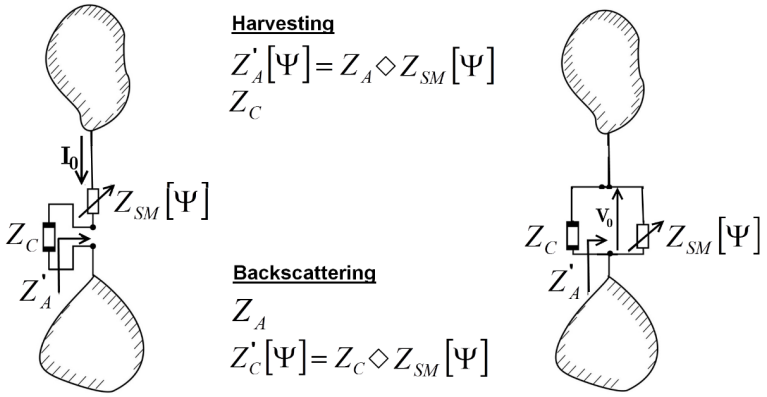

Figure 3.1.: Series (left) and parallel (right) interconnection of the sensitive equivalent lumped impedance of the SM (Z_{SM}) with indication of the corresponding equivalent antenna and microchip impedances for the harvesting and backscattering links. The symbol '$\diamondsuit$' indicates series/parallel connection.

models will be applied to describe realized gain and phase of the tag.

3.1.1. Harvesting mode

In the harvesting mode the sensitive material is considered as part of the antenna, so that the transfer power coefficient needs to be evaluated for an equivalent antenna impedance

$$Z'_A[\Psi] \equiv Z_A \diamond Z_{SM}[\Psi] \tag{3.2}$$

where the symbol $'\diamond'$ indicates the series or parallel connection. For calculation convenience the load can be taken into account as a lumped variable impedance $Z_{SM}[\Psi] = R_{SM}[\Psi] + j \cdot \chi_{SM}[\Psi]$ in case of series interconnection, or a lumped variable admittance $Y_{SM}[\Psi] = g_{SM}[\Psi] + j \cdot B_{SM}[\Psi]$ in case of parallel interconnection to

the impedance $Z_A = R_A + j \cdot \chi_A = \frac{1}{Y_A} = \frac{1}{g_A + j \cdot B_A}$ of the unloaded (blank) antenna (Fig. 3.1). Z_A can be estimated by simulations or measurements at the position of the RFID chip.

The input impedance of the loaded tag $Z'_A[\Psi]$ is definitely dependent on the value Ψ of the process under observation. It is now useful to express the performance indicator of an RFID tag, e.g. the realized gain $\hat{G_\tau}(\theta, \varphi)[\Psi] = G(\theta, \varphi)[\Psi] \cdot \tau[\Psi]$ in terms of the equivalent impedance/admittance of the SM loading.

From Fig. 3.1, the input power of the unloaded tag can be expressed as

$$P_A = \frac{1}{2} R_A \left| I_0^2 \right| = \frac{1}{2} g_A \left| V_0^2 \right| \tag{3.3}$$

while the power absorbed in the sensing load, for the series ($P_{SM,s}[\Psi]$) and parallel ($P_{SM,p}[\Psi]$) topologies is respectively

$$P_{SM,s}[\Psi] = \frac{1}{2} R_{SM}[\Psi] \left| I_0^2 \right| . \tag{3.4}$$

$$P_{SM,p}[\Psi] = \frac{1}{2} g_{SM}[\Psi] \left| V_0^2 \right| . \tag{3.5}$$

The gain of the loaded antenna can be calculated as

$$G_{s/p}(\theta, \varphi)[\Psi] = 4\pi \frac{I(\theta, \phi)}{P_A + P_{SM,s/p}[\Psi]} = \alpha_{s/p}[\Psi] G_0(\theta, \phi) \tag{3.6}$$

where $I(\theta, \varphi)$ is the radiation intensity, $G_0(\theta, \varphi)$ is the gain of the unloaded tag, and

$$\alpha_s[\Psi] = \frac{R_A}{R_A + R_{SM}[\Psi]} < 1 \tag{3.7}$$

$$\alpha_p[\Psi] = \frac{g_A}{g_A + g_{SM}[\Psi]} < 1 \tag{3.8}$$

is the degradation of the gain introduced by the SM-load perturbation for a series ($\alpha_s[\Psi]$) or parallel ($\alpha_p[\Psi]$) interconnection, which will negatively impact on the read-range performance of the sensor tag.

The power transmission coefficient of the loaded tag for the two configurations, can be hence deduced from equation (2.1) by substitution of $Z'_A[\Psi] = (Z_A + Z_{SM}[\Psi]) = (Y_A + Y_{SM}[\Psi])^{-1}$, so that:

$$\tau_s[\Psi] = \frac{4R_C(R_A + R_{SM}[\Psi])}{|Z_C + Z_A + Z_{SM}[\Psi]|^2} \tag{3.9}$$

$$\tau_p[\Psi] = \frac{4g_C(g_A + g_{SM}[\Psi])}{|Y_C + Y_A + Y_{SM}[\Psi]|^2} \tag{3.10}$$

The realized gain $\hat{G_\tau}[\Psi] = G[\Psi] \cdot \tau[\Psi]$ of the SM-loaded tag is hence finally calculated from equations (3.6) and (3.9) and (3.10) as

$$\hat{G}_{\tau,s}[\Psi] = G_0 \cdot (1 + \frac{R_{SM}[\Psi]}{R_A})^{-1} \frac{4R_C(R_A + R_{SM}[\Psi])}{|Z_C + Z_A + Z_{SM}[\Psi]|^2} \tag{3.11}$$

$$\hat{G}_{\tau,p}[\Psi] = G_0 \cdot (1 + \frac{g_{SM}[\Psi]}{g_A})^{-1} \frac{4g_C(g_A + g_{SM}[\Psi])}{|Y_C + Y_A + Y_{SM}[\Psi]|^2} \tag{3.12}$$

where the angular dependence has been omitted for notation simplicity. As shown later on, the above model can be also used to estimate the equivalent impedance $Z_{SM}[\Psi] = \frac{1}{Y_{SM}[\Psi]}$ of the sensitive materials at different levels of the agent under test. Once the SM electric properties are characterized through the equivalent admittance, the same equations can be hence used, in conjunction to predict and shape the overall sensor response. Some operative examples will be given in the next Chapters of the thesis.

3.1.2. Backscattering mode

In the backscattering mode, the sensitive material can be instead considered as part of the microchip, so that the equivalent microchip impedance is

$$Z'_C[\Psi] \equiv Z_C \diamond Z_{SM}[\Psi] \tag{3.13}$$

while the antenna impedance Z_A is considered static in this case. In the next reasonings regarding the backscattered mode, only the phase variations according to the lumped load change will be considered.

By introducing the effective chip impedance $Z'_C[\Psi]$ in (2.13), and by assuming a reference impedance modulation between a low and high values $Z_C^{ON} = Z_C$ and $Z_C^{OFF} \to \infty$, the following two expressions of the retrieved phase are obtained in cases of parallel (φ_p) and series (φ_s) topologies:

$$\varphi_p[\Psi] = C + arg\left(\frac{1}{Z_A + Z_{SM}[\Psi]} + \right.$$

$$\left. - \frac{1}{\left(Z_A + \left(\frac{1}{Z_C} + \frac{1}{Z_{SM}[\Psi]} \right)^{-1} \right)} \right) \tag{3.14}$$

$$\varphi_s[\Psi] = C + arg\left(- \frac{1}{Z_A + Z_C + Z_{SM}[\Psi]} \right) \tag{3.15}$$

where the quantity $C = -2k_0 r + 2\Phi(\underline{\hat{r}})$ will now remain constant by keeping the set-up fixed all along the observation of the phe-

nomenon under interest. Finally, denoting with $\varphi[\Psi(0)]$ a reference initial state, then the differential phase

$$\triangle\varphi(t) = \varphi[\Psi(t)] - \varphi[\Psi(0)] \leftrightarrow f(Z_{SM}[\Psi]). \tag{3.16}$$

will depend on the parameter Ψ throughout the only impedance of the sensitive material since the other contributes in C are accordingly dropped out. Above equation is the phase sensing formula and will enable to easily model and control the response of the device.

3.1.3. Asymptotic analysis

In order to better understand the role of the interconnection topology for the sensitive material and the reaction of the phase, of the transmission coefficient and of the gain to the external stimuli, the equations in (3.9),(3.10) (3.14) and (3.15) are now numerically evaluated for two extreme conditions and without any hypothesis on the tag layout. The sensitive material has been assumed to have a dominant resistive or capacitive behavior, e.g. by separately considering the two limits $C_{SM}[\Psi] \to 0$ and $R_{SM}[\Psi] \to \infty$ for resistive and capacitive SM, respectively.

Fig. 3.2 shows the curves of $\varphi[Z_{SM}]$ and $\tau[Z_{SM}]$ for the four above edge cases referred to a realistic microchip impedance $Z_C = 25 - j237\,\Omega$ (NXP G2il [45]). The case of perfect matching of the unloaded antenna impedance ($Z_A = Z_C^*$) to the IC was considered at the fixed frequency $f = 868MHz$ (European RFID band). The phase response saturates for large values of R_{SM} or X_{SM} while the most sensitive responses (steepest slopes of the curves) are apparent for small values of SM resistance or capacitance. The series connection of a resistive SM (Fig. 3.2C) does not provide any phase sensing capability while it produces a huge degradation of the power harvesting (through the parameter τ).

Requirements over the communication performances may be formalized as constraints over the power transfer coefficient τ caused by the variation of the external agent. For instance having fixed the communication constrain to $\tau > \tau_{min} = 0.5$, the useful phase ranges (shadowed areas in the Fig. 3.2) are resumed in Tab. 3.1.

The most convenient results are found for the cases of capacitive SM in both parallel and series interconnections, while a resistive SM is effective for phase sensing only in parallel connection and however it provides a more modest phase change.

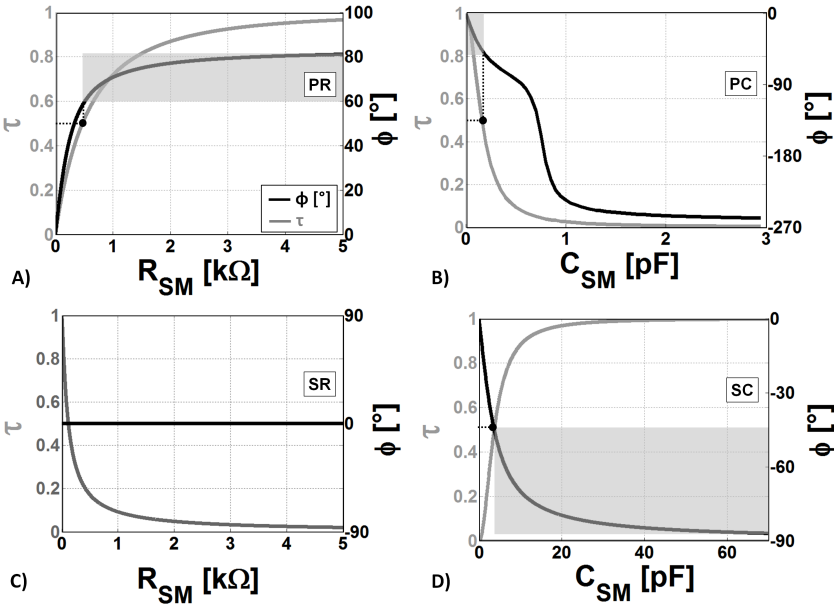

Figure 3.2.: Phase and power transmission coefficient vs C_{SM} and R_{SM} variations: A) parallel-loaded tag with resistive behavior (PR); B) parallel-loaded tag with capacitive behavior (PC); C) series-loaded tag with resistive behavior (SR); D) series-loaded tag with capacitive behavior (SC). The shadowed regions indicate the range of the SM's impedance and of phase response corresponding to a power transfer coefficient $\tau > 0.5$.

It is worth noticing that the SM variation will produce a degradation of the gain as well, quantified by the previously introduced degradation factors $\alpha_s[\Psi]$ and $\alpha_p[\Psi]$ for series and parallel interconnections. From definitions in (3.7) and (3.8), it is clear that the only factor which influences the antenna gain is the resistance or

Table 3.1.: Useful phase range for sensing for $\tau > 0.5$

P-R	P-C	S-R	S-C
20°	50°	0	50°

conductance (R_{SM}, g_{SM}) of the chemical load, while the capacitance variations are completely irrelevant. Fig. 3.3 shows the curves of $\alpha\,[R_{SM}]$ for the two topologies in case of fully resistive behavior. It can be observed that the trends are completely inverted for the two configurations, and could be used as additional sensing parameters even though the decrease of α will negatively impact on the read-range performance of the sensor tag.

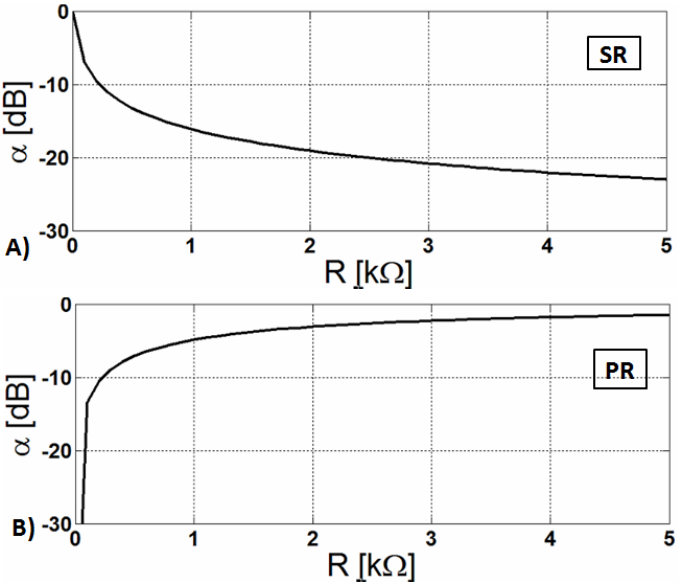

Figure 3.3.: Degradation coefficient α of the gain as defined in (3.7) and (3.8) introduced by the chemical perturbation R_{SM}: A) parallel-loaded tag with resistive behavior (PR); B) series-loaded tag with resistive behavior (SR).

4. RFID Antennas Suitable to Ambient Sensing

This chapter introduces the general purpose antennas capable of hosting a distributed or lumped sensitive material. Several layouts, having different sizes, materials and characteristics, are presented and described in this chapter for what concerns their communication performance.

Several planar layouts with maximum dimensions of a credit card and able to host distributed or lumped sensitive materials, are here described and characterized in their communications performance. The antennas are presented as general purpose *SM-host,* completely unspecific in order to react to the presence of humidity, gases, temperature, etc. However, for the reader convenience, a first high-level classification is given according to the SM they are hosting in this specific research and the parameter they are sensitive to (vapours or temperature).

Convenient tuning mechanisms are implemented in some layouts in order to enable custom shifts and on-site corrections of the tag response at the desired frequency in the global RFID band, without demanding for significant geometrical modifications. This features are potentially useful to modify the dynamic range of the sensor and its sensitivity with a minimal change to the antenna layout. Previous equivalent lumped-element models of the loadings will be exploited in next chapters to predict the sensor's response to the different processes under test.

4.1. Tags suitable to temperature sensing

4.1.1. Planar dipole over sensitive substrate

A threshold sensor is an RFID "thermal switch" or fuse based on a threshold physical phenomenon, such that a material changes its state when the external temperature overcomes a given threshold, and the event is permanently written into a physical memory. A small UHF RFID tag has been designed to work as a threshold temperature sensor. The tag integrates a paraffin wax, which serves as substrate layer and at the same time as distributed SM to sense the heat exposures. A narrow-band passive tag dipole antenna is designed to monitor the dielectric changes of its substrate material. Once the tag is exposed to a certain temperature, known as the threshold temperature value, the dielectric properties of the paraffin layer will change [46]. This affects the permittivity of the paraffin layer and eventually the effective permittivity of the whole substrate. The change in the permittivity alters the input impedance of the tag antenna.

The described small narrow-band symmetric dipole tag antenna (Fig. 4.1) has been simulated by Ansoft HFSS [47]. The tag was designed and fabricated on a multi-layer substrate, constituting FR4 ($\epsilon = 4.1$), thin plastic bag ($\epsilon = 3$) and a layer of commercial paraffin wax [48] ($\epsilon = 2.1$). Alien Higgs 2 IC was used in the tag antenna [49] with sensitivity equal to -14 dBm. The tag is matched to a center frequency of 870MHz using a T-match as an impedance transformer [29]. The overall dimension of the tag is equal to $44mm \times 30mm$.

To reduce the size, the antenna structure is folded with a V-structure making the tag antenna more compact and giving the current a longer path to accommodate the desired wavelength. The small size and the use of thin microstrip lines contribute in making the tag antenna narrow band and more sensitive to any structural or dielectric changes in the substrate.

A prototype of the threshold sensor is shown in Fig. 4.2. Paraplast type of paraffin wax is used to make the substrate layer by melting the waxy pellets of paraffin into a cake frame [48] and then integrating it in a vacuum plastic bag to avoid spillage. The sensor RFID

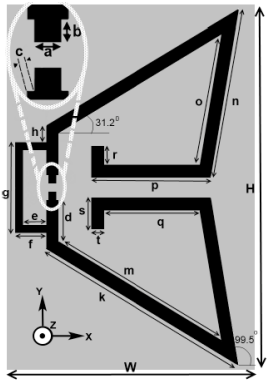

DIMENSIONS OF THE SENSING TAG

Line	Length (mm)	Width (mm)		Line	Lengtha (mm)	Width (mm)
a	1	-		u	3	1.5
b	1	-		n	20.5	1.5
c	0.25	-		o	16	1.5
d	5	1.5		p	14.4	1.5
e	2.75	1		q	11.6	1.5
f	3.75	1		r	2.25	1.5
g	11	1		s	3.75	1.5
h	1.92	1.5		t	1.5	-
k	27	1.5		H	44	-
m	23	1.5		W	30	-

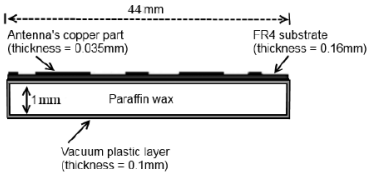

Figure 4.1.: Geometrical parameters of the designed threshold sensor tag antenna.

tag was measured using Tagformance RFID measurement device [50], connected to a linearly polarized reader antenna.

The measured realized gain of the tag antenna is analyzed using the path loss measurement data from the Tagformance measuring equipment, as [51],

$$G_r = \frac{P_{chip}}{L_{fwd} \cdot P_{to}^{in}} \tag{4.1}$$

where P_{chip} refers to the sensitivity of the IC, set to -14 dBm. L_{fwd} is the forward path loss from the transmitter to the tag antenna, and P_{to}^{in} represents the turn-on power. The maximum simulated and measured realized gain at –x axis direction of the tag antenna can be seen in Fig. 4.3, showing a very good agreement.

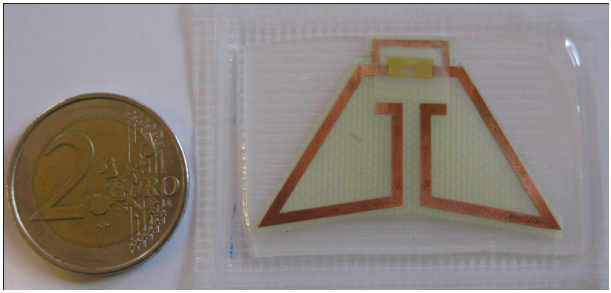

Figure 4.2.: Fabricated prototype of the threshold sensor tag antenna.

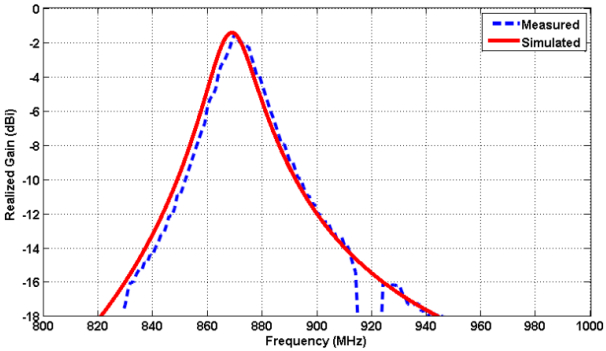

Figure 4.3.: Simulated and measured realized gain at '-x direction' in Fig. 4.1.

4.1.2. Two ports planar dipole

A second class of temperature sensors (<200°C) include an instantaneous RFID sensor with a SM capable to continuously react to the change of temperature. An external thermistor is connected to the tag's antenna that, when exposed to time-variant temperature, will modify the electromagnetic response of the tag detectable by the reader from remote. The sensing information is hence transmitted by an analog manner and the conversion to a meaningful temperature data is achieved at the reader side by using calibration curves.

The considered instantaneous temperature sensor layout is a symmetric folded two-ports dipole (Fig. 4.4 A), with a T-match section exploited to tune the input impedance of the tag to the G2XM microchip in TSS0P8 package (power sensitivity $p_C = -15dBm$) [45]. Two-ports grid formulas, specified in [38, 39], may model the behavior of the tag, where the first port is representing the IC and the second the lumped sensing element.

Fig. 4.4 shows the simulated and measured realized gain vs. frequency of the un-loaded tag. The temperature sensing is analogically performed by a COTS thermistor integrated into the MLA layout, able to change the radiation characteristics of the tag.

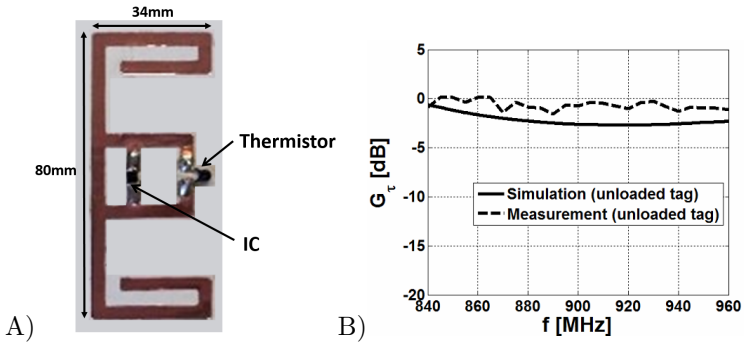

Figure 4.4.: A) Prototype of temperature sensor tag integrating a thermistor able to change its electric properties according to temperature variations; B) Simulated and measured realized gain vs. frequency of the un-loaded tag along broadside direction.

4.2. Tags suitable to chemical sensing

4.2.1. H-slot fed folded-patch

The first device for chemical sensing is a modified version of the wearable antenna presented in [34, 52]: a folded planar structure over a 4mm-thick Teflon substrate provided with a radiating edge and a sensing H-shaped slot (Fig. 4.5). The length L controls the antenna resonances and is about a quarter of wavelength, while the shape factor of the slots can be properly designed to achieve the required input inductive reactance to match the capacitive impedance of the RFID microchip. A ground plane on the back short-circuited to the upper patch favors smaller dimensions and decoupling from the material the tag is attached on. A distributed chemical material for vapors sensing can be deposited just inside the slots since they host high value of electric field [14] and are the most sensitive part of the antenna. In order to reduce the area of chemical deposition and further increase the electric field over the apertures, the H-slots are loaded by two rectangular conductive patches. In this way each half glasses-like profile may be considered as a combination of six slot-lines [52] whose characteristic impedances are

affected by the dielectric properties of the chemical material spread on top (Fig. 4.6). Since the vapor absorption is expected to produce a change of the sensitive material's dielectric properties, a variation of both input impedance and gain of the antenna may be remotely detected by the reader as sensing parameters.

Finally, the field distribution is not uniform inside the glasses-like slots and hence the most sensitive areas, i.e the portions where the field is maximum, are the central gap (hosting the RFID IC) and the upper horizontal and inner vertical slots. The radiation pattern of the antenna (Fig. 4.7) has a maximum directed towards the slot of radiation of the upper edge.

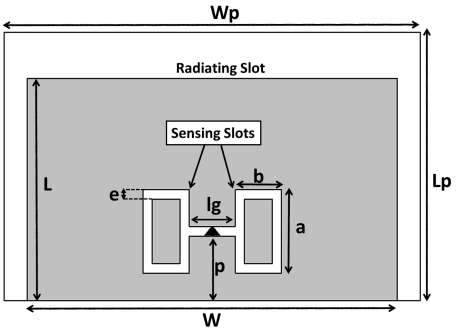

Figure 4.5.: Layout of the H-slot tag sensor.

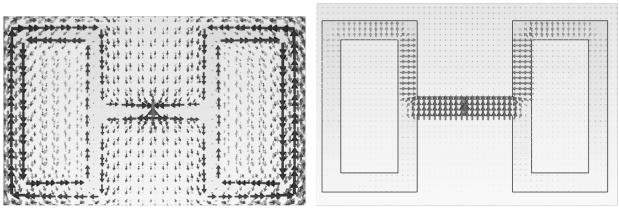

Figure 4.6.: Current (left) and aperture field (right) distribution on the sensitive glasses-like slots computed by FDTD.

A first prototype of the polymer-doped tag (Fig. 4.8) has been de-

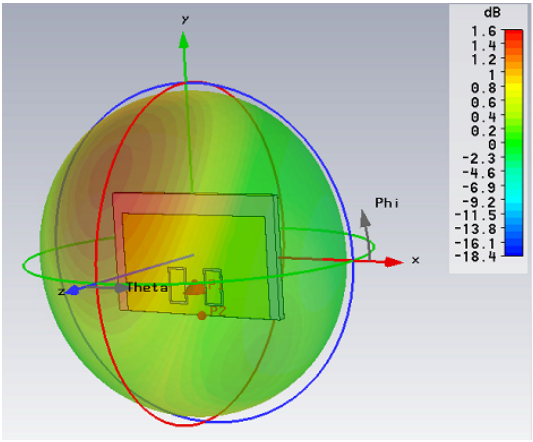

Figure 4.7.: radiation pattern of the H-slot fed folded-patch.

signed and fabricated according to the guidelines described in [52] (size listed in Tab. 4.1). The tag is matched to the G2iL NXP IC with $Z_C = 25 - j237\Omega$ and power sensitivity $P_{chip} = -18dBm$ [45]. The design procedure has been optimized for the unloaded tag, i.e. without chemical material deposition on the glasses-like slots.

The communication performances of the unloaded tag have been characterized for what concerns the realized gain G_τ (2.9) by means of both simulations and measurements [53]. Simulations have been performed by CST Microwave Studio, a Finite-Difference Time-Domain (FDTD) tool [54], while the measurements have been carried out by means of a UHF long-range reader based on the ThingMagic M5-e ASIC [55] whose output power can be controlled by 0.5dBm steps. The reader's antenna was a 5dB linear polarized patch, placed 50cm apart from the radio-sensor. Reflections from ground and side walls were minimized by using absorbing panels. Once known the reader gain G_R, the reader-tag distance d, the polarization factor η_p between the reader and the tag and the measured turn-on power P_{in}^{to}, e.g. the minimum input power required by the reader's unit to activate the remote microchip to send back its code, the realized gain is estimated by eq. (2.9). Results are

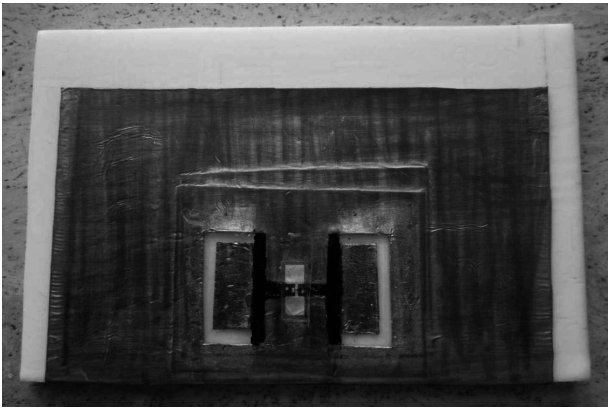

Figure 4.8.: RFID sensor prototype over a Teflon substrate 4mm thick with a partial polymer filling (in black) on the sensing glasses-like slots.

shown in Fig. 4.9. From (2.7) it is possible to determine the maximum read range, $d_{max} = 8m$, by considering 3.2W EIRP, which is the highest emitted power from the reader allowed by European regulations.

Table 4.1.: Size in millimeters of the parameters in Fig. 4.8.

Parameter	Value [mm]
a	18
b	10
e	2
p	14
L	48
Lp	58
lg	10
W	80
Wp	90

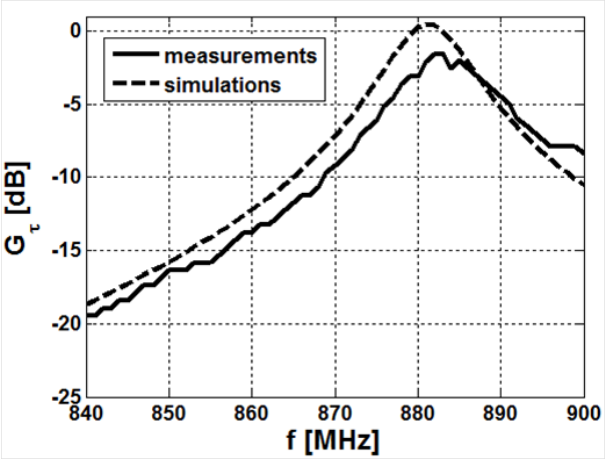

Figure 4.9.: Measured and Simulated realized gain along the antenna axis (broadside observation) for the unloaded sensor tag in Fig. 4.8.

4.2.2. "Square smile" antenna

Smaller layouts are often needed in order to simplify the integration into small objects. Miniaturization generally produces a remarkable degradation of the antenna bandwidth as well as of the radiation efficiency. As a consequence this can negatively affect the interoperability in different Countries and the stability of the performances with respect to the specific placement.

Fig. 4.10a shows the shape of a miniaturized sensing tag antenna which is a variant of the previous layout (Fig. 4.5). The layout

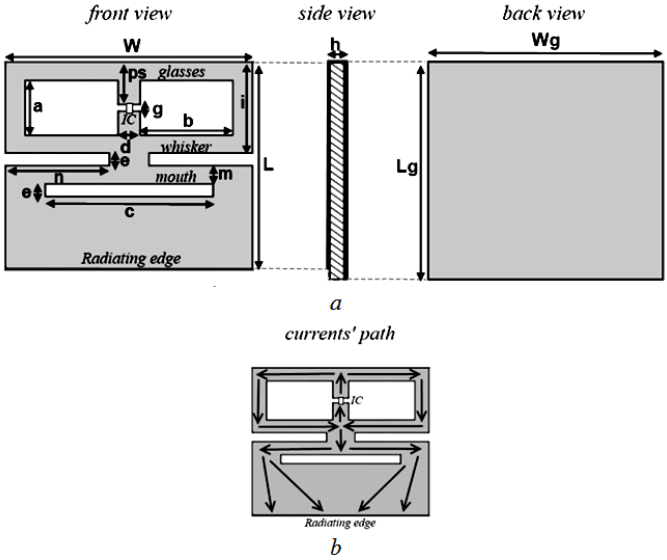

Figure 4.10.: Layout of the miniaturized wearable tag on 3 mm thick EPDM foam (external size: Lg=35mm, Wg=45mm, h=3mm). a) Geometry and parameters b) Schematic path of the electric currents over the top part of the tag.

is similar to a "square smile" and comprises a folded patch (the "head") to achieve a partial decoupling from the object/person it is attached on, connected to the RFID microchip by a H-shaped slot (the "glasses") to balance the microchip impedance. The presence

of the "whisker" slot (size n) and of the "mouth" (size c) permit to extend the current path from the microchip terminals toward the radiating edge (Fig. 4.10b). In this way the electrical length of the antenna increases and hence the antenna's resonance shifts toward a lower frequency, producing miniaturization. As in the previous case of H-slot antenna, thanks to presence of a high electric field, the "glasses" but even the "whisker" and "mouth" may be used as sensing slots to be doped by a distributed chemical material.

In order to provide an example of the tuning capability with respect to parameters {n, c}, the antenna has been simulated by FDTD considering a microchip impedance $Z_C = 13 - j151\Omega$ (Impinj Monza 4 IC, power sensitivity: -18dBm [56]) and a 3mm-thick substrate (*Ethylene-Propylene-Diene Monomer* EPDM foam) of dielectric properties $\varepsilon = 1.21$, $\sigma = 4 \cdot 10^{-4} S/m$. By observing in Fig. 4.11 the power transfer coefficient τ, it is worth noticing that the variation of mouth and whisker produces only a shift of the optimum frequency, preserving the peak value which is instead mainly controlled by the shape factor of the H-slot. In particular, changing the size n of the whisker-like slots, a significant and coarse change of the resonance frequency (12.5MHz/mm) is produced, while adjusting the mouth's length c, a finer tuning of the resonance is possible (2.5 MHz/mm). Simulations demonstrated that the radiation gain of the miniaturized antenna is almost insensitive to the change of the whisker and mouth parameters and is comprised between -7dB and -7.5dB at 868MHz.

The proposed layout therefore offers a two-steps tuning, which makes it easy to re-adapt a same overall shape of the antenna to different frequencies and placement. It is indeed visible (Fig. 4.11b) how the same antenna may be adapted for the European RFID band (866-869MHz) or USA RFID band (902-928 MHz) by just acting on the whiskers length. In practical applications, the length of mouth and whisker can be easily modified by adding or removing narrow strips of adhesive copper, as shown later on. The resulting external size is about half than the H-slot antenna previously presented.

A 4.5cm x 3.5cm prototype of the miniaturized tag (Fig. 4.12) has been first designed for application at the European RFID frequency f=868MHz, and hence fabricated by using aluminum adhesive sheet

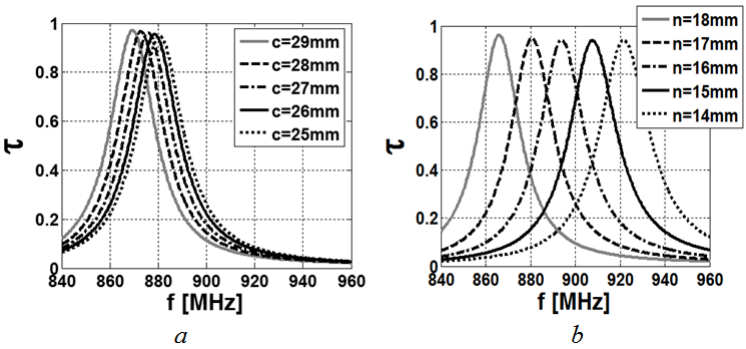

Figure 4.11.: Parametric exploration of the simulated power transmission coefficient for various lengths of a) the mouth parameter "c" and b) the whisker parameter "n" Size fixed in [mm]: L=34; Lg=35; W=43; Wg=45; a=9; b=16; d=10; e=2; g=1; h=3; i=15; ps=7, m=3. The frequency shift produced by 4mm variation of c and n is respectively 10MHz and 50MHz.

carved by a computer-controlled cutter. The size of this kind of antenna is suitable to integration into ID cards.

The communication performances of the tag have been experimentally verified with respect to the realized gain $G_\tau = G_T \cdot \tau$ measured by means of the turn-on method as described above. In Fig. 4.13a and b the measured and simulated data referred to the frontal direction (tag and reader antennas are aligned) are in good agreement, especially at the reference European frequency 868MHz, where the realized gain reaches -7dB. The estimated free-space read range, calculated for a reader emitting a fixed power $P_{EIRP} = 3.2W$, is almost 4m in case of reader with circular polarization ($\chi = 0.5$) and above 5m in case of reader with linear polarization ($\chi = 1$), where χ represents the polarization efficiency.

In order to demonstrate the simple manual tunability of the tag, the previous prototype has been modified with the purpose to move the peak of the power transfer coefficient toward the US RFID frequency f=910MHz. As suggested by Fig. 4.11, the whisker size n has to be shortened by three millimeters (from 18 to 15mm) and

a *b*

Figure 4.12.: RFID miniaturized wearable aluminum prototype, over a 3mm EPDM black foam having dimensions as reported in Fig. 4.11 and mouth and whisker parameters c=29mm, n=18mm. a) Top view of the prototype; b) prototype placed on high lossy laboratory phantom. The arrow indicates the direction of realized gain measurements.

this has been practically achieved by adding two aluminum strips on the whiskers, as shown in Fig. 4.14.

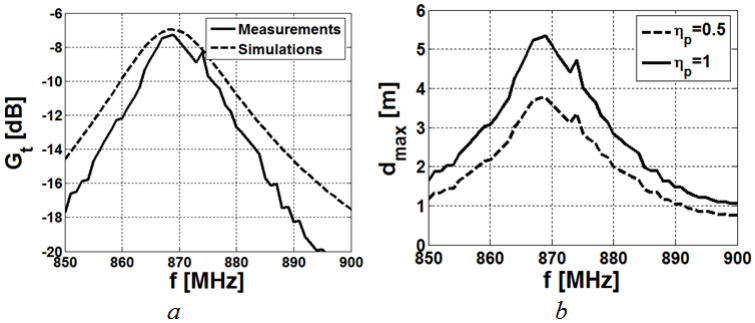

a *b*

Figure 4.13.: a) Measured and simulated realized gain of the miniaturized wearable tag in the frontal (broadside) direction. b) Estimated maximum read range in the free-space in case of reader with circular and linear polarization..

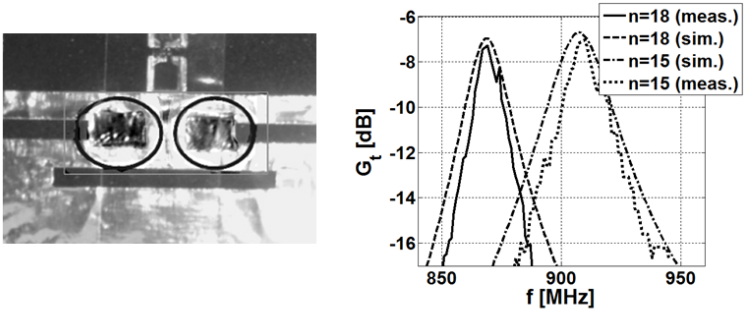

a *b*

Figure 4.14.: a) Square smile" prototype with additional strips of aluminum to shorten "n" from 18mm to 15mm. b) Measured and simulated realized gain for the tag in the frontal (broadside) direction with n equal to 18mm and 15mm.

4.2.3. Doubly-folded patch antenna

As introduced in chapter 3 a possible approach to RFID *sensing engineering* is to describe the complex interactions between sensitive material, antenna and volatile compounds as simple lumped-element circuits, that is possible when the loading sensitive material is in a very localized displacement. A general purpose chemical drop-loaded tag is here introduced, which, as will be shown in next Chapters, can be used as highly sensitive chemical radio-sensors and, at the same time, to easily estimate the electromagnetic UHF parameters of the specific SM during gas exposure.

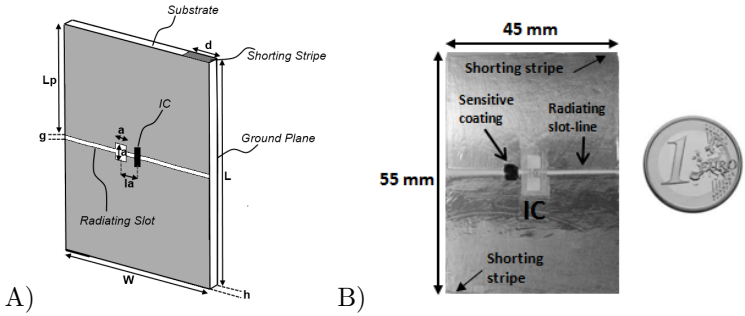

Figure 4.15.: A) Layout and B) fabricated prototype of the miniaturized sensor tag. The Sensitive Material (SM) will be deposited inside a $a \times a$ niche along the radiating slot.

The considered tag employs a slot-line layout and a tuning mechanism able to shift the antenna response at each frequency of the global UHF RFID band (865-928MHz). This feature can hence potentially useful to modify the dynamic range of the sensor and its sensitivity. The SM is assumed to be placed into a small $(\frac{\lambda}{100} \times \frac{\lambda}{100})$ niche and modeled with a lumped element model as introduced in sec. 3.1 to mathematically separate the effect of the SM from the response of the un-loaded (blank) tag. The gas sensing application and SM characterization will be illustrated experimentally in next Chapters.

The antenna layout is composed of two co-planar patches of size $\{W, L_p\} < \lambda/4$ forming an open-circuit non-resonant slot-line, as

shown in Fig. 4.15. The RFID microchip is placed in the middle of the radiating slot. The opposite corners of the two patches are connected to the ground plane by means of two thin vertical stripes so that the current path is lengthened along the overall diagonal (Fig. 4.16A) with great benefit to antenna miniaturization. The resonance frequency is hence mostly determined by the length $\sqrt{(2L_p)^2 + W^2}$ of the diagonal, the maximum gain is related to the width W of the layout. A fine tuning of the operating frequency is possible by acting on the size d of the shorting vertical stripes, in order to produce a frequency shift of the tag's resistance and reactance.

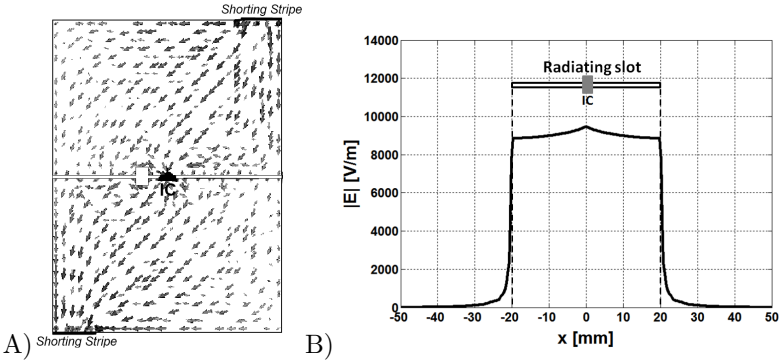

Figure 4.16.: A) Typical paths of electric current lines over the top surface of the tag (size as in Tab.I) which are lengthened by the two opposite adjustable shorting stripes. B) Absolute value of the electrical aperture field along the slot line (x direction) in absence of the niche.

Since $W < \lambda/4$, the open-circuit slot hosts a strong and slowly variable aperture-field, as shown in Fig. 4.16B and hence it is the most sensitive part of the antenna, suitable to contain the sensor which will be deposited into a niche close to the microchip. The radiation pattern (Fig. 4.18) is fully broadside in this case, making the communication reader-tag more reliable with respect to previous antenna layouts, where the maximum gain was not in the broadside direction.

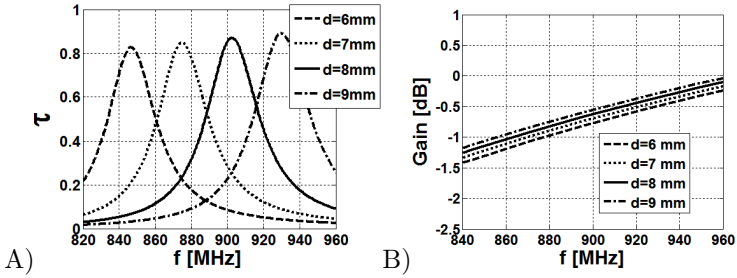

Figure 4.17.: Parametric analysis of the power transmission coefficient (A) and gain (B) of the unloaded tag, obtained by FDTD simulations, for some widths d of the shorting stripes (Fig. 4.15), having fixed the other sizes of the tag as in table Tab. 4.2.

All the electromagnetic simulations have been performed by FDTD methods. Fig. 4.17A shows a parametric simulation of the power transfer coefficient τ of the tag, considering a microchip transponder *NXP G2il* IC [45]. The antenna is assumed to include a 3mm-thick Forex slab as substrate with parameters $\epsilon = 1.55$, $\sigma = 6 \cdot 10^{-4} S/m$. The external size is $40mm \times 55mm$, e.g. half the surface of a credit card, corresponding to $0.12 \cdot \lambda \times 0.15 \cdot \lambda$ at 868MHz; detailed dimensions are listed in Tab. 4.2. Variations of the width d of the shorting stripes produce a significant monotonic and linear frequency shift of the power transfer coefficient as large as 30 MHz/mm, with a slight but negligible change in the peak value. The gain of the tag (Fig. 4.17B) is instead much less sensitive to the change of d, so that the profile of the realized gain of the tag, with respect to the control parameter, is mostly related to the frequency shift of the power transfer coefficient.

The peak of the power transfer coefficient is quite stable ($0.8 < \tau < 0.9$) for $6mm \leq d \leq 9mm$ and hence the antenna may be tuned to European RFID band (866-869MHz) or USA band (902-928 MHz) by just small geometrical changes. In practical applications, the size of the stripes can be easily modified by adding or removing narrow pieces of adhesive copper. A prototype of the miniaturized sensor tag (Fig. 4.15B) has been fabricated with the same sizes as in Tab. 4.1 by properly carving and wrapping an adhesive copper sheet

Table 4.2.: Size in millimeters of the parameters in Fig. 4.15.

Parameter	Value [mm]
L	55
Lp	27
W	40
g	1
a	3
d	7.5
g	1
h	3
la	4.5

on the Forex substrate. As in previous cases, the communication performance of the unloaded tag has been characterized in terms of realized gain. The corresponding results are shown in Fig. 4.19 in comparison with FDTD simulations. By considering 3.2W EIRP, the maximum emitted power from the reader allowed by European regulations and a circular polarized reader's antenna ($\chi = 0.5$), the estimated free-space maximum read range (from (2.7)) is about $7m$.

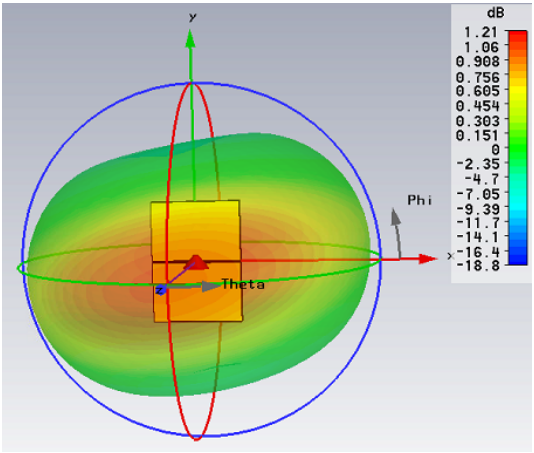

Figure 4.18.: radiation pattern of the H-slot fed folded-patch.

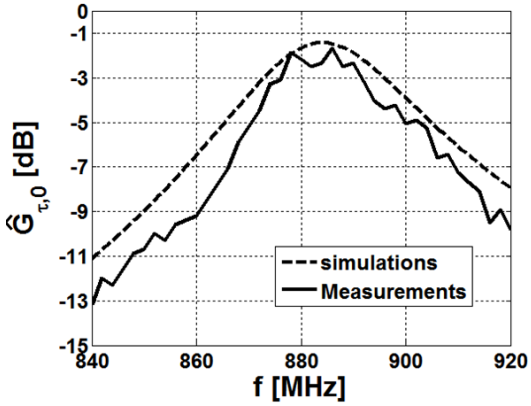

Figure 4.19.: Measured and simulated realized gain along the antenna's broadside direction for the unloaded ("blank") sensor tag of Fig. 4.15.

Part II.

Temperature Sensing

There are several environmental factors, affecting the quality and state, of people, objects and environments. Among them, temperature is considered as one of the most important environmental parameters that can influence the performance or quality of several items and products, as well as, in the medical context, it reveals physiological and pathological situations for humans and environments. [57, 58]. The most common devices for temperature monitoring are battery- and memory- operated sensors. These types of sensors usually need external power supplies and hence can't be used to tag every product or object. In several daily, industrial, environmental and healthcare-oriented applications there is a recognized need to move from a wired or powered thermal diagnostic architecture to a wireless one, involving lightweight autonomous or semi-autonomous sensors. The aim is to reduce the overall mass of testing equipments, to gain freedom in sensors placement, to enable last-minute implementations, to simplify the hardware interface, to definitely speed-up the integration schedule and reduce the cost of the sensors. Since passive sensors are targeted for their relatively low cost and easier implementation RFID sensors [59] have received the most attention. Some RFID microchips equipped with an integrated temperature sensor and with a local Analog to Digital Converter, are nowadays available to monitor temperature [25, 26] as will be better detailed in the Appendix. However they require more power to turn the IC on, due to their additional complex circuitry, affecting the overall read range in the passive mode. Moreover, these RFID sensors are still limited in their range of temperature ($-40°C \div 64°C$) and are able to work only when supplied with a continuous RF power or an external battery, to log the temperature into the memory.

In this part, two different kind of analogical temperature sensor will be introduced. The first one is a threshold sensor, exploiting a distributed load, i.e. a paraffin substrate, able to change its properties over a certain temperature in a non-reversible way. The second one is an instantaneous sensor based on a lumped thermistor-loaded dipole. A first experimental analysis in comparison with models presented in sec. 3.1 will be reported in this part.

5. Threshold Temperature RFID Sensor with Distributed Load

The chapter describes a RFID passive sensor integrating paraffin wax as a distributed load and substrate material in order to obtain a threshold heat sensor device. Paraffin wax acts as a distributed material sensitive to temperature variations, a *thermal fuse* irreversibly changing the narrow band tag's properties. The sensor tag is able to detect, store and transmit data on the thermal history of environments and objects.

An RFID "thermal switch" or *fuse* is based on a threshold physical phenomenon, such that a material changes its state when the external temperature overcomes a given threshold, and the event is permanently written into a physical memory. For instance the thermal-controlled event could be the melting of a ice region (low-temperature threshold) loading the tag's antenna [20], or the geometric changes of Shape Memory Alloys such as the Nitinol [22]. In these cases the temperature change induces an abrupt variation of the antenna response so that the microchip is activated or not depending on the temperature violation of a predefined level. These devices could have application to the assessment of food and drugs integrity as well as to the detection of fire and over-heating of domestic devices.

This chapter describes a new low cost and small analogue type of passive UHF RFID threshold heat sensor. The device integrates a paraffin wax, which serves as substrate layer of the antenna and at the same time as distributed SM to sense the heat exposures. In order to maximize the effects of this change, a sensitive nar-

row band passive RFID tag based on a miniaturized folded dipole antenna was designed and presented in sec. 4.1.1. Once the tag is exposed to a certain temperature, known as the threshold temperature value, the paraffin layer changes its physical and chemical properties. These changes eventually affect the dielectric properties of the substrate, with a distributed effect on the antenna's properties as previously introduced in the part I of the Thesis. An irreversible shift in the tag's operating frequency is remotely detected by the reader after heating. The change on the tags performance, incurred due to the changes in the permittivity of the substrate, can be analyzed at any instance and does not require a continuous RF power or any other external power source. Due to intrinsic fragility of paraffin, in practical applications the sensing tag should be carefully packaged with the product, to avoid any accidental damage. However, in many applications the use of external force can also damage the product inside the package. This will make the tag unreadable, indicating that the quality of the product has been lowered or been damaged.

5.1. The sensitive material: Paraffin wax

Paraffins are straight-chains or branched saturated organic compounds [60]. They are a form of hydrocarbons. Composition of organic compounds in a paraffinic hydrocarbon is C_nH_{2n+2}. The state of paraffin can be determined with its average molecular weight. Solid form of paraffin at room temperature, also referred as paraffin wax, is considered to have a molecular weight from $C_{20}H_{42}$ to $C_{40}H_{82}$. Paraffin wax is mainly a mixture of paraffins and cycloalkanes [60]. It is mostly found as white odorless, tasteless, waxy solid, at the room temperature. In the electrical industry paraffin waxes have been used mainly for insulation. Among their characteristics are low dielectric loss, high resistivity values, flexibility, ductility, and low thermal expansion coefficient. The paraffin waxes can be classified based on their molecular weight, melting point and the mixture of other additives such as the percent of oil content. The melting point of paraffin wax varies approximately in the range from 40°C to 80°C [46, 60]. Paraffin wax can acquire three different

forms of crystal shapes, plate crystal, mal crystals, and needle crystals. Temperature plays a major role in changing the characteristics of paraffin wax such as density, dielectric constant, crystal shape, and molecular structure. The increase in temperature expands the volume of paraffin wax and decreases its density, depending on its melting point with respect to the room temperature. The decrease in density means fewer numbers of molecules per unit volume, causing less interaction with the electric fields and therefore, resulting in a decrease in the dielectric constant value. According to [60], some of the physical characteristics of paraffin wax are summarized in Tab. 5.1.

Characteristic	Value
Density at 100^0c	0.75-0.79 g/cm^3
Density (solid wax)	0.9 g/cm^3
Average molecular weight	376-587 g/mol
Viscosity at 98.9°c	3.19 – 12.59 mm^2/s
Expansion coefficient in solid	0.0009-0.0016 cm^3/g
Expansion at melting	0.122-0.137 cm^3/g
Typical Melting point	+40 – +81 ^{0}C
Typical Boiling points	+215 – +300+ ^{0}C
Solubility in water	Insoluble
Electrical resistivity	10^{16} – 10^{18} Ω/cm^3

Table 5.1.: Physical characteristics of paraffin [60]

According to the literature, the dielectric constant value of paraffin wax can be between 2 to 2.6 at room temperature, depending on the type of paraffin wax and its molecular weight.

5.2. The planar dipole over sensitive substrate

The threshold sensor device (Fig. 5.1 left), described in detail in sec. 4.1.1, is a miniaturized folded dipole antenna (overall dimensions equal to $44mm \times 30mm \times 1mm$) integrating a Paraplast type of paraffin wax [48] as substrate and thermal fuse.

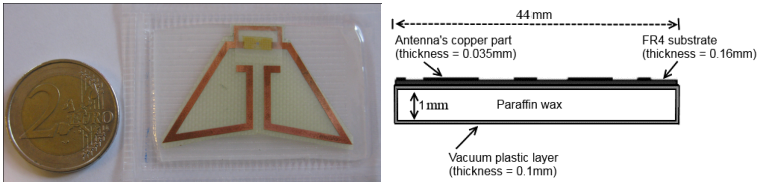

Figure 5.1.: Fabricated prototype of the threshold sensor tag antenna (left) and schematic representation of its side view (right).

Paraplast type of paraffin wax is used to make the substrate layer by melting the waxy pellets of paraffin into a cake frame. According to the specification provided by the supplier, the solid Paraplast paraffin wax is 99% pure with 1% of additives. The properties of paraffin start changing at 36 - 40°C and the melting was observed to start around 50°C – 56°C. The relative dielectric constant value of Paraplast paraffin wax in this experiment was 2.1 ± 0.1 at room temperature, as measured by the Agilent dielectric probe [61]. The paraffin wax substrate was placed in a vacuumed plastic bag to avoid spilling during heat measurements using a multilayer substrate approach, as shown in (Fig. 5.1 right). Once exposed to heat, the paraffin wax somehow retains the changes in its physical characteristics even if it is brought back to its previous temperature, unless it is reprocessed and formed. The change in the characteristics of paraffin wax layer affects the whole substrate of the sensor tag, resulting in a change in the total effective reflection coefficient of the multilayer substrate[60].

5.2.1. Numerical analysis

The transfer of power between the complex source impedance (tag antenna) and the complex load impedance (IC) is analyzed in simulation using the equation of the power reflection coefficient [62]

$$|\Gamma|^2 = \left| \frac{Z_C - Z_A^*}{Z_C + Z_A} \right| \tag{5.1}$$

To have an optimal power transfer and maximum read range, it is desirable to have a lower value of the power reflection coefficient at the operating frequency band. Fig. 5.2, shows the simulated power reflection coefficient of the tag antenna, designed to operate at a center frequency of 870MHz. As illustrated in the figure the tag has a narrow bandwidth ($\approx 10MHz$), which gives an advantage of sensing even a small change in the dielectric substrate.

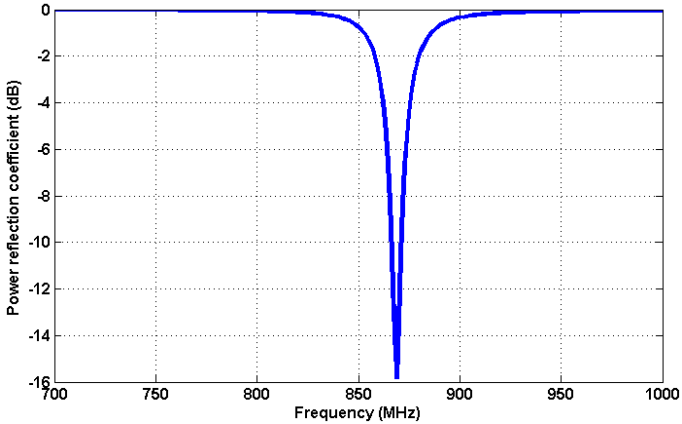

Figure 5.2.: Simulated power reflection coefficient of the RFID tag antenna.

The shift in the resonance frequency of the tag antenna, due to possible change in the dielectric constant values of the paraffin wax layer [46] during heating, can be seen in Fig. 5.3. The paraffin wax used in the proposed antenna substrate is considered having a dielectric constant change from around 2.2 to 1.8. The narrow band tag antenna helps to maximize the effects of change in the resonance frequency.

This type of sensor tag detects the exposure of various goods and products to high temperatures by a detuning effect due to change of the paraffin layer. The detuning affects the realized gain of the antenna and accordingly the the required turn-on power to activate the tag and the read range at the operating frequency as shown later on.

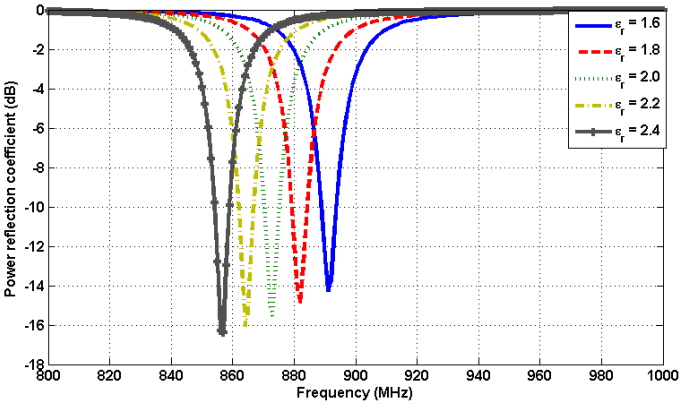

Figure 5.3.: Simulated power reflection coefficients of the sensing tag due to various dielectric constant values of the paraffin wax layer.

5.2.2. Prototype and experimentation

The heat sensor tag was measured in an EMC chamber with a custom made measurement setup environment (Fig. 5.4). The measurement setup comprises a linearly polarized reader antenna connected to the Tagformance measurement device [50] (with a minimum power step resolution of 0.1dBm), absorbing panels, hot air blower, and an RFID threshold sensor tag to be measured.

The RFID sensor tag is placed horizontally, facing upwards on top of the Styrofoam boxes. The tag is placed 1m far apart from a linearly polarized reader antenna, connected to the Tagformance. The RFID tag was heated by a hot air blower, up to the melting the paraffin wax layer. Due to the placement of the tag and the use of a vacuum bag surrounding the paraffin wax substrate layer, the shape of the paraffin substrate layer was kept almost the same. The turn-on power measured before and after the heating of the RFID sensor tag antenna is shown in Fig. 5.5.

It is clearly visible that the heating of the tag produces a frequency shift on the minimum turn-on power shift of about 15-20MHz. According to the results, after heating the tag antenna, around 6 dBm

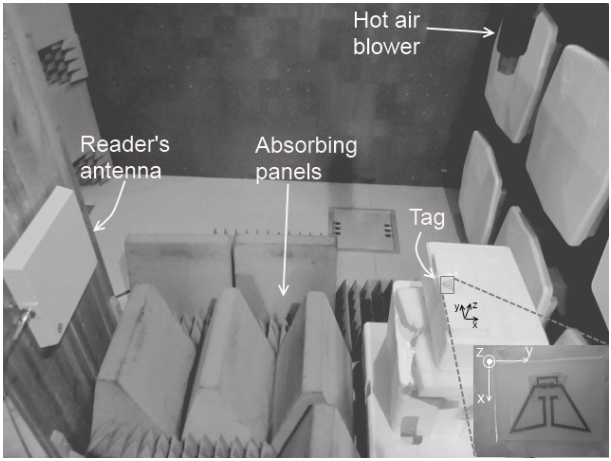

Figure 5.4.: Measurement setup of the heat threshold sensor tag.

more are required to power up the IC on the desired frequency of 870MHz with respect to the initial condition. Due to the use of a narrow band RFID tag antenna design, the read range at 870 MHz has been reduced to more than half (from 7m to 2.5m).

Fig. 5.6 shows the measured threshold torn-on power at 870 MHz with respect to the temperature change, during the heating and cooling processes of the tag. Measurements were carried out in the measurement environment as in Fig. 5.4.

The turn-on power increases with the rising of temperature, until the paraffin wax is fully melted. After melting, the tag is left to cool down slowly at room temperature. Slight increase in the required transmitted power can be seen during the cooling and re-solidification process of the paraffin wax layer. It is worth noticing that once the tag is detuned, due to the melting of paraffin wax layer, it cannot return to its original state, even if brought back to ambient temperature and solid form.

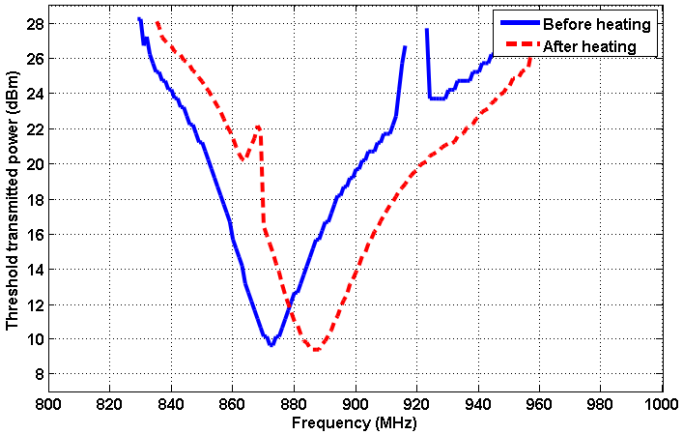

Figure 5.5.: Measured turn-on power at '-x direction'.

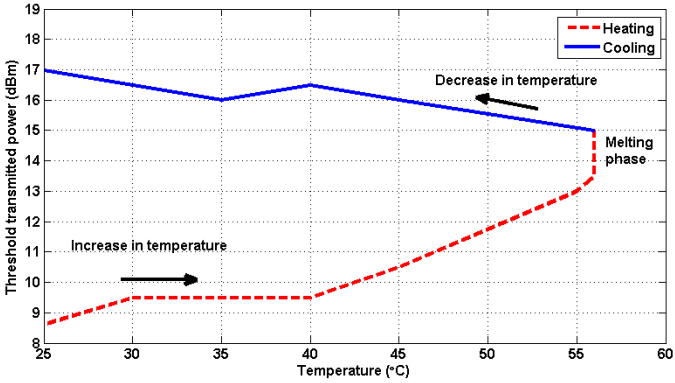

Figure 5.6.: Measured turn-on power with respect to temperature at 870MHz, while heating and cooling of the tag, at '-x direction'.

5.3. Experimentation on consumer products

To demonstrate the use of this type of heat sensing tag, some measurements were made on typical consumer products and boxes. Tagformance RFID measurement device was used to measure the tag antenna in the anechoic chamber by Voyantic Ltd. (Fig. 5.7). The chamber contains a rotating table on which the tag is placed, 50cm distant from a linearly polarized reader antenna connected to the Tagformance measurement device, and absorbing panels on each side.

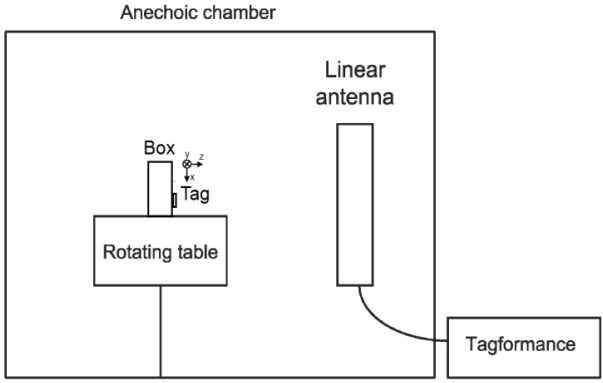

Figure 5.7.: Voyantic Ltd. Anechoic chamber set-up.

The tag antenna was attached to the exterior of the packages as shown in Fig. 5.8. The performance of the RFID heat sensor tag were analyzed on two different types of packages. First the RFID heat sensing tag is attached and measured on an empty white paper box, and then a similar RFID tag is attached on top of a box containing metallic cans of food items. As previously, the tag is measured before and after heating. The temperature of the hot air was around 50 – 60 °C.

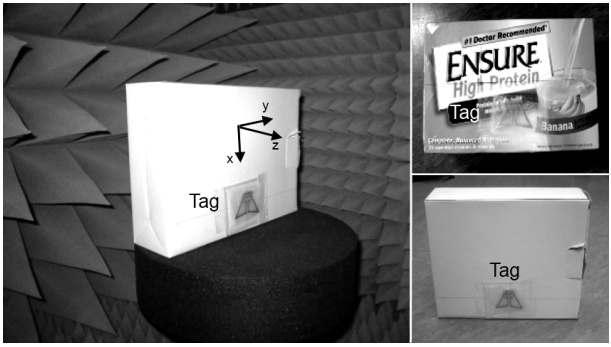

Figure 5.8.: Heat sensing tag on consumer products.

5.3.1. Measurement results

The change in the turn-on power of the sensor tag due to heat on top of an empty paper box is shown in Fig. 5.9.

The frequency shift is equal to 25 MHz producing an increase of the turn-on power at 865MHz, from 7 dBm to 16 dBm. The maximum read range is accordingly reduced from almost 6 meters to less than 2.8 meters.

The turn-on power of the tag placed on top of a box of metallic cans is instead shown in Fig. 5.10. The higher values of power required to activate the tag with respect to the previous measurement is due to the metallic background of the tag, which negatively affects the communication performance of the dipole.

In this case the tag has a frequency shift of almost 30 MHz. Accordingly, the tag attached to the package of metallic cans cannot be read by the measurement equipment on the desired frequency of 865 MHz after heating. It can be observed that these types of sensor tags are more affected due to heat when placed on top of a package containing metallic cans, increasing the “on-off” effect of the threshold sensor.

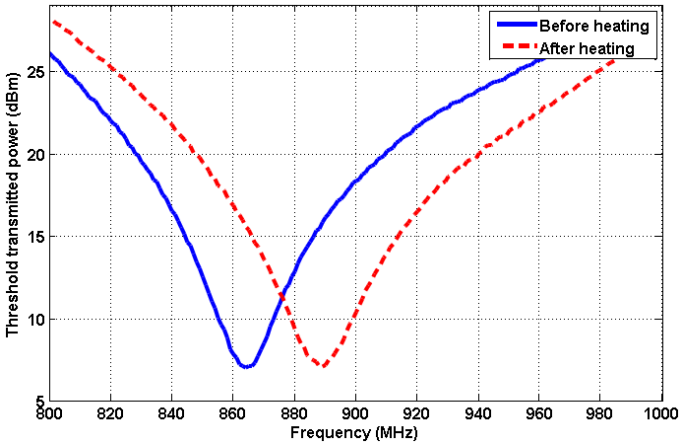

Figure 5.9.: Measured turn-on power variation on an empty paper box at +z axis.

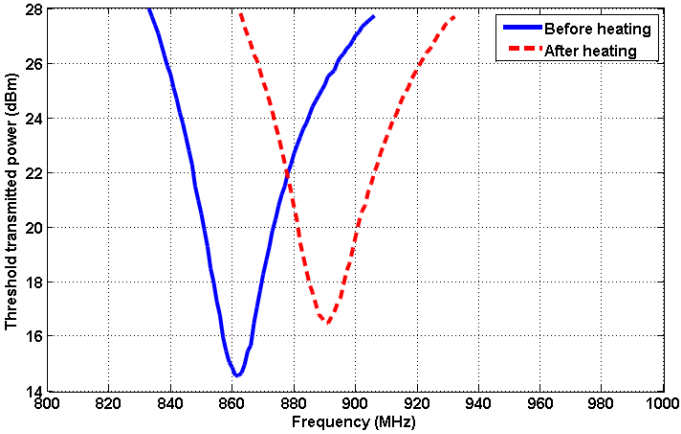

Figure 5.10.: Measured turn-on power variation of sensor tag attached to on a box of metallic cans at +z axis.

5.3.2. Conclusions

A threshold temperature sensor tag has been described using a multi-layer substrate. Paraffin wax acts as the distributed heat sensitive layer of the substrate, which changes its dielectric properties when exposed to temperatures close to its melting point. The exposure to heat causes the melting of paraffin and a frequency shift of the turn-on power of the tag. These changes are irreversible even if the tag is brought back to the same temperature. This type of heat sensing tag can be useful in many applications including supply chain operations and transportations of various heat sensitive drugs and food items. As the proposed sensor tag is low cost, it can be placed on large variety of common packages to qualify and display the quality status of the products.

6. Instantaneous Temperature RFID Sensor with Lumped Load

The chapter describes a RFID passive sensor including an external thermistor that modifies the electromagnetic response of the tag's antenna according to temperature variations. The thermistor acts as a lumped sensitive material reversibly and continuously changing the tag's properties.

Differently from the threshold sensor described in chapter 5, an instantaneous sensor is able to continuously react to the change of temperature. A first example of RFID passive instantaneous temperature sensor was given in [23], where a (distilled) water region incased close to the tag is used as distributed sensitive load.

This chapter shows a first attempt to evaluate the performance of a newly developed continuous passive RFID sensor tag for medium-high temperature monitoring (<200°C) [63]. The sensor includes a standard low-cost RFID microchip, conventionally used in logistics, plus an external thermistor connected to the tag's antenna. When the tag is exposed to time-variant temperature, the electromagnetic response will change accordingly being detectable by the reader from remote. The sensing information is hence transmitted by an analog manner and the conversion to a meaningful temperature data is achieved at the reader side by using calibration curves.

6.1. Numerical analysis

The dynamic ranges and the sensitivities of a generic RFID tag hosting a lumped thermistors in parallel to the IC are here evaluated without any hypothesis on the tag layout. The lumped sensitive material, i.e. the thermistor is assumed to have a completely resistive behavior. Three COTS NTC thermistor, whose resistance variations with temperature can be found in [64], have been considered for this analysis: $1k\Omega$, $5.6k\Omega$ and $18k\Omega$ measured in DC at ambient temperature (i.e. 25°C). The realized gain, the power transmission coefficient, the Analog Identifier, and the phase are numerically calculated from equations 3.10, 3.12, 3.14 and 2.11 in a range of temperature within 0°C and 150°C. Fig. 6.1 shows the curves of $G_\tau[R_{SM}]$, $\tau[R_{SM}]$ $AID[R_{SM}]$ and $\varphi[R_{SM}]$ for the three thermistors individually loading a generic antenna with a realistic microchip impedance $Z_C = 16 - j148\,\Omega$ (NXP G2xl [45]). The case of perfect matching of the unloaded antenna impedance ($Z_A = Z_C^*$) to the IC was considered at the fixed frequency $f = 868MHz$ (European RFID band). It is worth mentioning that the profile of the sensitivity curve, and thus of the temperature resolution, may be shaped as needed by using a proper thermistor resistance: in particular a better sensitivity to lower temperature can be achieved by smaller-resistance thermistors, while for higher temperatures a higher resistance is recommended, in order to avoid an excessive degradation of the communication performance of the tag.

This preliminar analysis is useful to understand the achievable dynamic ranges and sensitivities of a thermistor-loaded temperature sensor tag. However, in reality, the impedance values of COTS thermistor are not available at radio-frequency, since they are characterized only at DC. As shown below, the measured impedance of a COTS thermistor at RF is greatly different with the one measured at DC, and a parasitic capacitance needs to be considered in parallel to the thermistor resistance.

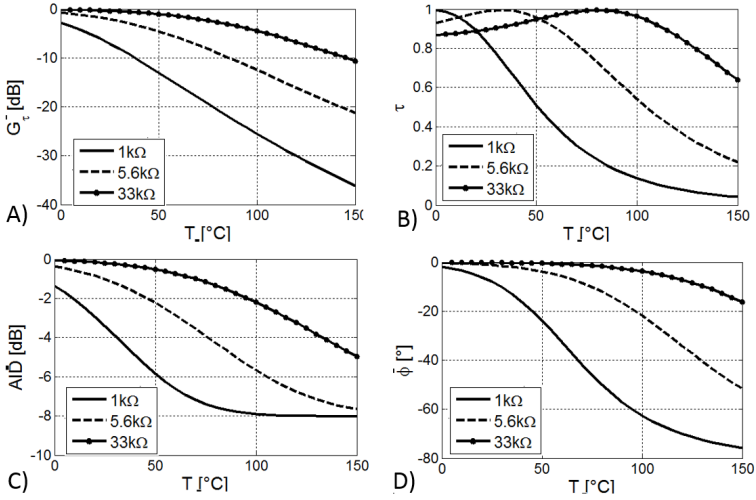

Figure 6.1.: Realized gain (A), power transmission coefficient (B), Analog Identifier (C), and phase (D) variations vs. temperature of a generic tag antenna loaded by three lumped thermistors.

6.2. The thermistor-loaded sensor

The considered temperature sensor tag is a symmetric meander-line antenna presented in sec. 4.1.2. The temperature sensing is analogically performed by a COTS thermistor integrated into the MLA layout. The thermistor's declared resistance is $47K\Omega$ at 25°C at DC and may change up to two order of magnitudes according to temperature variations. However its radio-frequency impedance and dynamic response were completely unknown so that the lumped element was preliminary evaluated by connecting the thermistor to a SMA connector and using a VNA for impedance measurement after calibration (set-up shown in Fig. 6.2). The equivalent RF impedance of the thermistor at 870MHz was hence estimated as a parallel connection between a resistance and a parasitic capacitance $Z_{th}[T] \equiv R_{th}[T] \parallel C_{th}[T]$, both dependent on the temperature T. The equivalent resistance decreases from $2.2k\Omega$ down to 200Ω as

the temperature increases from 25°C to 160°C, while the parasitic capacitance increases from 0.3 pF to 0.7 pF in the same condition.

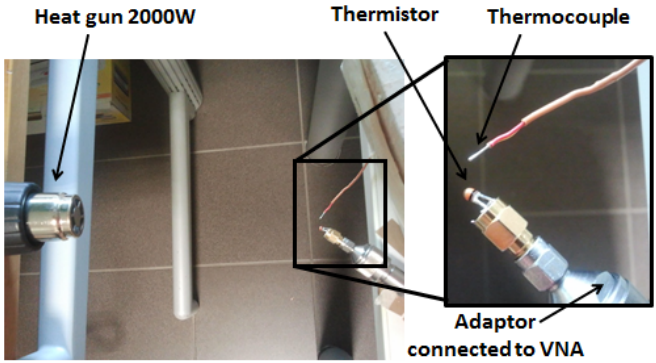

Figure 6.2.: Set-up for the thermistor characterization at the frequency of 870MHz

shows the simulated (by FEKO [65]) realized gain vs. frequency for two different temperatures. On moving from the ambient temperature to 160°C, a 5.5dB dynamic range of the antenna response is predicted: it will be converted into temperature resolution as explained in the experimental section.

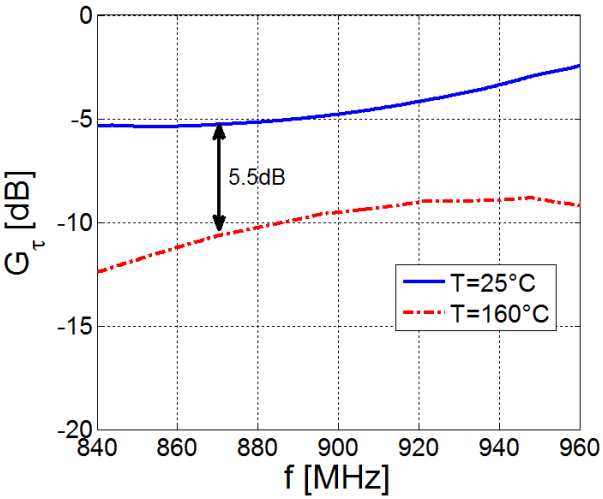

Figure 6.3.: Simulated realized gain of the MLA in Fig. 4.4 along broadside direction for different conditions.

6.3. Laboratory experimentation

The temperature sensing capabilities of the tag have been checked during heating in a controlled environment.

Measurements were carried out by means of the ThingMagic M5 reader [55], placed 50cm apart from the tag and emitting fixed power (3.2W EIRP). The sensing performances of the RFID tag have been analyzed dynamically when the temperature rapidly changes from ambient conditions up to saturation (from 30°C to 105°C), using a 2000W heat gun to increase the temperature (Fig. 6.4). As shown in Fig. 6.5, the backscattered power $P_{BS}[T]$ of the tag is able to follow the the change of temperature with a 5 dB dynamic range. The RFID sensor revealed a slower response with respect to the thermocouple, due to the thermal inertia of the selected thermistor and the tag support. After cooling the sensor fully recovered up to the initial level of backscattered power.

In order to test the reproducibility capabilities of the sensor, dur-

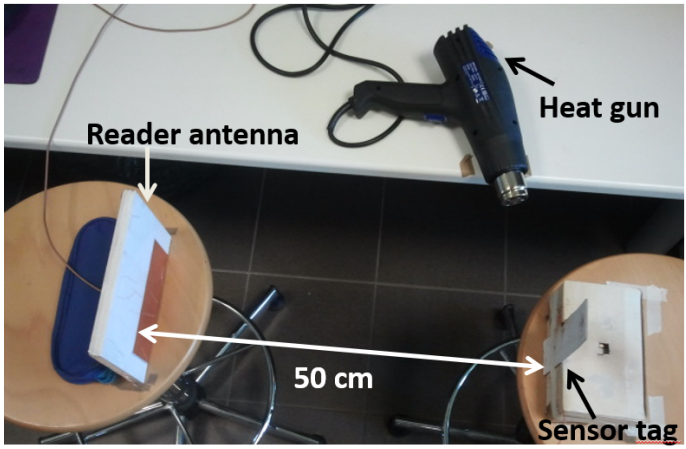

Figure 6.4.: Set-up for the RFID temperature sensor measurements.

ing a second experiment the tag has been exposed to cyclic heating and recovery from 30°C to 200°C. The IC was covered by protective layers in order to avoid damages of its functionalities at high temperatures.

The change of the response curves (Fig. 6.6) follows the exponential temperature variations profiles with dynamic ranges of about 8dBs. The sensor exhibits high reproducibility during different cycles and full capability of recovery right after the end of heating, with less than 0.5dB hysteresis.

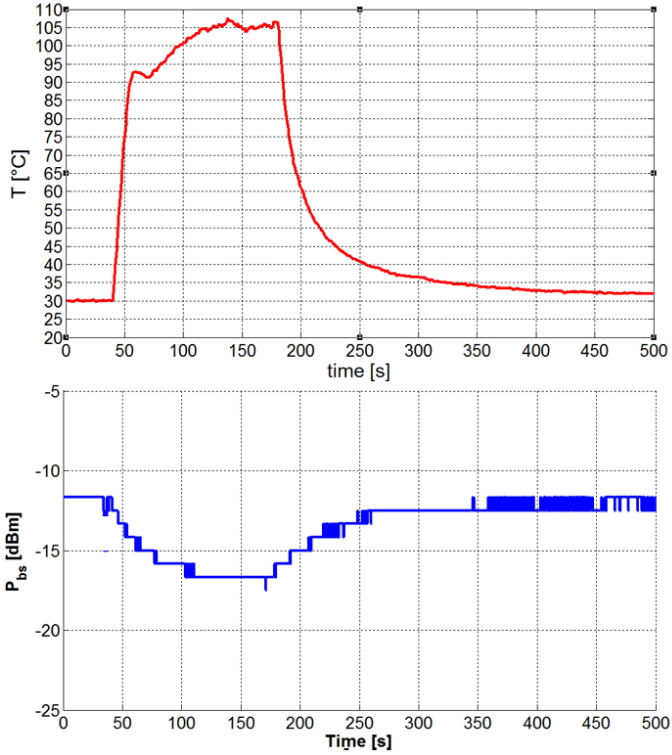

Figure 6.5.: Top) Thermocouple-measured variation of temperature from ambient conditions up to 105°C. Down) Backscattered power response of the sensor tag at 868 MHz.

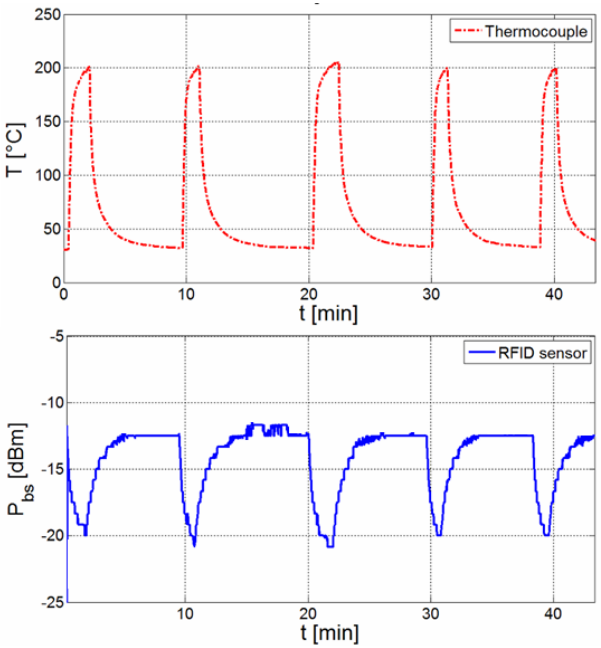

Figure 6.6.: Top) Thermocouple-measured variation of temperature during five cycles of heating by a 2000W heath gun and ambient cooling. Down) Backscattered power response of the sensor tag at 868 MHz.

6.4. Conclusions

Although real-scenario measurement and calibration curves should be required to better assess the estimated results, the presented thermistor loaded sensor shows that wireless sensing of temperature up to 200°C by battery-less RFID devices in the UHF band can be feasible. The possible resolution of the continuous sensor tag could approach 1°C by a proper design of the sensor and selection of an appropriate thermistor. Of course, further investigation and experiments need to be put into practice in order to select the most suitable thermistor for real applications and to optimize the sensor reponse. Sensing parameters such as AID or phase are recommended for future experimentations in order to mantain a reasonable communication performance in terms of realized gain. Moreover, a continuous improvement of the sensitivity of the chips is expected in the next years (about 3dB every 2 years according to a rather established trend), allowing in principle a wider power margin useful to improve the temperature resolution of the tag and even more reliable read ranges.

Part III.

Volatile Compounds Sensing

Fast and reliable detection of volatile compounds in the air is a key issue in many daily and industrial applications. People wellness in living and medical environments may benefit of a continuous and reliable monitoring of critical parameters such as the presence/level of several gases. Conventional monitoring methods involve wired sensors or even wireless devices generally provided with a local power source that fixes the sensors lifetime before battery replacement or recharge [66, 67, 68]. However, only battery-less, and hence simpler devices can ensure a true pervasive distribution, due to their reduced cost and to the theoretically infinite life. The sensing function may be in principle played by the RFID antenna itself that it is coated by a layer of a chemically sensitive material whose dielectric properties are influenced by the adsorption of a volatile compound [14]. However, most of the chemical sensitive materials are mostly characterized only in DC [69], and hence the design of these class of sensors suffers from the lack of information about the SM's electromagnetic parameters in the UHF RFID band.

Among the different environmental parameters, the observation of humidity is of primarily interest in the assessment of the air quality in living and controlled rooms, in the monitoring of the conservation state of foods, in the preservation of walls, exhibition spaces, historical buildings, libraries and archival collections. Additionally, humidity is critical in many biomedical applications concerning the healing degree of wounds [70] and the storage and delivery of pharmaceutical and biological products.

Some early experiments of how integrating humidity sensors into UHF RFID tags were recently presented in [16, 15, 18, 71]. These papers demonstrated that the RFID response may be affected by an external chemical receptor reacting to the water absorption. Nevertheless, important issues, concerning the full characterization of the tag as a sensor, are still in question. Several of these topics will be explored in next three Chapters, such as the effects of the sensitive material amount on the tag, the recovery capabilities in cyclic exposure, the hysteresis, the robustness, the reproducibility, techniques to characterize at RF and minimize the amount of the SM needed while maximizing sensitivity and communication performance, and not last the control over the response of the radio-sensor and the cross-sensitivity to multiple physical parameters.

7. Characterization and Effects of Chemical Sensitive Loadings

In this Chapter a new family of polymer-doped tags is proposed in order to characterize the effects of chemical loadings when exposed to ambient humidity or other gas. A sensitive chemical species based on PEDOT:PSS is used to load two different folded-like patch tags. The communication and sensing capabilities of the radio-sensors are investigated by means of experimental analysis during humidity exposures that show how to control and balance above opposite requirements by a proper deposition of the sensitive material.
A key-issue of the wireless gas sensing by RFIDs is the capability to select and characterize chemical sensitive materials when exposed to different gases. An open-circuit shielded slotline layout is proposed as a tool to estimate the electromagnetic equivalent parameters of the SM during the gas exposure.

This chapter explores the possibility to integrate different chemical paints into passive UHF tags with full attention to both communication and sensing issues and their mutual relationships. Among the different polymers showing sensitivity to four selected gases (ethanol, octane, ammonia and humidity), *poly (3,4-ethylenedioxythiophene) :poly (styrenesulfonic acid)* PEDOT:PSS [72] was selected for further experimentations. Such a conducting polymer shows significant and reversible modification in its electrical properties when exposed to changing humidity. It can be easily manufactured on industrial scale using various deposition techniques [73]. For sens-

ing purposes, it is often deposited into interdigital capacitors and, if characterized in DC, it shows monotonic exponential variation of resistance when exposed to humidity [74]. However, only little knowledge is currently available about the radiofrequency features of the PEDOT:PSS as a sensing material, even without integration with antennas.

In this chapter, the sensor tags presented in sec. 4.2.1 and in sec. 4.2.3 suitable to host a distributed and a lumped load of chemical coatings, respectively, are utilized for detailing the sensitive material effects during sensing of humidity. The achievable sensitivity and the communication performance of the sensor-tag are characterized depending on the amount of deposited polymer on the "H-slot fed folded-patch" (sec. 4.2.1). Starting from the lumped electric model proposed in sec. 3.1, this Chapter further investigates that idea by exploiting a miniaturized doubly-folded patch antenna hosting one drop of chemical material (sec. 4.2.3), which can be useful to easily estimate the electromagnetic UHF parameters of the specific SM during gas exposure.

The described devices could have interesting applications in the assessment of the air quality within living and controlled rooms, in the monitoring of the conservation state of foods, in the preservation of walls, and even in the medical field, e.g. to monitor the healing degree of wounds.

7.1. Materials and Methods

The first step of this analysis consisted in selecting chemical sensitive coatings able to respond to gas exposures in the UHF RFID band, since there is no information in literature on their electrical properties at RF.

7.1.1. Volatile compounds

The selected volatile compounds were ethanol (alcohol), octane (hydrocarbons), ammonia (weak bases) and water. This choice is based on the broad chemical properties of the compounds and their presence in several common environments.

7.1.2. Sensitive coatings

The set of preliminary selected coatings is listed in Tab. 7.1: four polymers (Pedot:PSS, polypyrrole, PDAC and doped PSS), two polypyrrolic macrocycles (a phthalocyanine and a metalloporphyrin), two carbon based materials (SWCNT and carbon black) and a hybrid organic (porphyrin coated Zinc oxide nanorods). Some of these materials, such as the organic polymers, are commercially available and already exploited for their electrical properties as DC sensors. The rest of proposed coatings have been previously used in DC but coupled with different transducers [75], [76]. The large part of the investigated sensitive materials are not selective, they rather can interact with a wide range of compounds from Lewis acid-base, hydrogen bonds (acid and basic), dipolar, $\pi - \pi$ interactions, and induced dipole. All of them, even with different intensities, are used to bind ethanol, ammonia and water, while the latter is the only interaction available for the detection of octane. This cross-selectivity has been exploited in the past for the development of sensor arrays.

The toxicity of previous materials is a topic of interest in order to preserve the human health while handling this kind of chemical sensors. Pedot:PSS, Phthalocyanine, Polypyrrole, PDAC and Doped PSS are completely biocompatible and not harmful. Some of them are even used in cosmetics. ZnO Nanorods and MnTPPS are considered non-harmful unless inhaled in high volumes. Carbon black have traditionally been used therapeutically, without obvious adverse effect. Studies of workers exposed to carbon blacks revealed respiratory symptoms or irritation including impaired lung function arising from deposition of dust in the lungs. However, surveys of carbon black workers have not permitted any firm conclusions on carcinogenicity to be drawn. The toxicity of carbon nanotubes has been an important question in nanotechnology. The data are still fragmentary and subject to criticism. Preliminary results highlight the difficulties in evaluating the toxicity of this heterogeneous material. Parameters such as structure, size distribution, surface area, surface chemistry, surface charge, and agglomeration state as well as purity of the samples, have considerable impact on the reactivity of carbon nanotubes. However, available data clearly show

Table 7.1.: Sensitive coatings used for the RFID sensors.

Sensor no.	Sensitive coatings	
1	**Pedot:PSS**	*poly(3,4-ethylenedioxythiophene) poly(styrenesulfonate)*
2	**SWCNT**	*Single Wall Carbon Nanotubes*
3	**Carbon black**	
4	**Phthalocyanine**	
5	**Polypyrrole**	
6	**ZnO Nanorods**	*Monocarboxytetraphenylporphyrin functionalized ZnO nanorods*
7	**MnTPPS**	*Manganese-Tetra-(sulfonatophenyl)porphyrin*
8	**PDAC**	*poly diallyldimethylammonium chloride*
9	**Doped PSS**	*Doped poly(styrenesulfonate)*

that, under some conditions, nanotubes can cross membrane barriers, which suggests that, if raw materials reach the organs, they can induce harmful effects such as inflammatory and fibrotic reactions [77]. Therefore, common safety precautions for chemicals have been considered during the fabrication of the chemical doped sensors.

The RFID wireless transducer (Fig. 7.1) is the basic device previously described in sec. 4.2.3. It comprises a planar tag antenna folded on a rigid substrate and an RFID microchip transponder and, as it will be shown later on, it can be used for both gas sensing and characterization of the sensitive materials. Several prototypes of the miniaturized sensor tag were manufactured by properly wrapping an adhesive carved copper sheet on the Forex substrates. Each coating listed in Tab. 7.1 was carefully poured on top of the sensing niche of nine different tags, using a fine droplet.

7.1.3. Measurement metrics and procedures

The UHF long-range reader ThingMagic M5 [55] was used to interrogate the tags during dynamic exposures to gases providing a 0.5dBm resolution in the turn-on power measurements within the 840-960MHz band. Tag sensors were placed inside a custom exposure cell where vapors are flown in and out (Fig. 7.1). The cell is a $13cm \times 10cm \times 2cm$ box made by Polyoxymethylene (POM), a thermoplastic polymer whose features of high resistance, good dielectric properties and impermeability allow reducing the analyte adsorption on the internal surfaces and avoid the electromagnetic interference with the tag antenna placed inside the cell. Two mass flow controllers and a remote controller connected to a PC have been used to split dry air flux into a carrier and a diluting part; the carrier is bubbled through the volatile compound of interest and afterwards mixed with the diluting part to achieve the desired concentration level injected in the measurement cell. During the exposures to gases the sensor tag is placed inside the measurement cell 45cm away from a 5dB linear polarized patch that serves as reader antenna (Fig. 7.2) and the room temperature has been kept constant at 22°C in order to consider only the signal variations due to vapor concentration changes. Reflections from ground and from side walls are minimized by means of absorbing panels. All the volatile compounds are finally disposed off by means of specialized chemical fume extractors.

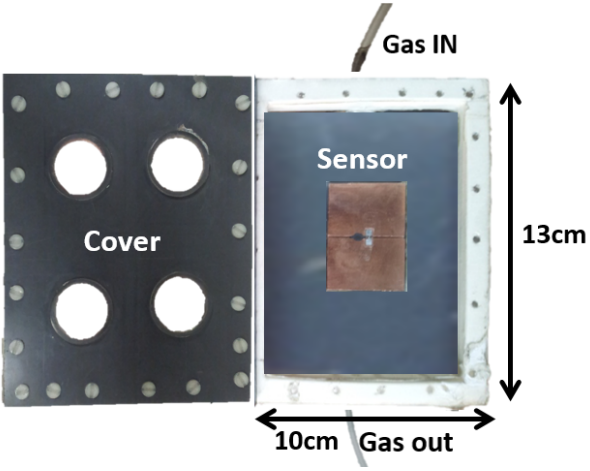

Figure 7.1.: Picture of the open airtight measurement cell made of POM containing the doubly-folded chemical doped patch antenna. The plastic cell's electromagnetic effect is negligible, due its thickness and low permittivity.

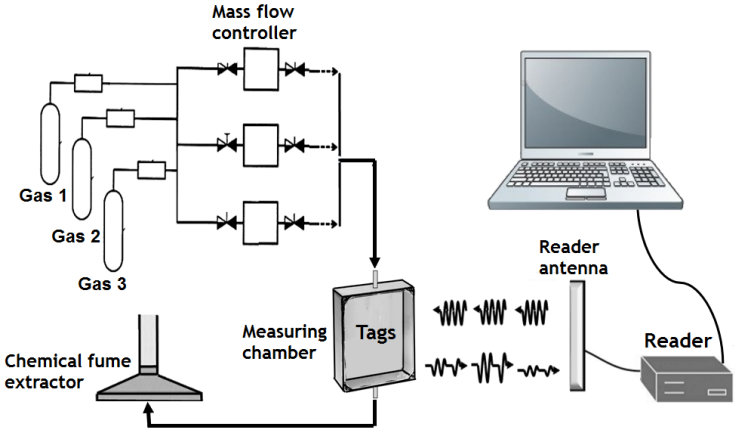

Figure 7.2.: Sketch of the experimental set-up involving a controlled gas delivery system.

7.2. Preliminary Selection of Coatings for UHF sensing

A first characterization of each sensor coated with the sensitive materials listed in Tab. 7.1 was carried out by exposing the coated tags to a saturated concentration of the four test vapors in order to select the most responsive ones. The measurement protocol consists to flow dry air through the system for 1 hour to establish a system baseline, then to flow a selected gas at its saturated concentration for 30 minutes (exposure time) and subsequently to flow dry air to clean the sensor surfaces for 1 hour and 30 minutes (recovery time). In this way the reliability of the sensor was quantified for each coating. Fig. 7.3 shows a typical profile of the measured normalized turn-on power (case of Pedot:PSS coated tag) during humidity exposure with indication of the achieved dynamic range. The maximum variations of the turn-on power in each performed measurement are summarized in Tab. 7.2. In all cases, polypirrole and porphyrins coated ZnO nanorods gave negligible responses ($< 1dB$), practically masked by the resolution of the reader; hence they are not suited to radiofrequency sensors of the considered gases. Pedot:PSS, SWCNT, PDAC and doped PSS, exhibited the most substantial changes of turn-on power response to at least a subset of the four gases under test.

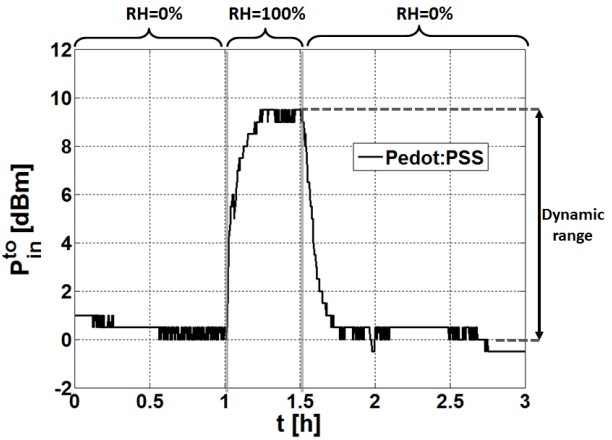

Figure 7.3.: Example of measured time evolution of the turn-on power normalized to its baseline value. The sensor is functionalized with Pedot:PSS and monitored during 1 hour of dry air to achieve the baseline value, 30 minutes exposure to saturated water vapor and 1 hour and 30 minutes recovery in dry air. The 0.5 dBm minimum step of the data distribution is due to the resolution of the reader.

Table 7.2.: ΔTurn-on Power values

Sensitive Material	Moisture (0-100%)	Ethanol (0-100%)	Ammonia (1 mol) (0-100%)	Octane (0-100%)
Pedot:PSS	**H.R.** $\boldsymbol{\Delta \geq 4dB}$	**H.R.** $\boldsymbol{\Delta \geq 4dB}$	L.R. $\Delta \leq 1dB$	L.R. $\Delta \leq 1dB$
SWCNT	L.R. $\Delta \leq 1dB$	L.R. $\Delta \leq 1dB$	**H.R** $\boldsymbol{\Delta \geq 4dB}$	L.R. $\Delta \leq 1dB$
Carbon black	L.R. $\Delta \leq 1dB$	M.R. $1dB < \Delta < 4dB$	L.R. $\Delta \leq 1dB$	L.R. $\Delta \leq 1dB$
Phthalo-cyanine	L.R. $\Delta \leq 1dB$	M.R. $1dB < \Delta < 4dB$	M.R. $1dB < \Delta < 4dB$	**H.R.** $\boldsymbol{\Delta \geq 4dB}$
Polypyr-role	L.R. $\Delta \leq 1dB$	L.R. $\Delta \leq 1dB$	L.R. $\Delta \leq 1dB$	L.R. $\Delta \leq 1dB$
ZnO Nanorods	L.R. $\Delta \leq 1dB$	L.R. $\Delta \leq 1dB$	L.R. $\Delta \leq 1dB$	L.R. $\Delta \leq 1dB$
MnTPPS	L.R. $\Delta \leq 1dB$	M.R. $1dB < \Delta < 4dB$	L.R. $\Delta \leq 1dB$	M.R. $1dB < \Delta < 4dB$
PDAC	**H.R.** $\boldsymbol{\Delta \geq 4dB}$	L.R. $\Delta \leq 1dB$	**H.R.** $\boldsymbol{\Delta \geq 4dB}$	**H.R.** $\boldsymbol{\Delta \geq 4dB}$
Doped PSS	**H.R.** $\boldsymbol{\Delta \geq 4dB}$	**H.R.** $\boldsymbol{\Delta \geq 4dB}$	L.R. $\Delta \leq 1dB$	L.R. $\Delta \leq 1dB$

H.R. = High Response; M.R. = Medium Response; L.R. = Low Response.

7.3. Effects of Sensitive Material Amount

After showing the different selectivity and response of several sensitive coatings, the effects of the sensitive material amount amount were characterized with the tag antenna described in sec. 4.2.1 and represented in Fig. 7.5 left. This layout is a distributed SM-loaded tag hosting a chemical coating deposition within the H-slot. Since there is no decoupling from the operative and structural point of view between antenna and sensor, the proposed device has to be characterized and optimized from both perspectives. In particular, the sensing capabilities in this case are paid in terms of a worsening of the tag's realized gain (and hence of the read distance) along with the humidity exposure. It is hence important to balance two opposite requirements, e.g. to pursue a useful sensitivity at the minimum degradation of the communication. The amount of deposited polymer is expected to be an effective parameter to tune the communication/sensing performances as demonstrated in the following experiments.

7.3.1. Pedot:PSS

Among the sensitive coatings in Tab. 7.1, Pedot:PSS was selected for further characterization during humidity exposures. The conductive polymer is available commercially as Clevios PH 500, a homogenized water based dispersion [78] generally used for conductive coatings with a PEDOT to PSS ratio of 1:2.5 (Fig. 7.4). Like other polymers containing sulfonic acid groups, PEDOT:PSS is strongly hygroscopic and takes up moisture when handled under ambient conditions. At room temperature, it naturally solidifies so producing a thin film of about $35\mu m$ thickness. Since Pedot:PSS is a lossy material, the absorption of electromagnetic energy is higher than in air. The polymeric film is able to almost instantaneously absorb water from the environment which is incorporated into the films. Consequently water produces an increase of the layer thickness, especially remarkable for films with high PSS content up to 30% (as in the considered case).

PEDOT:PSS is well known within the antenna and RF community since, thanks to its characteristics, it has been recently used as

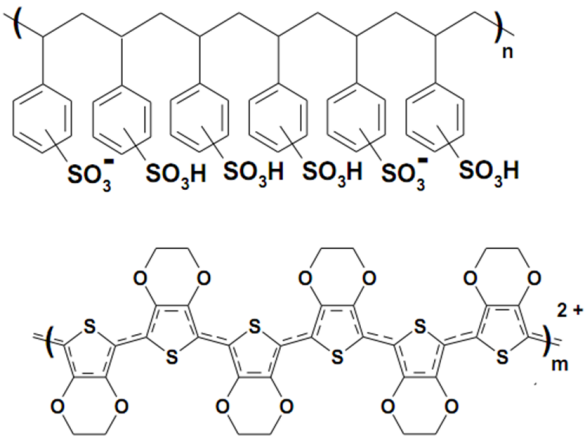

Figure 7.4.: *Poly (3,4-ethylenedioxythiophene):poly (styrenesulfonic acid)* PEDOT:PSS chemical formula.

conductive material for printed antennas applications [79]. Optical translucency of PEDOT:PSS allows to hide an antenna or make the antenna virtually invisible [80, 81] when mounted on a transparent substrate, such as the screen of a laptop or PDA, while the ductility permits to attach the polymer on flexible fabrics and plastic substrates.

7.3.2. Communication performance vs. Pedot:PSS amount

The communication performances of the doped tag have been evaluated at ambient humidity in terms of realized gain G_τ versus the amount of polymer deposition inside the glasses-like slots according to the layouts in Fig. 7.5 right. From the measured profiles in Fig. 7.6, it is worth observing that there would be only a negligible degradation in communications on moving from the blank tag to the deposition F obtained with a single polymer drop just behind the microchip. For the other cases, it is instead apparent that, by filling the central slot and the two upper horizontal slots (as

suggested by Fig. 4.6), the peak of the realized gain sensibly shifts and attenuates of about 8dB. Accordingly, the activation distance would be reduced from $8m$ to $3.5m$.

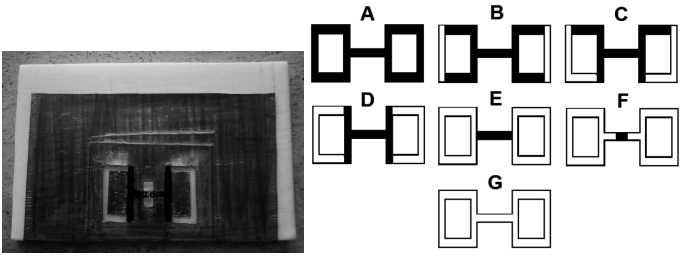

Figure 7.5.: Left) RFID sensor prototype with a partial polymer filling (in black) on the sensing glasses-like slots. Right) Some layouts of polymer deposition inside the glasses-like slots. The first geometry (A) corresponds to a complete loading of the slot, the last one (G) to an unloaded (blank) tag.

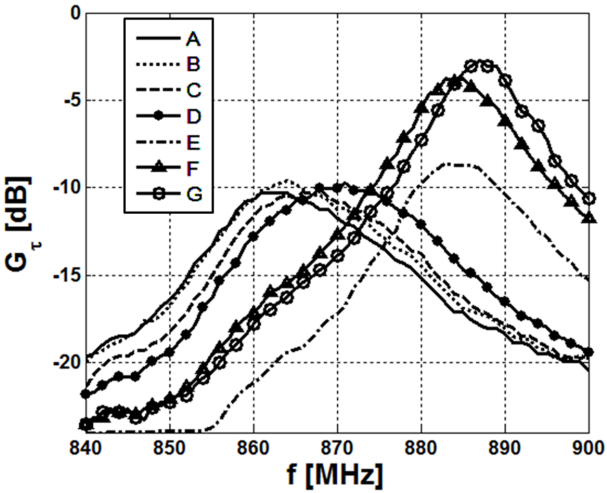

Figure 7.6.: Measured realized gain along the antenna axis (broadside observation) for different polymer depositions as in Fig. 7.5.

7.3.3. Sensing performances vs. Pedot:PSS amount.

The sensing performances of the RFID tag have been analyzed dynamically when the humidity inside the box of Fig. 7.7 gradually changes from ambient conditions up to saturation, for the most representative polymer deposition layouts (cases A, D and F in Fig. 7.5). The saturation has been gradually obtained by placing the tag inside a closed plastic chamber partially filled with water (Fig. 7.7). When the chamber is closed, the relative humidity approaches RH=100% (wet air), while in case the cover is removed, the humidity is that of the ambient air (RH =50%). The measurements have been performed at room temperature of 24°C, to be considered stable all along the process.

The considered sensing metrics are the turn-on power $P_{to}^{in}[RH]$ and the normalized backscattered power $p_{BS}[RH]$ as defined in sec. 2.2. The backscattered power is deduced from the RSSI (Received Signal Strength Indicator), provided by the reader, and then transformed

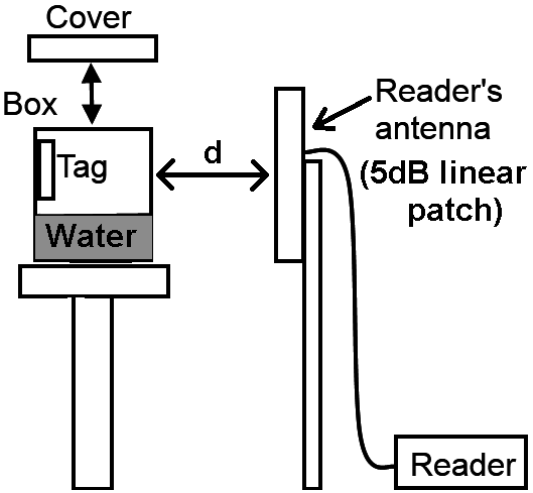

Figure 7.7.: Measurement set-up: the sensor tag is placed into a sealed plastic chamber partially filled with water at a distance d=50cm away from the reader's antenna. The plastic chamber, thanks to its low permittivity, does not significantly affect the response of the tag.

through the following conversion rule (specific for the used reader)

$$P_{BS} = 0.8RSSI + 24 - G_{LNA} - 96 - 0.8RSSI_{th} \tag{7.1}$$

The sensors were not conditioned prior to operation. Fig. 7.8 shows the measured variation of the turn-on power $P_{in}^{to}[RH]$ with respect to the increase of humidity at the frequencies where, case by case, the turn-on power is minimum. To improve the readability, a mean-square interpolation is superimposed to the stair-step distribution of the measurement data caused by the coarse output power resolution ($0.5dBm$) of the UHF ThingMagic m5 reader [55].

All the measured tags detect the variation of the humidity according to an exponential profile so that the turn-on power increases of about $3.5dB\ to\ 6dB$ depending on the specific PEDOT:PSS depo-

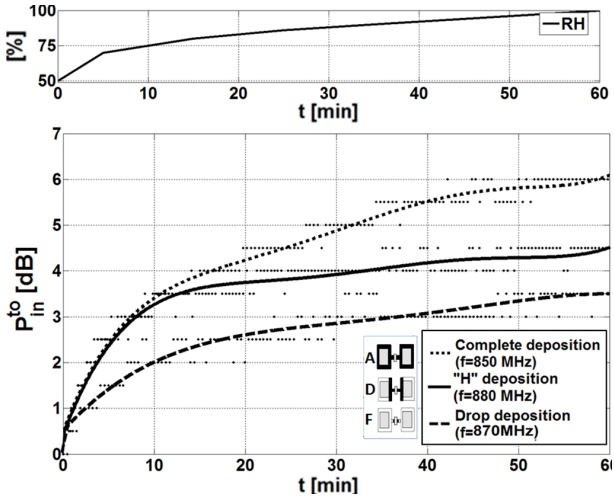

Figure 7.8.: Top) Measured variation of humidity inside the plastic box. The RH level variation with time has been monitored by means of a digital hygrometer placed inside the box. Bottom) Measured turn-on power normalized with respect to its initial value, e.g at ambient RH, for three different polymer depositions into the H-slot. Data (discontinuous dots) have been fitted by a mean square interpolation.

sition. The wider is the area covered by the polymer, the greater is the water absorption and thus the dynamic range of the sensor. It is moreover worth noticing that during the very early grade of the exposure, e.g. for 50%<RH<75% (t < 10min), the responses of layout A (full deposition) and layout D (H-like deposition) are indistinguishable while the overall saturation threshold is instead 2dB higher for the case A. Finally, even the single-drop layout F offers the possibility to track the humidity change with an interesting overall 3.5dB dynamic range.

As for conventional sensors, also in this case it is possible to determine the *calibration curves* (see sec. 2.3). Fig. 7.9 shows the normalized values of turn-on and backscattered power with respect to the initial condition. The profiles appear almost linear, especially at

low humidity grades and so it is possible to extract the sensitivity of the devices, e.g the slope of the linearized curves, as the power difference generated by 1% change in the RH level, (eq.2.16 where $\xi = \{P_{in}^{to}, p_{BS}\}$). The values for the three depositions of Fig. 7.9 are listed in Tab. 7.3. In the lower part of the dynamic ranges, the backscattered power metric appears more sensitive to humidity variations than the turn-on power indicator, while no remarkable difference may be observed close to the saturation. It is finally worth noticing that the deposition layout corresponding to a single polymer drop (case F) has a nearly halved sensitivity with respect to the full-deposition tag A. However, at least for low humidity grades, its sensitivity is fully comparable with the one achieved in [16, 15], further demonstrating the possibility of reducing the amount of sensor deposition without affecting the performance of the described tag.

Table 7.3.: Sensitivities $[dB/RH]$ of measured turn-on and backscatter power.

	$RH_{low}-RH_{high}$	Case A	Case D	Case F
$S_{P_{in}^{to}}$	$50\% - 80\%$	0.13	0.12	0.08
	$80\% - 100\%$	0.1	0.05	0.05
$S_{p_{BS}}$	$50\% - 80\%$	0.18	0.2	0.12
	$80\% - 100\%$	0.13	0.05	0.05

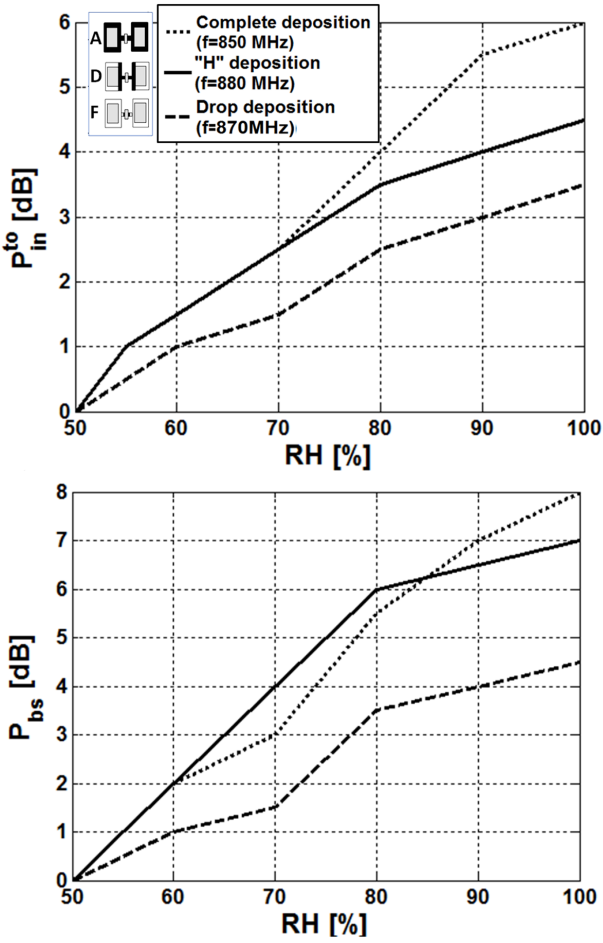

Figure 7.9.: Calibration Curves of the humidity RFID sensor in Fig. 7.5 left for different amount of polymer deposition. Top) Turn-on power; Bottom) Backscattered power.

7.4. Sensitive Material Characterization

In order to obtain the Pedot:PSS electrical properties at UHF a general-purpose procedure was implemented using the doubly-folded patch tag (Fig. 7.1), whose layout has been presented in sec. 4.2.3. The SM is assumed to be placed into the small ($\frac{\lambda}{100} \times \frac{\lambda}{100}$) niche and modeled with a lumped element model in parallel to the NXP G2il IC [45]. The circuit model is shown in Fig. 7.10. Pedot:PSS characterization is illustrated numerically and experimentally as follows.

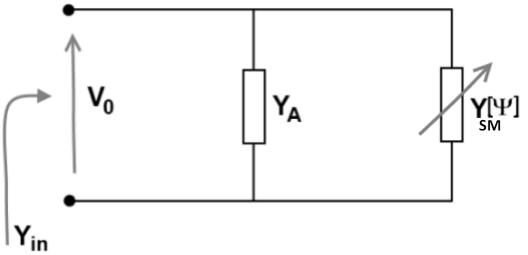

Figure 7.10.: Slotline's equivalent circuit model with the SM equivalent admittance $Y_{SM}[\Psi]$ in parallel to the input admittance of the unloaded antenna Y_A.

7.4.1. Experimental Procedure

The tag's capability to be used in the electromagnetic characterization of SMs is discussed and demonstrated by exposing the tag to humidity variations. The measured realized gain of the chemical loaded tag for two different grades of relative humidity (RH), e.g. ambient level (RH=40%) and saturation (RH=100%), are compared with that of the "blank" tag. Variation of relative humidity levels in parallel by a digital hygrometer placed within the chamber, at the purpose to provide a reference dataset. The presence of the polymer induces a significant frequency shift of the tags' response towards higher frequencies with respect to the blank configuration and such a shift is proportional to the grade of humidity. The peak

value of the gain of the loaded tag at humidity saturation (100%) overcomes the frequency limit of the reader (960MHz) and therefore it cannot be appreciated by the measurement.

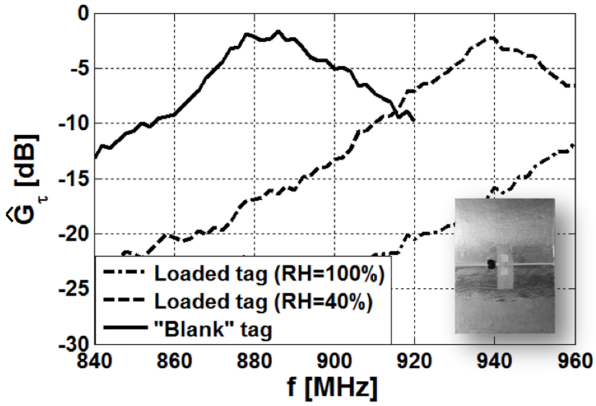

Figure 7.11.: Measured realized gain in the broadside direction for the chemical-loaded and "blank" tags. Measurements have been performed within the range of frequencies allowed by the reader (840MHz-960MHz).

In order to evaluate the effects of the SM in the whole considered range of humidity (40% to 100%), the loaded tag has been manually re-tuned to keep the operative frequency of the tag around 900MHz. Starting from the tuning chart in Fig. 4.17, the requested 35MHz shift towards lower frequencies in condition of ambient humidity has been practically achieved by reducing the length d of the shorting strip lines from 7.5mm to 6.5mm. The new measured realized gains of the retuned chemical-loaded tag for different levels of humidity can be now fully appreciated by the reader (in Fig. 7.12), and the system is now ready to estimate the equivalent SM parameters.

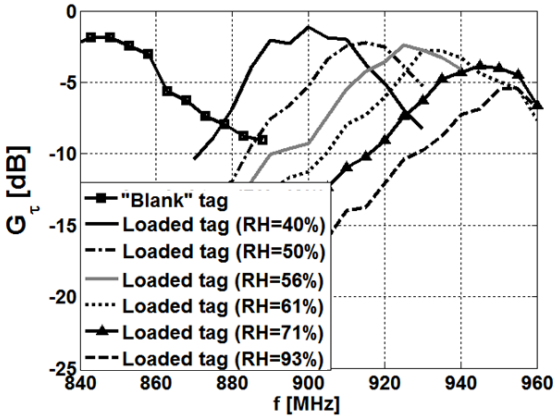

Figure 7.12.: Measured realized gains of the re-tuned ($d = 6.5mm$) "blank" and chemical-doped tags in the broadside direction for different levels of humidity.

The assumed equivalent admittance of the Pedot:PSS is hence a parallel connection of a resistance and a capacitance$\{R_{SM}[RH_n],\, C_{SM}[RH_n]\}$ as in (3.1) whose values at discrete humidity grades $\{RH_n\}$ are here identified with the following procedure involving the lumped model of Fig. 7.10 and eq. (3.12).

i) The realized gain $G^{meas}_{\tau,f_i}[RH_n]$ of the loaded tag is measured at some frequencies $\{f_i\}$, in several different humidity concentration, starting from ambient air ($RH = 40\%$) up to fully wet air ($RH = 100\%$), as previously shown in Fig. 7.12;

ii) the input impedance ($Z_A = \frac{1}{Y_A}$) and the gain (G_0) of the unloaded tag are obtained by FDTD simulations;

iii) the lumped model $G^{mod}_{\tau,f_i}(R_{SM}[RH_n], C_{SM}[RH_n])$ in (3.12) is finally inverted to identify the unknown parameters of the SM by minimizing, at every considered humidity concentration RH_n, the following error function:

$$\Delta_{tot}[RH_n] =$$

$$\sum_{i=1}^{3} \frac{\left| G^{meas}_{\tau,f_i}[RH_n] - G^{mod}_{\tau,f_i}(R_{SM}[RH_n], C_{SM}[RH_n]) \right|^2}{\left| G^{meas}_{\tau,f_i}[RH_n] \right|^2} \tag{7.2}$$

with $f_i = \{f_{Gmax,RHn},\ f_{Gmax,RHn} \pm 10MHz\}$, where $f_{Gmax,RHn}$ refers to the frequency corresponding to the peak of the measured realized gain of the loaded sensor at the considered humidity level RH_n.

An example of parameter identification of the PEDOT:PSS resistance $R_{SM}[RH_n]$ and capacitance $C_{SM}[RH_n]$ is shown in Fig. 7.13, where the error isolines Δ_{tot} obtained from (7.2) are referred to the humidity RH=56%.

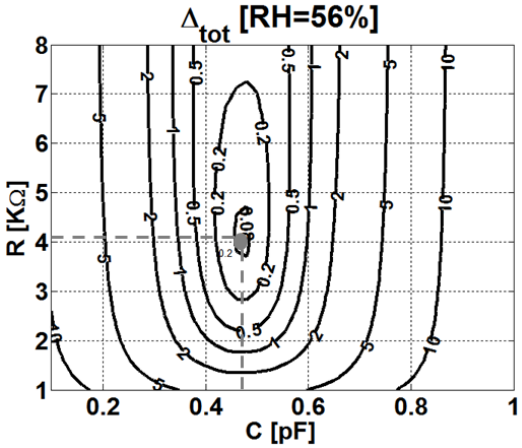

Figure 7.13.: Isolines of the global error $\Delta_{tot}[RH = 56\%]$ for the parametric identification of the equivalent resistance R_{SM} and capacitance C_{SM} of the PEDOT:PSS drop corresponding to the humidity RH=56%. The gray circle indicates the couplet (R_{SM}, C_{SM}) minimizing the error in (7.2).

The estimated values of $C_{SM}[RH_n]$ and $R_{SM}[RH_n]$ as a function of the humidity grade from 40% to 100% are summarized in Fig. 7.14.

The obtained samples for both resistance and capacitance have been fitted by a mean-square interpolation, using a second order polynomial

$$\begin{bmatrix} R_{SM}[RH] \\ C_{SM}[RH] \end{bmatrix} \simeq \sum_{k=0}^{2} \begin{bmatrix} a_{R,k} \\ a_{C,k} \end{bmatrix} RH^k \tag{7.3}$$

with $\{a_{R,k}\}_{k=0..2} = \{17,\ -0.32,\ -1.7 \cdot 10^{-4}\}$, and $\{a_{C,k}\}_{k=0..2} = \{-0.31,\ 0.02,\ -1 \cdot 10^{-4}\}$. It is clearly visible how the optimized resistance of Pedot:PSS decreases with a greater water absorption due to power loss, while the capacitance of the polymer increases because of its higher permittivity. Both the values tend to saturate close to RH=100%.

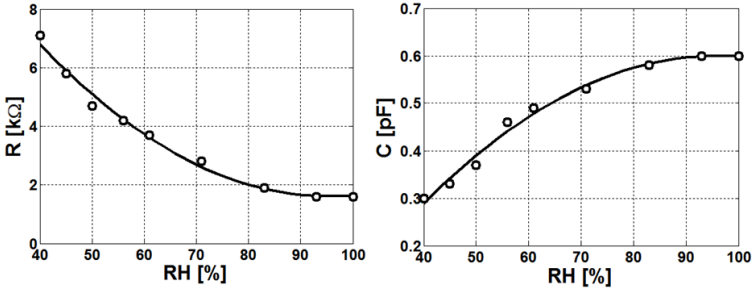

Figure 7.14.: Estimated values (circles) of the capacitance C_{SM} and resistance R_{SM} of Pedot:PSS for different levels of humidity between 40% and 100%. The data have been fitted by a second-order mean square interpolation (continuous lines).

For a cross-check, Fig. 7.15 compares the measured and calculated realized gains at two humidity levels RH={40%, 71%} showing a satisfactory agreement nearby the peaks of the tags responses.

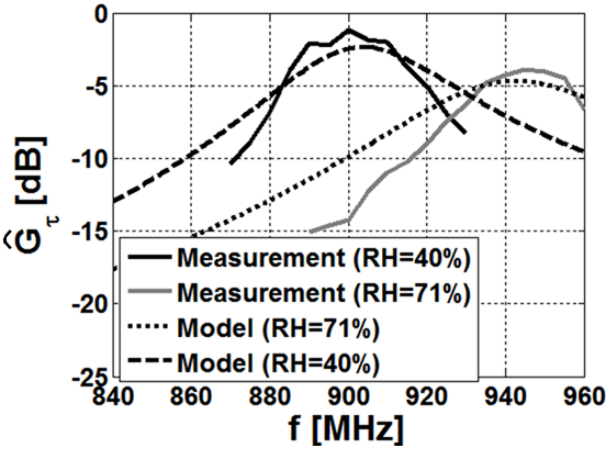

Figure 7.15.: Measured and estimated realized gain for two different RH levels along the antenna axis (broadside observation) by using the identified values of capacitance C_{SM} and resistance R_{SM} of the Pedot:PSS load.

7.5. Conclusions

This chapter described the characterization process of a sensitive coating suited to be integrated into an UHF RFID transducer. Pedot:PSS, Doped PSS, SWCNT and PDAC revealed significantly sensitive, at different extent, to the tested volatile compounds: water, ethanol, ammonia and octane.

The complete integration of PEDOT:PSS as a distributed or lumped chemical load into RFID tags has been reported in this chapter, aiming to test the effects of the polymer amount on the communication and sensing performance for humidity detection. It was demonstrated that the sensitivity and dynamic range can be controlled by the amount and the displacement of polymer into the sensing slots of a distributed loaded sensor.

The equivalent lumped-element model of the chemical loading in parallel to the IC (chapter 3) can be used to characterize the electrical properties of the SM at UHF frequencies. Thanks to the

presence of the ground plane, which decouples the two presented antennas from their location, this kind of tags are moreover suitable to harsh environments and body-centric applications.

8. Design and Experimentation of RFID Gas Sensors through Amplitude or Phase Control

A key-issue of the wireless gas sensing by RFIDs is the capability to control the sensor's response while minimizing the amount of chemical sensitive material required to dope the tag antenna. Previously proposed circuit models (chapter 3) modelling a general purpose RFID transducer hosting lumped sensitive elements (sec. 4.2.3) can be applied to investigate, fully characterize and master the communication and sensing capabilities of RFID loaded sensors. Numerical analysis and experimentation are performed in order to balance the two above opposite requirements by studying signal amplitude- and phase- oriented measurements for the detection of humidity.

As earlier demonstrated, a possible approach to RFID sensing engineering is to describe the complex interactions between SM, antenna and volatile compounds as simple lumped-element circuits, that is possible when the loading SM is a very localized displacement. Starting from the lumped electric model proposed in sec. 3.1, this Chapter further investigates that idea by exploiting the doubly-folded drop-loaded tag, which can be useful to support the design of an effective and highly sensitive chemical radio-sensor. The considered tag employs a slot-line layout and a tuning mechanism (see

sec. 4.2.3) able to shift the antenna response at each frequency of the global UHF RFID band (865-928MHz). This feature is hence potentially useful to modify the dynamic range of the sensor and its sensitivity, as detailed below.

Signal amplitude-oriented sensing is numerically studied and experimented in order to define the sensitivity, the recovery capability and the hysteresis during cyclic exposures to humidity. the Analog Identifier (AID) is used as a set-up invariant sensing parameter.

Nowadays many RFID readers are capable to provide power information in a fully coherent way and extract the phase of the demodulated signals backscattered by the tag. Early experiments with phase detection were only focused to spatial tracking of people and objects [35]. For the first time, phase of the backscattered signal is here exploited as an additional chemical sensing carrier.

The following tests performed on the proposed sensor allow the validation of the models proposed in chapter 3, the evaluation of the robustness of the phase-measurement to the mutual reader-tag position and the quantification of the achievable resolution, for several dynamic ranges, for both signal amplitude- and phase-oriented RFID measurements.

An RFID sensor-tag will be finally experimented in a real world application.

8.1. Signal Amplitude Design Example

Having estimated in sec. 7.4.1 the PEDOT:PSS equivalent lumped parameters $\{R_{SM}, C_{SM}\}$, the model of eq. (3.12) is now applied to optimize the response of the radio-sensor (sec. 4.2.3). The sensitivity of the PEDOT:PSS lumped-loaded tag to humidity, at the RFID European frequency f=868MHz, is increased by properly modifying the geometrical parameter d of the tag (Fig. 4.15). The equivalent admittance $Y_{SM}[RH]$ of Pedot:PSS is estimated by (7.3), while the input impedance $Y_A[d]$ and the gain $G_0[d]$ of the unloaded tag are obtained by FDTD simulations. By representing (Fig. 8.1) the predicted realized gain $\hat{G}_\tau[d, RH]$ of the Pedot:PSS-loaded tag with respect to increasing humidity concentrations, it is clearly evident

that the slope of the curves (corresponding to the device's sensitivity) and their absolute value may be tuned by adjusting the size d of the shorting stripes. In particular, the choice d=8.5mm permits to achieve the best compromise between the absolute value of realized gain all along the RH variation (affecting the read range), the sensitivity to RH, the dynamic range and finally the monotonicity of the $RH \leftrightarrow \hat{G}_\tau$ profile. In this case, the gain degradation factor defined in (3.8) is $\alpha[RH = 40\%..100\%] = 3.5dB$ (Fig. 8.2) and therefore the span of dynamic range of the tag response in Fig. 8.1 is mostly imposed by the impedance mismatch, e.g. by the change of τ.

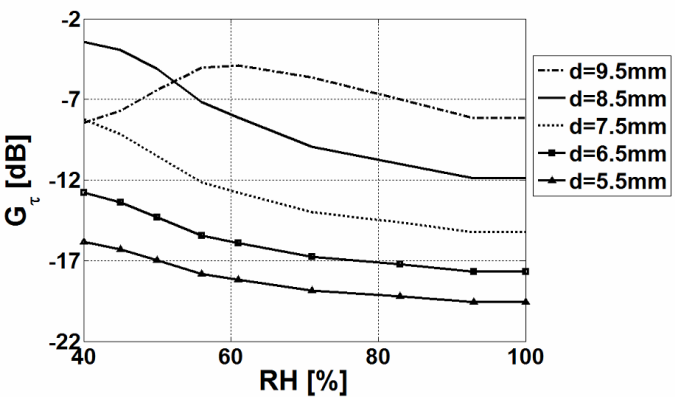

Figure 8.1.: Estimated values of the sensor tag's realized gains $\hat{G}_\tau[d, RH]$ at 868MHz according to the model in (3.12).

The performance of the retuned sensor ($d = 8.5mm$) are finally characterized by measuring the turn-on power $P_{to}^{in}[RH]$, the backscattered power $P_{BS}[RH]$ and the Analog Identifier AID, at fixed frequency f=868MHz during dynamic exposures to humidity and subsequent recovery in order to evaluate the real achievable dynamic ranges, sensitivities and hysteresis. Fig. 8.3 shows the measured normalized variation of the sensing indicators for a single 1.5-hour cycle of exposure/recovery. Measured data are interpolated by mean-square.

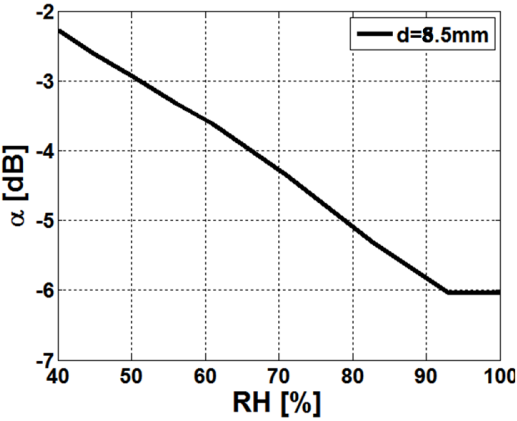

Figure 8.2.: Estimated values of the gain degradation factor (eq. 3.8) at 868 MHz caused by the chemical loading.

The change of the response curves follows the exponential humidity profile with dynamic ranges for turn-on power, backscattered power and AID of 17dB, 23dB and 9dB, respectively. These values are higher than those predicted by the model as the parameter identification of Y_{SM} is less accurate for frequencies far from the gain's peaks, as visible in Fig. 8.1. The recovery process down to the ambient humidity (RH=40%), right after the end of humidity exposure, takes around 30min, even if just 20min are enough for the sensor to recover almost completely. The hysteresis is less than 1dB. Finally, Fig. 8.4 shows the *Calibration Curves*. The profiles appear almost linear for the backscattered power, while the turn-on power saturates for humidity levels greater than 80%.

The sensitivity values for the indicators of Fig. 8.4 are listed in Tab. 8.1.

Among previous signal amplitude-related sensing parameters, the backscattered power metric appears as the most sensitive to humidity change with 0.44dB/RH sensitivity between 40% and 80% relative humidity. The Analog Identifier, even if less sensitive than other indicators, is however very interesting since it does not require an accurate control of the measurement set-up and it is hence the

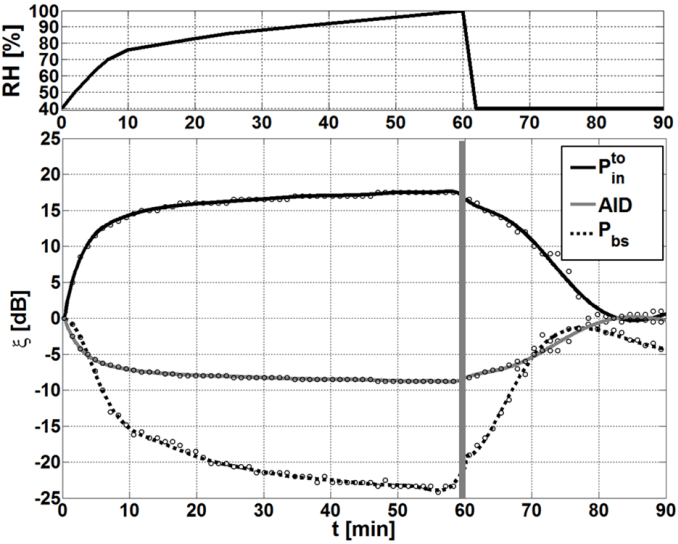

Figure 8.3.: Top) Measured variation of relative humidity during one hour exposure from ambient air (RH=40%) to saturated air (RH=100%) and 30 minutes recovery, as measured by a digital hygrometer. Down) Sensing curves at 868 MHz normalized with respect to the initial value, e.g at ambient RH. Data (circles) have been fitted by a mean square interpolation.

right choice for mobile readers.

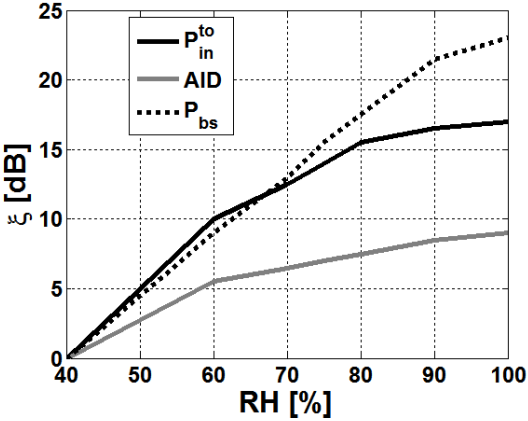

Figure 8.4.: Calibration Curves of the RFID sensor from Fig. 8.3. Turn-on power, backscattered power and AID are represented as a function of humidity.

Table 8.1.: Sensitivities $[dB/RH]$ of measured turn-on power, backscatter power and Analog Identifier.

	$RH_{low}-RH_{high}$	[dB/RH]
$S[P_{in}^{to}]$	$40\% - 80\%$	0.39
	$80\% - 100\%$	0.08
$S[AID]$	$40\% - 80\%$	0.19
	$80\% - 100\%$	0.08
$S[p_{BS}]$	$40\% - 80\%$	0.44
	$80\% - 100\%$	0.28

8.1.1. Cyclic response to humidity

In order to test the recovery and reproducibility capabilities of the sensor, the tag has been exposed to cyclic increasing concentrations of humidity. In these measurements, the molecules to be detected were separately vaporized with concentrations precisely dosed by the controlled flow-system presented in sec. 7.1.3. The reader antenna was 50cm away from the tag and dry air was used as a carrier gas.

The turn-on power P_{in}^{to} variation is visible in Fig. 8.5 when the tag was subjected to several exposure and recovery cycles (15 min and 20 min, respectively) by different percentages of humidity. The effects are fully reversible and proportional to the concentration of humidity, with a negligible hysteresis.

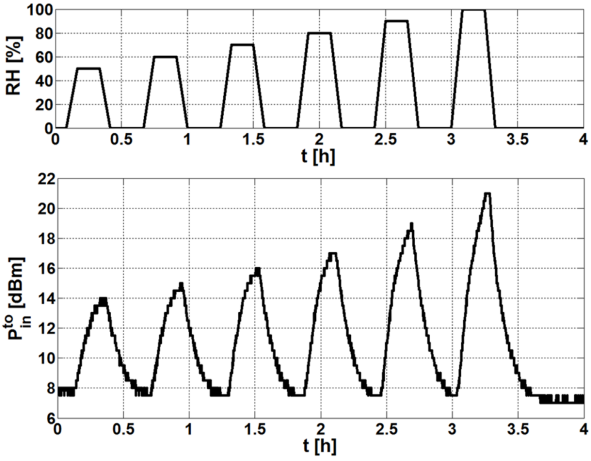

Figure 8.5.: Measured turn-on power during cyclic humidity exposures and recoveries at frequency f=868MHz**.**

8.2. Phase Design Example

A different sensing approach, exploiting the phase of the backscattered signal as sensing carrier, is here investigated. The same tag layout (sec. 4.2.3) doped by Pedot:PSS is evaluated numerically and experimentally for what concern the phase dependence to humidity changes.

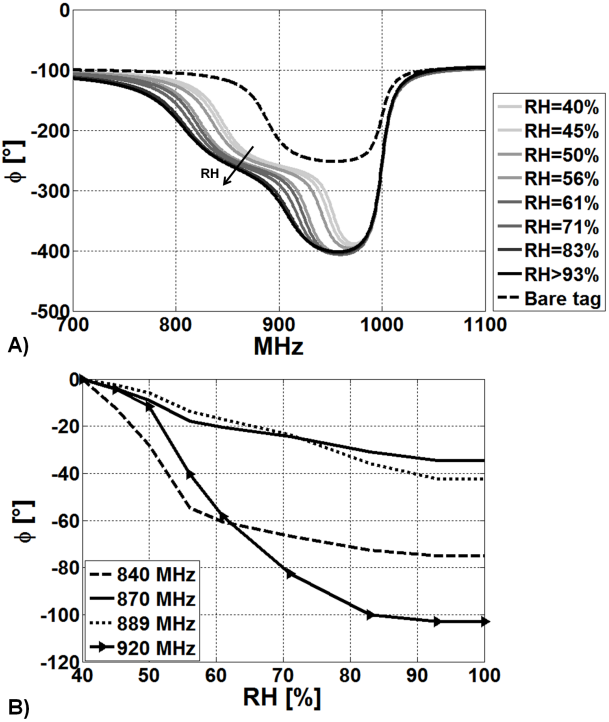

Figure 8.6.: A) Simulated phase variations of the RFID backscattered signal as a function of the relative humidity (RH) and of the frequency. B) Estimated calibration curves of the humidity sensor at four selected frequencies in the worldwide UHF RFID band.

Fig. 8.6A shows the estimated phase vs frequency responses for am-

bient humidity (RH=40%) up to saturation (100%) by application of Eq.(3.14) where the impedance Z_A of the unloaded tag antenna was obtained by numerical simulations. It is worth noticing that phase curves monotonically decrease vs the moisture increases but according to different dynamic ranges and sensitivity that are dependent on frequency (Fig. 8.6B). The phase response however saturates above 1GHz, where the impact of the SM impedance becomes negligible.

Fig. 8.7 finally shows some possible tag's responses (phase and power transmission coefficient) on changing the width d of the shorting stripes e.g. $5.5mm < d < 9.5mm$. The dynamic range of the phase may reach up to $\Delta\varphi$=100° for d=5.5mm, even if the most useful trade-off between phase range and power transfer coefficient degradation could be obtained for d=9mm ($\Delta\varphi = 90°$ and $\tau > 0.5$).

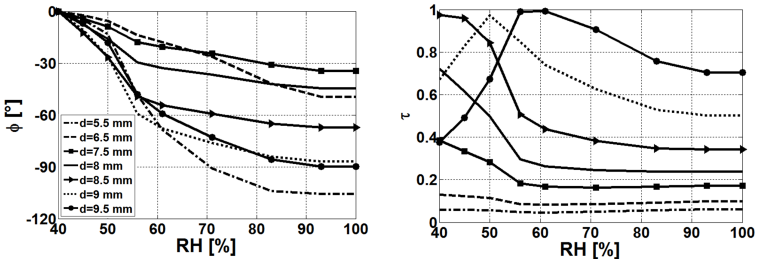

Figure 8.7.: Simulated calibration curves of phase and the power transmission coefficient vs humidity as a function of the antenna tuning parameter d**,** at the fixed frequency of 868MHz**.**

8.2.1. Experimental results

A measurements campaign has been carried out to corroborate the theoretical findings on phase sensing, to describe the required signal processing and derive the achievable resolutions.

The experimental set-up for phase measurements comprises a ThingMagic M6 reader [82], locked at 868 MHz, having disabled the frequency hopping. The reader injects $P_{in} = 26dBmW$ power into a

$5dB$ linear polarized patch antenna. The humidity variations are obtained by the set-up shown in Fig. 7.7.

Phase measurements were performed for several tuning conditions of the tag (e.g. for some values of the tuning parameter d) that potentially provide different dynamic ranges as predicted by the numerical analysis in Fig. 8.7. Experiments were moreover repeated for different alignments between reader's antenna and tag to quantify the robustness of the proposed sensing method to the specific set-up.

8.2.1.1. Phase unwrapping and filtering

A first example of phase measurements considered a tag having tuning stripes with size d=7.5mm that, according to the diagrams in Fig. 8.7, should provide a modest phase dynamic range of about $\Delta\varphi = 35°$. Fig. 8.8B) shows the raw phase data as directly provided by the reader for a single 2-hours cycle of exposure/recovery. There are two clearly visible effects: *i*) the presence of phase wrapping during the exposure and *ii*) a remarkable fluctuation affecting the overall phase signal. Phase wrapping is originated by the receiving and demodulation circuit, at the reader side, so that the phase outcome is confined between 0 and 180°. A phase unwrapping correction $\varphi_{unwrap} = \varphi_{wrap} \pm \pi$ was hence applied to each data sample whose difference with the previous value was larger than $\frac{\pi}{2}$. In this way a continuous form of the phase was obtained making it usable for further processing. The resulting signal (Fig. 8.8C), after normalization by the initial phase, was then processed by an FFT to identify the frequency content (Fig. 8.8D) of the fluctuation. The signal is hence processed by a low-pass FIR (Finite Impulse Response) filter (order N=48 and cut-off $f_0 = 0.01Hz$) and follows the exponential humidity profile (Fig. 8.8C) up to saturation with the expected dynamic range of 35°, as foreseen by the circuit model. The achieved resolution (twice the standard deviation evaluated in the steady state portion of the response) of phase measurements after low-pass filtering is less than 2°.

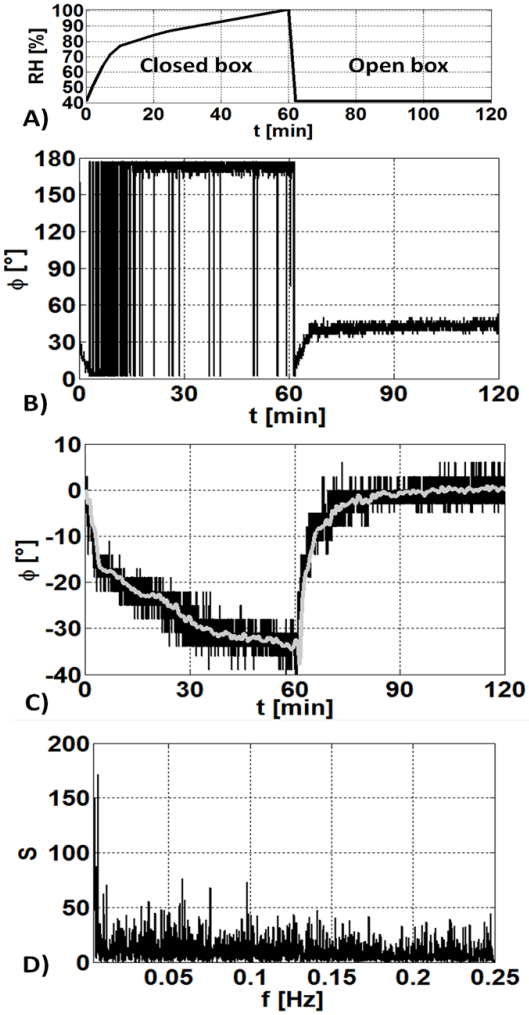

Figure 8.8.: A) Relative humidity, measured by a digital hygrometer, during one-hour exposure from ambient air (RH=40%) to saturated air (RH=100%) and one hour recovery. B) Raw phase measurement by the RFID set-up. C) RFID phase after phase unwrapping (black line) and after low pass filtering (grey line). D) Frequency spectrum of the unwrapped phase.

8.2.1.2. Sensitivity to set-up arrangement

In a second set of experiments, the tag was interrogated (see inset in Fig. 8.9) by the reader antenna from different distances ($30cm < r < 120cm$) and orientations ($\theta = \{0,30°\}$). For each fixed configuration the same measurement and processing as above were repeated. The obtained diagrams during 1h of exposure are superimposed in Fig. 8.9 after normalization for the initial condition for each experiment. In spite of the measurements being made within some weeks and with different tags (hence with a few manufacturing imperfection), the achieved dynamic ranges are in quite good agreement in all the cases. Profiles exhibit a reasonable similarity especially in the steeper part of the phase dynamic ($0 < \phi < 20°$) while some discrepancies are apparent in the flatter part of the response. The phase measurement for sensing was therefore reasonably stable with respect to the mutual position between the reader antenna and the tag, which however has to be kept fixed during the observation of the humidity changes.

This result was expected since the phase dependance on distance and orientation between antennas is embedded into the constant parameter C that is dropped out in the calculation of the differential phase in (3.16).

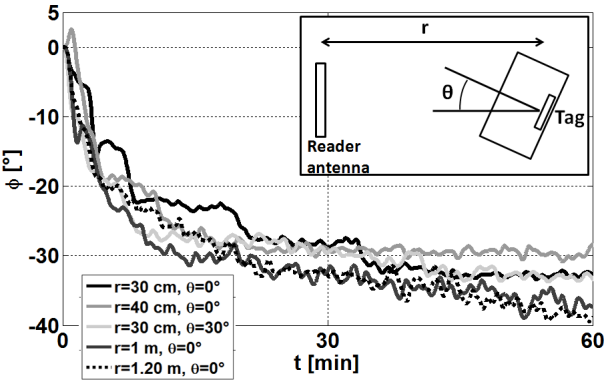

Figure 8.9.: Superposition of the sensor responses (differential phase) upon 1h exposure to humidity for different alignments and orientations between the reader PIFA and the tag: $30cm < r < 120cm$, $\theta = 0°, 30°$.

8.2.1.3. Wider dynamic ranges

In a third set of measurements, the size of tuning strips of the tags have been modified (7.5mm$\leq d \leq$9mm) in order to reproduce wider dynamic ranges as in the simulated profiles of Fig. 8.7. The corresponding tag's responses in the exposure and recovery cycles, after phase unwrapping and filtering, are shown in Fig. 8.10. The profiles are in reasonable agreement with the model so that the achieved span of the phase responses are $\Delta\varphi = \{35°, 45°, 60°, 82°\}$ for the cases $d = \{7.5,\ 8,\ 8.5,\ 9\}\, mm$, respectively.

Finally, the achieved four phase responses are used to derive the calibration curves $\Delta\varphi \leftrightarrow RH$ of the sensor (Fig. 8.11) that have to be compared with theoretical data (Eq. 3.14) derived from the circuit model in the previous section. Reasonable agreement is achieved concerning the dynamic ranges in all the four considered configurations, while the slopes of the curves (i.e. the sensitivities) exhibit differences between model and measurements in the cases

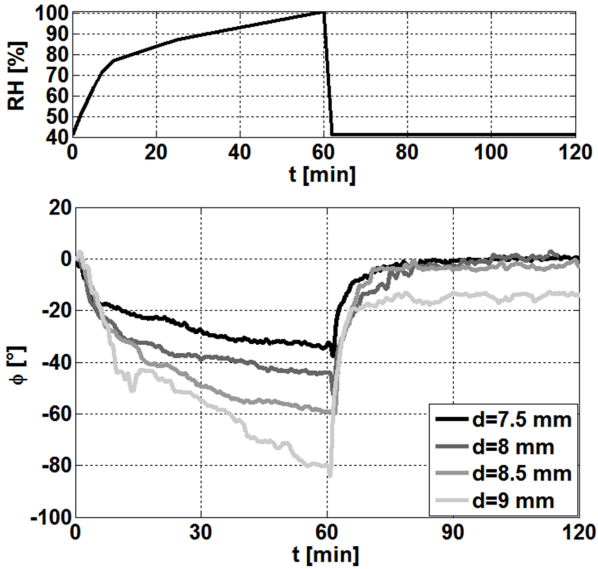

Figure 8.10.: Top) Relative humidity, measured by a digital hygrometer, during one-hour exposure from ambient air (RH=40%) to saturated air (RH=100%) and one hour recovery. Bottom) Phase response (after processing) of the test tag for different tuning conditions through the size d of the shorting stripes.

$d = 8.5mm$ and $d = 9mm$ (Fig. 8.11 C and D), probably due to a different speed of the sensor responses with respect to the change of humidity that, in the last two cases, would have required a larger exposure time to reach the saturation.

All the measured calibration curves appear almost linear from RH=40% to 100%, but with different slopes. It is therefore possible to extract the phase-sensitivities from 2.16, listed in Tab. 8.2, that span from 0.6 to 1.4 deg/RH depending on the selected tuning stripes' size. As predicted by simulations, the most sensitive tag configuration was that with d=9mm.

Table 8.2.: Sensitivities [°/RH] of measured phase variation.

$S\,[\varphi]\ [°/RH]$				
$RH_{low}-RH_{high}$	$d = 7.5$ mm	$d = 8$ mm	$d = 8.5$ mm	$d = 9$ mm
40% - 100%	0.6	0.75	1	1.4

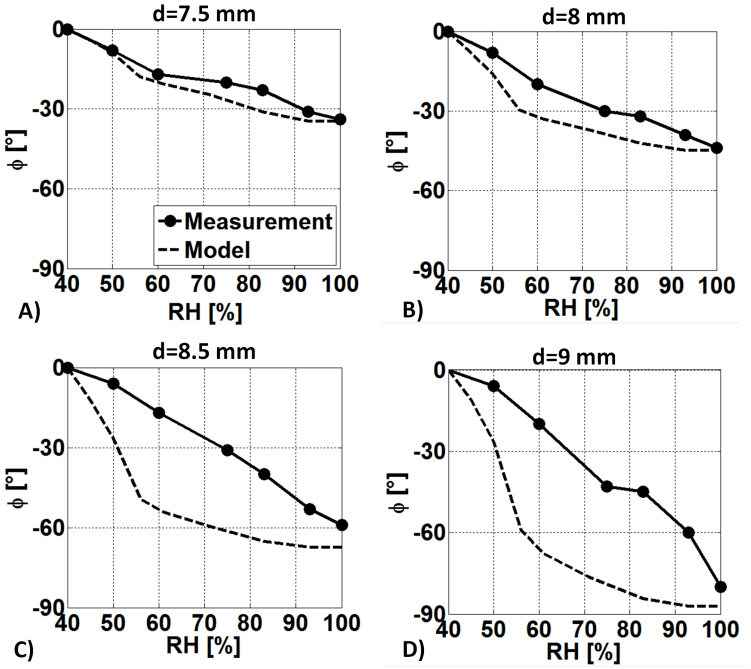

Figure 8.11.: Calibration curves $\Delta\varphi \leftrightarrow RH$ corresponding to the response in Fig. 8.10 and comparison with theoretical profiles obtained by the circuit model, considering four different sizes of the shorting stripes.

8.3. A Real Application

To discuss the response of the proposed humidity sensors in realistic conditions, one of these has been finally applied to monitor an overnight exposure. The Pedot:PSS loaded tag (case D of Fig. 7.5) has been placed outside an external wall and interrogated by the RFID reader installed on the inside with its antenna attached on the inner side of the windows. The distance between reader and tag is such to enable a robust RFID communication regardless the humidity grade**.** The RH and temperature levels have been monitored by means of a digital hygrometer placed outside, in close proximity of the tag. The experiment started at 6 p.m. in the evening on November 21st 2011 in Rome and ended at 2 p.m in the afternoon on November 22nd. The temperature was relatively stable in a range between 13°C and 17°C.

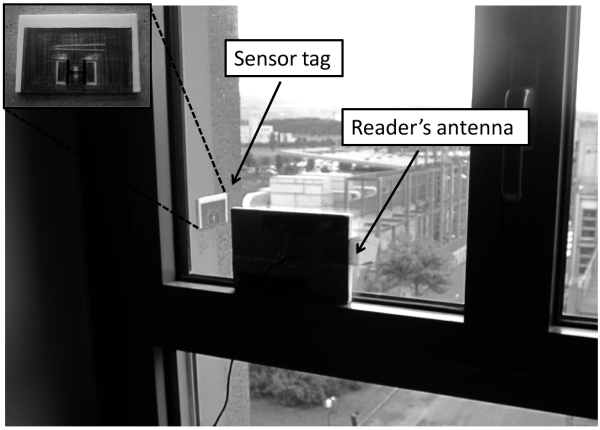

Figure 8.12.: Measurement set-up for the overnight humidity exposure.

The results in terms of normalized turn-on and backscattered power are shown in Fig. 8.13 at 880MHz. The tag's responses reasonably follow the profile of humidity during both increase (night) and reduction (morning). The dynamic range of variation of the sensor is

2.5dB for turn-on power and 3dB for backscattered power between the minimum (55%) and the maximum humidity (70%) detected during the night.

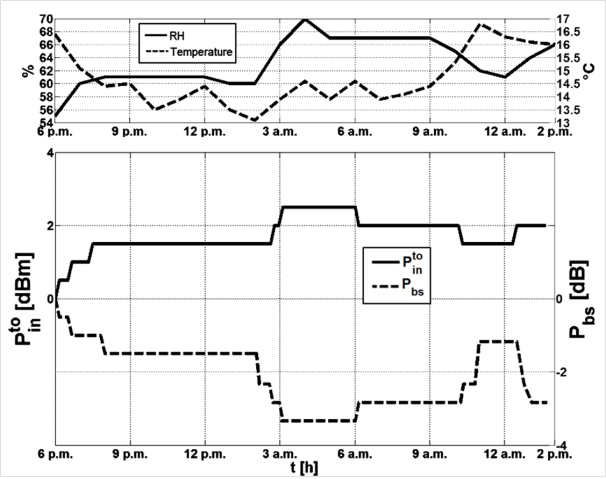

Figure 8.13.: Top) Measured external temperature and humidity variation during the night. Bottom) Measured normalized turn-on and backscattered power at 880 MHz during the overnight humidity exposure obtained with a moving window filter interpolation.

8.4. Discussions and Conclusions

It was demonstrated that the equivalent lumped-element model of the chemical loading in parallel to the IC (proposed in chapter 3) can be used to predict the sensor's response to the gas exposure. The dynamic range of the sensed data can be easily controlled by simple geometry tuning while reducing the degradation of energy scavenging, and hence of the read distance. It was moreover proved that not only signal amplitude-related parameters, but even the phase response of a chemically coated passive RFID tag may be

engineered to carry information about the change of the external environment.

When loaded with PEDOT:PSS for the detection of humidity concentration, the proposed sensor is able to provide a sensitivity of up to 0.4 dB/RH for power oriented sensing or up to 1.4°/RH for phase oriented sensing, at the cost of just a single polymer drop deposited right next to the microchip. Moreover, the water absorption is mostly completely reversible, and multiple measurements demonstrated a good repeatability at different days and conditions.

The experimental campaign on phase sensing revealed that a few signal processing (phase unwrapping and low-pass filtering) is required to reduce fluctuations and measurement artifacts. The resulting differential phase profiles are however rather insensitive to the set-up arrangement. The best considered tag antenna permitted to achieve up to 80° phase dynamic range constrained to $\tau > 0.5$.

It is worth comparing the performance of phase-based sensing with those of signal amplitude-based measurement over the same sensor tag, concerning the turn-on power (P_{to}^{in}) and the backscattered power (P_{bs}). The meaningful parameter for the final user is the resolution in humidity sensing δ_{RH} (in percentage) that is related to the dynamic range (DR) of the measured data and to the intrinsic resolution of the reader (δ_R). The interesting resolution can be hence computed as

$$\delta_{RH} = \frac{\Delta RH}{DR}\delta_R \tag{8.1}$$

being ΔRH the span of the humidity change in the experiments (here 40% to 100%). Results are reported in Tab. 8.3: It is visible that the resolution of the phase metrics is fully comparable with those of power metrics but with a substantially superior read performance.

Table 8.3.: Comparison among phase-based and power-based sensing for $\Delta RH = 60\%$

metrics	**DR**	δ_R	δ_{RH} [%]	**read range (r.r.)**
φ	82°	2°	**1.5**	$> 70\%$ max r.r.
P_{to}^{in}	17dBm	0.5dBm	**1.7**	$< 20\%$ max r.r.
P_{bs}	23dBm	0.8dBm	**2**	$< 20\%$ max r.r.

It is finally worth noting that SMs generally suffer from cross-sensitivity, e.g. they could react to multiple volatile compounds. Thus, the single device should be used in case a unique and known volatile species is present, as it happens in some controlled industrial processes. For a more general and un-controlled applications, instead, this class of RFID sensors can be arranged within a sensor array doped by different SMs forming a radio-chemical nose, as will be shown in next chapter.

9. RFID Array for Multi-Gas Detection

In previous chapters it has been demonstrated that tags coated by a proper sensitive layer are capable to sense some volatile compounds. The issue of cross-sensitivity and the possibility to develop an array of differently coated RFID sensors was not solved. This chapter investigates, through an experimental campaign involving the general-purpose sensor-antenna transducer introduced in sec. 4.2.3 and chapter 8, the potentiality of functionalized tags in the UHF RFID band to sense a multiplicity of volatile compounds, as well as the cross-sensitivity effects of different coatings in array configuration.

From experimentations presented in previous Chapters, it is was demonstrated how the variation of humidity can be measured at radiofrequency by using the PEDOT: PSS [83], [84] whereas the concentration of ammonia can be detected by SWCNT (Single Wall Carbon Nanotubes) [14]. In order to apply these RFID sensors to the real world, however, the uncertainty's problem of the response cross-sensitivity to different volatile compounds remains open. The examples presented up to date have mainly concerned with the detection of single volatile compounds. It is recommendable to study the performance of such sensors in real environment where mixtures of several gases are present. The problem of specificity is a common issue in chemical sensors. A typical solution, when specificity cannot be achieved, is the multiplication of sensors elements in order to form an array for the quantification and the identification of the mixture components. The important requirement for an array is that each sensor has a different selectivity. After the simil-

itude with natural olfaction, the arrays of gas sensors are typically nicknamed as "electronic noses" [12], [75].

In this chapter the potentiality of chemically functionalized tags working in the UHF RFID band (865-956MHz) and in particular the cross-sensitivity effects of different sensitive layers are analyzed. The very final goal is to set up the basis of array-oriented wireless passive sensors for the multivariate identification of vapors and gases.

The highly sensitive miniaturized planar RFID tag, already presented and characterized for humidity sensing in chapter 8, is used as a wireless transducer for a repeatable and uniform characterization procedure of different sensitive coatings exposed to different gases. Four effective materials such as Pedot:PSS, Doped PSS, SWCNT and PDAC revealed in sec. 7.2 a remarkable sensitivity to ammonia, ethanol, octane and water. Wireless sensing may be hence performed by narrow-band processing of the power response of the RFID tags as well as by the broadband extraction of features related to the resonance shift. The four sensors were used as an array and characterized by exposing them to saturated pressure of the four analytes of interest. It was finally observed how the inter-antenna coupling may affect the sensor capability of an array of UHF tags in terms of increased cross-sensitivity.

9.1. Univariate analysis

Pedot:PSS, Doped PSS, SWCNT and PDAC loaded tags selected from the procedure shown in sec. 7.2, were subjected to cyclic tests in order to appraise the reproducibility, dynamic ranges, response speed and the selectivity to the four gases under test. Three dilutions in dry air of the saturated pressure $\{50, 80, 100\}$ of water, ethanol, ammonia and octane, alternated with recoveries with the carrier gas (dry air) were fluxed in the measurement cell (Fig. 7.1). Each sensor was tested individually. The exposure time was fixed to 30 minutes while the recovery was 1 hour and 30 minutes. Each tag was interrogated by the reader at the frequency within the RFID worldwide band (860-960 MHz) where, case by case, the turn-on

power was minimum (corresponding to optimal read-range performance).

Fig. 9.1 and Fig. 9.2 show the measured variations of the turn-on power P_{in}^{to} (column A) and the analog identifier AID (column C) vs. time normalized to their initial values, with respect to the variations of the gas under test. Signals have been processed by a numeric low-pass FIR (Finite Impulse Response) filter with N=48 order at the purpose to remove the noise produced by the reader and the external environment. The maximum dynamic ranges are

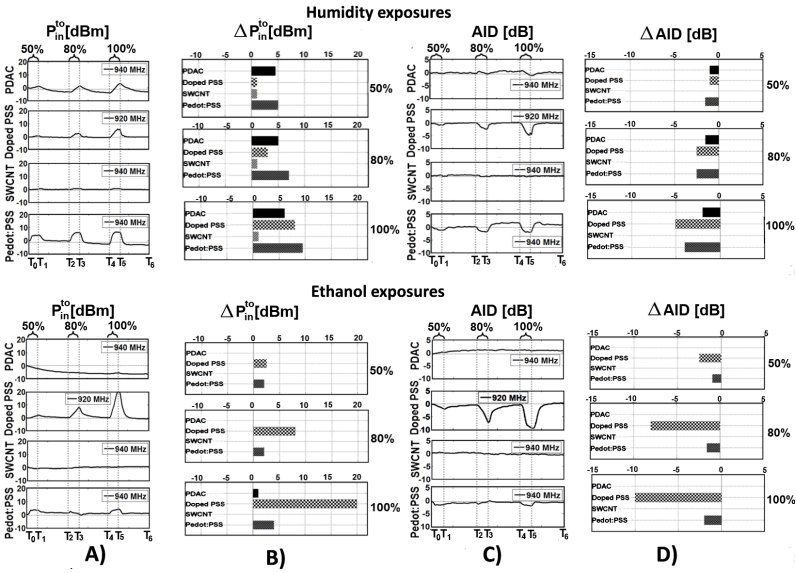

Figure 9.1.: A) - C) Measured variations of the normalized turn-on power and AID vs. time of the four chemical doped RFID sensors when exposed to 50% (between T0 - T1), 80% (between T2 - T3) and 100% (between T4 - T5) of humidity and ethanol, . Recovery by fluxing dry air takes place in T1 – T2, T3 – T4 and T5 – T6. T0=0min, T1=30min, T2=120min, T3=150min, T4=240min, T5=270min, T6=390min. B) - D) Measured Dynamic Ranges of the turn-on power and AID of the four chemical doped RFID sensors during dynamic exposures to 50%, 80% and 100% of humidity and ethanol.

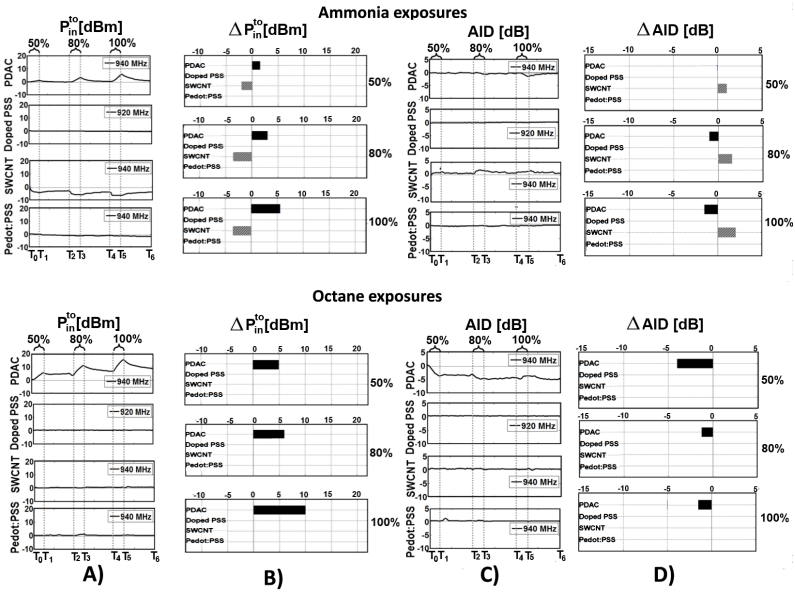

Figure 9.2.: A) - C) Measured variations of the normalized turn-on power and AID vs. time of the four chemical doped RFID sensors when exposed to 50% (between T0 - T1), 80% (between T2 - T3) and 100% (between T4 - T5) of ammonia and octane. Recovery by fluxing dry air takes place in T1 – T2, T3 – T4 and T5 – T6. T0=0min, T1=30min, T2=120min, T3=150min, T4=240min, T5=270min, T6=390min. B) - D) Measured Dynamic Ranges of the turn-on power and AID of the four chemical doped RFID sensors during dynamic exposures to 50%, 80% and 100% of ammonia and octane.

particularly remarkable for the couplets {Pedot:PSS, Humidity}, {PDAC, Octane}, {Doped PSS, Ethanol} wherein they span from 10 to 20dB. The AID curves, instead, have opposite trends and lower dynamic ranges with respect to the turn-on ones.

By applying a linear regression to the set of peak values of indicators corresponding to the three concentrations {50%, 80%, 100%} in Fig. 9.1 column B), D), it is finally possible to evaluate the sensitivity of each sensor defined in Tab. 9.1 as the slope of the linear regression (sec. 2.3). It is worth to notice that the couples {Pedot:PSS, Humidity}, {PDAC, Octane}, {Doped PSS, humidity}, {Doped PSS, Ethanol} gave maximum sensibility values, compatible with the resolution (0.1dBm) nowadays achieved by several state of the art readers.

Table 9.1.: Sensitivities $[dB/\%]$ of measured turn-on power and Analog Identifier

	$S[P_{to}^{in}]$				$S[AID]$			
	Moisture (50-100%)	**Ethanol (50-100%)**	**Ammonia (50-100%)**	**Octane (50-100%)**	**Moisture (50-100%)**	**Ethanol (50-100%)**	**Ammonia (50-100%)**	**Octane (50-100%)**
PDAC	0.05	0.02	**0.10**	**0.09**	0.02	0	0.03	0.01
Doped PSS	**0.13**	**0.35**	0	0	0.08	0.15	0	0
SWCNT	0	0	0.04	0	0	0	0.02	0
Pedot:PSS	**0.09**	0.04	0	0	0.05	0.02	0	0

9.1.1. Frequency domain analysis

A frequency-domain analysis was then performed in the (840MHz-960MHz) band at the purpose to better understand the phenomena of gas sensing by UHF RFID tags. The minimum of turn-on power is located at the frequency where the tag absorbs the maximum power, i.e. in resonance condition. The frequency responses to gas exposure in Fig. 9.3 show three different profiles. SWCNT v.s. ammonia produces only a change (decrease) in amplitude, proportional to the concentration of ammonia, while the resonance frequency remains almost unchanged all along gas exposures. The coating has in this case a dominant resistive behavior. Conversely, doped PSS v.s. water vapor shows instead an upward shift of the curves, and hence of the resonance frequency, while the minimum

turn-on power remains mostly stable during gas exposure. This coating can be hence considered as having a dominant capacitive behavior when exposed to water. Finally, PDAC v.s. ammonia combines the above two effects, e.g. produces both a shift towards lower frequencies and an increment of the minimum turn-on power proportional to the gas percentage, and hence can be regarded as a resistive-capacitive coating. Fig. 9.3 right finally shows the normalized variations of the resonant frequency and of the amplitude of turn-on power at resonance. In the countries where the RFID UHF band is sufficiently broad, as in USA (902 – 925 MHz), it is thus possible to perform sensing by also exploiting the frequency behavior of the tag.

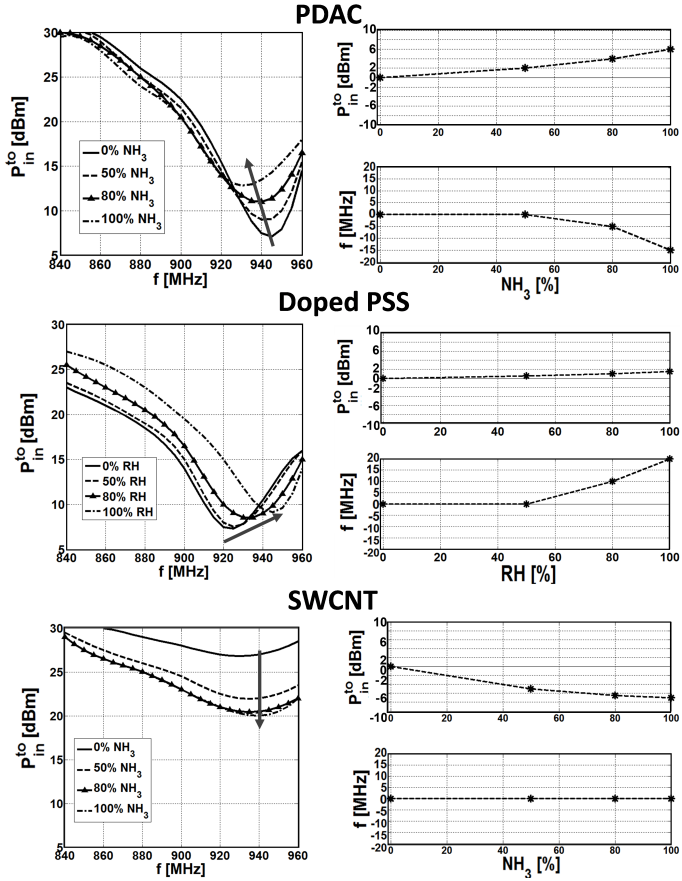

Figure 9.3.: Left) Measured turn-on power curves vs. frequency of PDAC exposed to ammonia, doped PSS exposed to humidity, and SWCNT exposed to ammonia. Right) Measured normalized variations of the minimum turn-on power and the operative central frequency as a function of the gas under test concentration.

9.2. Array Configuration

The four sensors were finally all placed inside the measurement cell at a same time in order to form an RFID sensor array as in Fig. 9.4. Tags #1 and #2 are aligned along the H-cut of the slot patterns, while tags #1 and #3 are aligned along the E-cut. The proximity of sensor tag antennas is a potentially source of uncertainty. Collision among RFID responses and inter-tag electromagnetic couplings are indeed expected to potentially modify the tag response with respect to isolated condition and definitely increase the cross-sensitivity of each sensor.

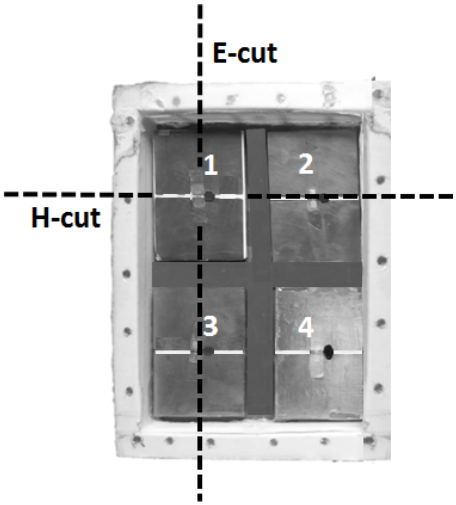

Figure 9.4.: Array of four sensor tags loaded by PDAC, doped PSS, SWCNT and Pedot:PSS, inside the measuring cell.

Packing many RFID tags in a limited space demands for special mathematical models as in [38]. A first-order estimation of the proximity effect is anyway obtained by the simulated scattering matrix $[S]$ whose independent elements are shown in Fig. 9.5. The maximum coupling arises between tags aligned along the E-cut (S_{13}) while coupling among tags placed along diagonals (S_{23}, S_{14}) are 7dB below. The array was then exposed to saturated percent-

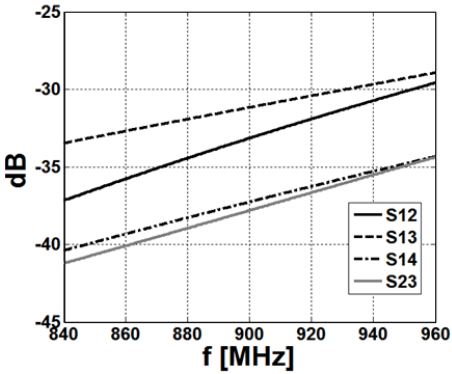

Figure 9.5.: Scattering parameters of the simulated array of blank tags.

ages of the four analytes of interest. Fig. 9.6 right shows the maximum variations of the turn-on powers at 940MHz after 30 minutes of exposure. As expected from the previous univariate analysis, the maximum responses were again obtained for the couples {Pedot:PSS, humidity}, {doped PSS, ethanol}, {SWCNT, ammonia} and {PDAC, octane}. These diagrams have to be compared with the ones in Fig. 9.6 left referred to standalone tags. The increase of cross-sensitivity is clearly visible in all the four exposures. For example, the octane that was detected by the only PDAC-loaded sensor, is instead revealed also by SWCNT- and Pedot:PSS-loaded sensors in case of the array configuration. The resulting sensing patterns are however highly different to each other, with interesting possibility to set-up a classification procedure.

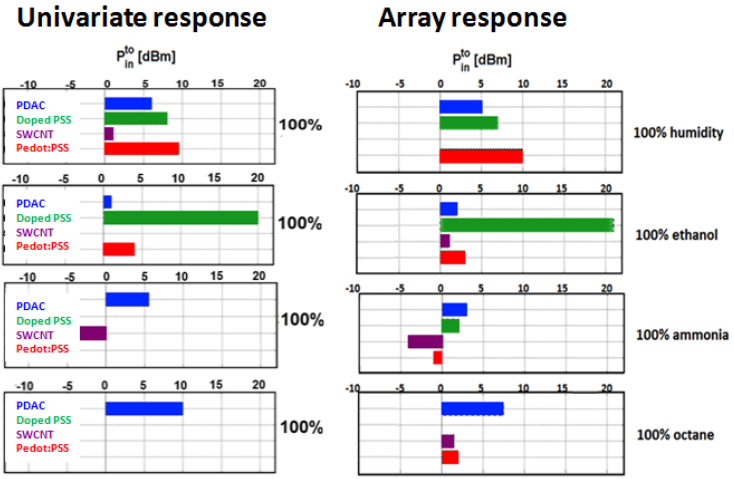

Figure 9.6.: Univariate (left) and array responses (right) in term of turn-on powers changes as exposed to the four analytes of interest.

9.3. Conclusions

This Chapter showed a detailed characterization of four coating materials, suitable to integration into an UHF RFID sensor array. Pedot:PSS, Doped PSS, SWCNT and PDAC revealed significantly sensitive, at different extent, to the tested volatile compounds: water, ethanol, ammonia and octane.

Sensing may be performed by measuring the variation of turn-on power or Analog Identifier at fixed frequency, as well as, by evaluating, in that countries allowing an RFID broad band interrogation, the changes of some frequency domain features such as the resonant frequency and the minimum value of the turn-on power. Packing four RFID sensors into a compact array induces an increase in cross sensitivity of each tag, because of the electromagnetic coupling, that should be accounted for a future classification procedure. Results look encouraging, even if a non-negligible effort is still needed to better characterize the sensor responses, due its slow speed, so

that the saturation was not always met in all the experiments. It was moreover apparent that the coatings were subjected to deterioration during the repeated exposures as a result of permanent chemical and mechanical interaction with the vapors. Thus, additional investigation should to be devoted to fabrication modality in order to achieve more reproducible and stable molecular films.

10. Conclusions and Future Research

The theoretical and experimental investigation proposed in this Thesis has drawn a possible path to focus the RFID research and technology to an IoT-based environment monitoring. The scientific contribution regarded mainly the development of completely new typologies of RFID passive sensors. Starting with a theoretical approach, the physics of the phenomena were investigated in detail for the particular case of Sensitive Material-loaded tags. Particular effort was given to merge very different fields such as Electromagnetism, Sensors and Materials. The criterions proposed for RFID sensing rely on power measurements, such as the turn-on power and the backscattered power collected by the reader, and on impedance-related parameters, such as the Analog Identifier and the phase. From the synergic study of all the sensing parameters and the investigation of functionalized RFIDs, such as distributed or lumped loaded tags, completely new techniques were introduced to fully master the RFID tag response. General properties and limitation of sensing have been explored by the help of equivalent circuits for parallel and series interconnections of lumped elements to the IC, while data processing issues, the achievable dynamic ranges, sensitivities and the measurement reproducibility have been investigated by means of numerical analysis and experimentations. Several case of studies concerning temperature, humidity and gas sensing were analyzed with the help of specialized antennas' layouts. It was therefore demonstrated that a functionalized passive RFID tag may be engineered to carry information about the change of the external environment. Moreover by the help of the equivalent circuit models it is possible to easily control the dynamic range of the sensed data while reducing the degradation of energy scavenging, and hence of the read distance. Great attention was

therefore given to balance the two opposite requirements, e.g. to pursue the maximum sensitivity at the minimum degradation of the communication.

While it is possible to find some electrical information about sensitive materials in DC, no significant data are currently available in the UHF RFID band, thus a specific characterization procedure was introduced for the first time to achieve the electrical properties and specificity to different measurands at RF. Several sensitive materials were tested in order to characterize the effects on communication and sensing performance of the sensor tags.

The integration of several passive sensitive materials onto the tag enabled the observation of key parameters ranging from temperature to gas sensing, necessary to the remote monitoring of environment in several scenarios. The amount and the proper displacement of the chemical materials into the sensing slots for vapours sensors tags was proved to be an effective parameter that changes the communication/sensing performances. The achieved sensitivities are higher than the state-of art of passive UHF RFID sensors and the communication performance degradation was kept under control.

In order to apply these ideas to the real world, however, the uncertainty's problem of the response cross-sensitivity to different environmental parameters was an obstacle to overcome. The examples presented up to date in literature have mainly concerned with the detection of a single measurand. A first attempt to solve the problem was given in this Thesis by the multiplication of sensors elements in order to form an array for the quantification and the identification of temperature and mixture gas components. In this way it was possible to set up the basis of array-oriented wireless passive sensors for the multivariate identification of vapors and gases. However, the increase in cross-sensitivity of each tag due to the proximity of the array elements, because of the electromagnetic coupling, should be accounted for a future classification procedure.

All the designed working prototypes corroborate the idea that, even if passive sensing architectures could sometimes suffer from weak sensitivity and poor selectivity, they can however offer great advantages in term of cost, reliability and scalability. They result extremely useful when traditional and powered solutions can not

be feasible, e.g. when the monitoring period is particularly long and complex or when sensors need to be integrated into daily objects or to be pervasively embedded into infrastructures. In these cases the sensors must be passive such to guarantee their "transparent" action for long period, without the need of maintenance.

In spite of the many advantages, several issues are still open and even challenging, especially concerning the reliability of the sensors and the true autonomy of the reader's node. Moreover, many other possible research paths may be currently envisaged, based on the fruitful synergy between the Material Science and the Electromagnetism potentiality to develop, in the next years, new devices and new knowledge. The promising results disclosed several unsolved questions and future research perspectives:

1. Chemical sensors still require to be mastered to gain a full reproducibility of deposition, stability of performance and resistance over time. A dedicated research activity, involving a strong interactions with chemical engineers, is required to set-up a more standardized procedure to characterize SM at radiofrequency, in order to provide an extensive database of useful chemical receptors and their sensitivity to a meaningful set of volatile compounds.
2. It is currently unknown if the SM-based RFID sensors would provide meaningful data set in case of placement into real environments. They are exposed to dust and dirty and to random and unpredictable change of environmental parameters such as temperature and humidity as first. Further theoretical and experimental efforts are hence required to make data retrieval and processing more robust at the purpose of more accurate data-inversion procedures.
3. Beside the technological issues, extensive experimental campaigns should be planned over medium scale against reference data-set to compute statistics and estimate the overall accuracy and resolution of this class of sensors.
4. The readers are currently a serious bottleneck in the massive adoption of RFID in IoT-based environment monitoring since most of available models are only oriented to logistics, e.g. to provide the ID of the tag rather then to produce stable

power and phase signals with high resolution. Furthermore, they exhibit high cost and usually require a PC-network infrastructure to work with. A true integration of RFID technology into an IoT infrastructure would instead require a full RFID node with autonomous computation power and wireless data connectivity toward the cloud. Hand-held, fully autonomous readers are already available, but they are nevertheless still overpriced and underperforming. Even tethered low-cost readers are 3-4 times more expensive than a WI-FI router, that should be considered as a cost target. Possible solutions could exploit the integration of low-cost embedded systems such as Arduino and Raspberry Pi, but specific research effort should be devoted to identify processing architectures and common interfaces. The true diffusion of these systems may probably happen when smart phones will be used as UHF RFID readers. Several of them already integrate the HF RFID interfaces and it is reasonable to expect that soon they will be equipped wit more RF interfaces, including the UHF RFID dedicated one.

5. Finally, in spite of the EPC is a standard protocol, the proprietary software libraries for the control of readers are heavily manufacturer-dependent so that a general purpose, and possibly open-source development framework could really simplify the design and implementation of high level applications.

Appendix A: Other Research

Passive Temperature Radio-Sensors for Concrete Maturation Monitoring

> A planar "T" like passive UHF RFID temperature sensor is here proposed for application inside the fresh concrete at the purpose to hydration monitoring during the curing procedure into caissons.
>
> Since the concrete's electromagnetic parameters significantly change along with the drying process, the antenna modeling and design consider both the electromagnetic and the chemical phenomena.

Wireless monitoring of civil infrastructures health during construction and lifetime, is nowadays collecting growing interest in the emerging paradigms of Wireless Sensor Networks and Internet of Things [85]. Majority of civil structures are built by assembling precast concrete blocks (segments), which are transported to the construction site after casting and curing. Curing is the process wherein the concrete is protected from loss of moisture and kept within a reasonable temperature range. The result of this process is an increased strength and decreased permeability. The accelerated curing, instead, consists in heating the ashlar of fresh concrete according to a controlled manner so that the artifact develops good mechanical strength in a few hours, rather than after the conventional 28 days [86]. This process known as *"curing concrete"* brings significant economic benefits, it speeds up the fabrication process and increases the reliability of the structures. It is crucial, however, to monitor the internal temperature in order to be able to adjust the oven heating during the process and accordingly to control the maturation of the block. Moreover, starting from temperature in-

formation, it is possible to derive parameters such as the degree of hydration, and the mechanical properties of the block. Conventional monitoring methods involve thermocouples which measure the temperature at the center of the ashlar. The technological limits are the high costs and the presence of cables that must be removed when the process is completed. For these reasons, the maturation quality of the ashlar is checked only for some samples.

Battery-less and wireless RFID technology could instead enable a true pervasive displacement of temperature sensors for concrete. Temperature RFID analog sensors have been presented previously in this thesis with their potentialities and current issues. However, a true spread of the autonomous RFID temperature sensing will be probably boosted by a new family of RFID microchips equipped with an integrated temperature sensor and with a local Analog to Digital Converter [25]-[26]. Accordingly, the temperature information is read from the tag straight away in a digital form.

Fig. .1 describes possible scenarios, where RFID-powered systems could support pervasive temperature sensing for curing concrete applications. A distributed network of battery-less tags with sensing capability is wirelessly interrogated by hand-held or fixed RFID readers during all the maturation process. The use of passive RFID temperature sensors in the UHF band, that are directly embedded into concrete ashlars for structural health monitoring, is instead still an unbeaten path.

This contribution presents a novel design of a passive RFID temperature sensor suited to deep integration into concrete. The tag's layout includes an external radiative part connected to a two-conductors transmission line immersed inside the concrete. Sensing is performed by the EM4325 IC [25] able to work as conventional RFID transponder as well as to provide temperature measurements in the [-40°C,+64°C] range (in passive mode) with a resolution of 0.25°C. Computer simulation and then extensive laboratory experimentation in real conditions demonstrated that, despite of the low sensitivity of the IC and the high losses of concrete, the proposed RFID sensor tag provides reasonable communication performance in passive mode with read ranges up to 2 meters, and fast and reliable temperature sensing capabilities that look comparable with that of more invasive and costly wired measurement systems.

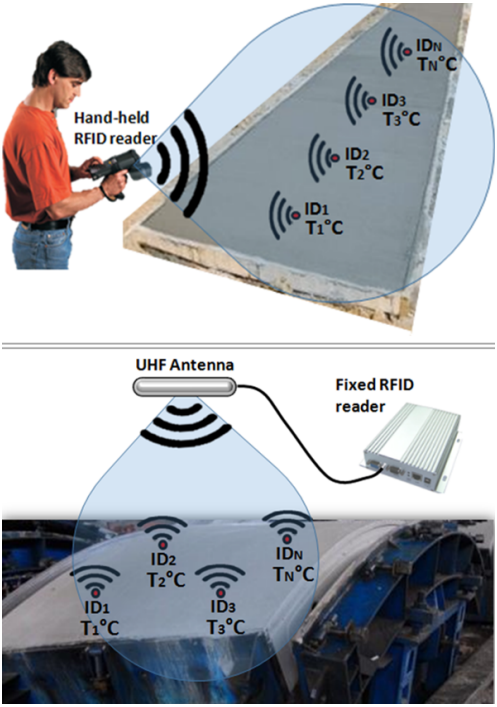

Figure .1.: Scenarios of RFID-powered systems for curing concrete monitoring: RFID passive sensors buried within concrete are wirelessly interrogated by hand-held readers (top) for applications such as the spritz beton in galleries, or by fixed readers (bottom) for temperature monitoring during the ashlar heating inside ovens.

RFID Communication in the Concrete

Concrete is a mixture of cement, water and aggregated composites. A malleable compound is obtained by mixing proper amounts of each constituent, which naturally gets the final mechanical strength in approximately twenty-eight days. The casting of fresh concrete is directed in form-works of the desired shape, usually made of wood, plastic or steel.

It is well known how the electromagnetic field is highly affected by the dielectric properties of the medium: Since concrete is a lossy material, its influence on RFID antennas working in close proximity to it needs to be carefully taken into account. Concrete dielectric properties, such as the permittivity $\varepsilon(T, m, p, f, \frac{w}{c}, c)$, and the conductivity $\sigma(T, m, p, f, \frac{w}{c}, c)$, are generally related to the temperature T, the external humidity m, the frequency f, the time t spent from casting, the location p, the water-cement ratio w/c and the type of cement c.

The dielectric properties of concrete are available from [87, 88, 89] for different ranges of frequencies and degree of hydration h_y, i.e. the ratio between the amount of hydrated cement and the initial amount. By fitting data from previous references it is possible to estimate the trend of conductivity and permittivity at UHF frequencies during concrete maturation process (Fig. .2), which will be used in the following numerical analysis. It is worth noticing that while the conductivity decreases proportionally to the degree of hydration, the trend of the permittivity is not monotonic and reaches its peak at about one-fifth of the maturation process.

The aim of the proposed RFID sensor is to ensure the communication with the reader while performing temperature measurements at the center of the ashlar of concrete. In order to preliminary evaluate the performance of an RFID tag designed to work in close proximity of the concrete, two configurations were simulated by a MOM solver: a $\lambda/2$ dipole in air lying at the concrete-air interface and the same antenna immersed 15 cm deep inside concrete (Fig. .3 top). Fig. .3 bottom shows the computed radiation gains along the *z>0* direction. It is clearly visible how the maximum gain of the dipole immersed in concrete is below -100dB making this device completely unreadable from outside. The dipole placed on the in-

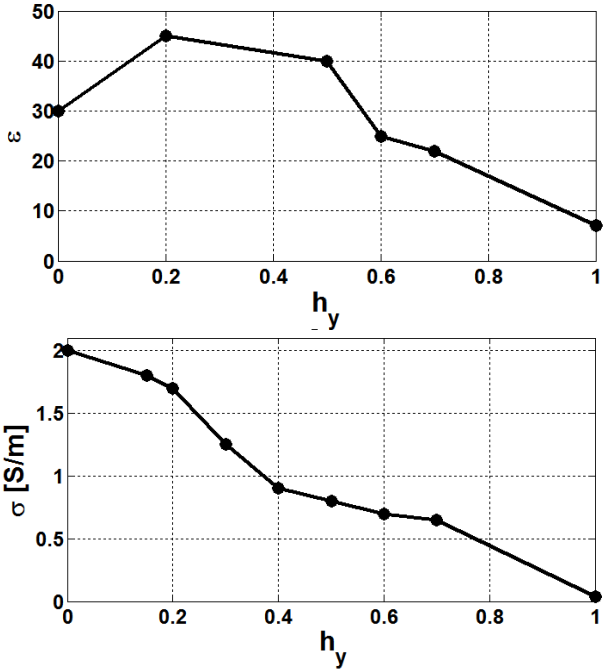

Figure .2.: Top) Permittivity of concrete vs. degree of hydration (f=868MHz); bottom) conductivity vs degree of hydration (f=868MHz).

terface concrete/air exhibits instead a gain of the order of -10dB and more, that may enable in principle the communication with a remote reader.

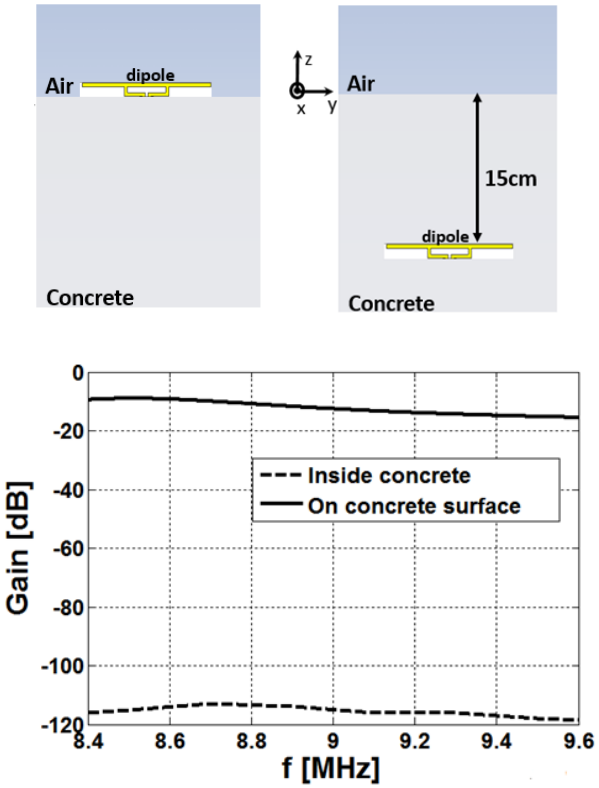

Figure .3.: Top) $\lambda/2$ dipole antennas simulation set-up. Concrete was simulated with a degree of hydration $h_y = 0.5$ (see Fig. .2), having infinite dimensions in x and y directions; Bottom) simulated gain along the $z>0$ direction in the UHF global RFID band of the two dipoles.

Design of the Probe-tag Temperature Sensor

To sense the concrete temperature at the required depth a probe-augmented T-match dipole is here considered. The antenna structure (Fig. .4) includes three physical and functional blocks.

1) A harvesting part, that is external to concrete, consisting of a simple dipole antenna able to collect the electromagnetic energy radiated from a reader. The antenna lies on a dielectric slab, a 4mm-thick Forex substrate ($\varepsilon_r = 1.55$ and $\sigma = 6 \times 10^{-4} S/m$) which acts as mechanical support. The dipole is connected to a T-match which plays as input impedance adapter in order to balance the chip impedance and ensure the maximum power transfer.

2) A probe consisting of a two-conductors transmission line made by parallel tracks (microstrips) connected to the T-match of the dipole. The line is suited to convey the energy collected by the antenna to the inner part of concrete. The strips are insulated from both sides by the same Forex slab where the antenna is placed in, at the purpose to prevent an excessive degradation of the communication performance. The two conductors are placed at a distance $d < \frac{\lambda}{100}$ such that their overall radiating effect is negligible. In order that all the power is transferred from the antenna to the load (i.e. the microchip), the length of the line lf must be a multiple of $\lambda/2$ in the medium. Therefore, the line is a balanced structure, whose length was designed, in first approximation as $lf = \frac{1}{2}\frac{\lambda}{\sqrt{\varepsilon}}$, with ε permittivity of concrete at an intermediate stage of maturation $h_y = 0.5$, and subsequently tuned and optimized by electromagnetic simulations.

3) The EM4325 microchip placed at the line termination having the functionality of radio, data storage, and temperature sensor. The IC position inside concrete defines the point of temperature sampling. The EM4325 is a device of size $6.4mm \times 3mm$ (version TSSP08) having impedance $Z_{chip} = 23.3 - j145\Omega$ at 868MHz and power sensitivity $P_{chip} = -8dBm$ in passive mode). The temperature sensor integrated in the chip exploits the principle of the link current-voltage transistor, enabling temperature monitoring in the range [-40°C, +64°C] with 0.25°C resolution in passive mode. The

temperature RFID tag will be hereafter denoted as *T-Tag*.

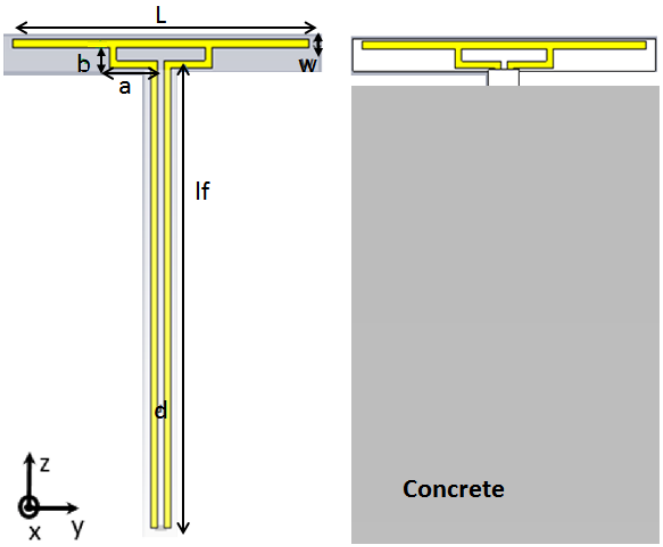

Figure .4.: Layout (left) of the probe-tag sensor on 4mm-thick Forex substrate for placement inside the concrete (right).

The communication performance of the T-Tag have been evaluated in terms of the realized gain. The T-Tag has been tuned to the EM4325 IC (by acting on the T-match parameters $\{a,b\}$) in the case of concrete's permittivity and conductivity corresponding to an intermediate hydration level $h_y = 0.5$, e.g. at half the maturation process. A power transmission coefficient $\tau = 0.95$ was achieved at 868MHz for an antenna with dimensions as in Tab. .1. Accordingly, the simulated realized gain (along $z>0$ direction) is shown in Fig. .5 top. The G_τ remains stable at a value of roughly -10dB till half the process dynamic range, while it improves of about 5dB at the end of maturation, due to the decrease of conductivity and losses of concrete (Fig. .2). By applying free space Friis formula, having considered the realized gain along $z>0$ direction and a reader's emitted power EIRP = 3.2W (the maximum allowed by regulations in Europe) in linear polarization, the estimated maximum reading

distance during the process is shown in Fig. .5 bottom. The reader-tag communication is therefore feasible up to 1m at every time and the maximum read range reaches almost 2 meters in case of dry concrete.

Table .1.: Size in [mm] of the parameters in Fig. .4.

L	a	b	w	d	lf
92	56	6	2	2	137

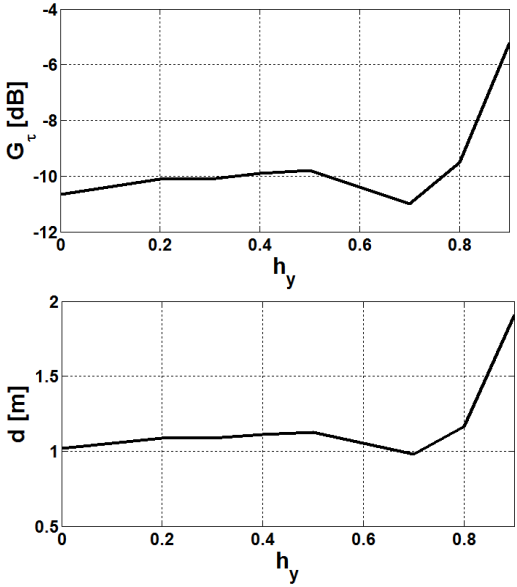

Figure .5.: Simulated realized gain (top) and estimated maximum read range (bottom) of the T-tag, as a function of degree of hydration (f=868 MHz).

Experimental characterization

Communication Performance

Several prototypes of the T-tag were fabricated for experimental tests. One of the T-tags was immersed in a caisson filled with fresh concrete to measure the realized gain in realistic conditions (Fig. .6).

The communication performance of the T-tag were characterized in terms of realized gain defined as in eq. 2.9, by means of both simulations and measurements in two different states of concrete maturation.

Measurements were carried out by means of the ThingMagic M5-e reader [55] driven by a proprietary control software. The reader's antenna was a broad-band 5dB linear polarized patch, placed 50cm away from the radio-sensor. The measured and simulated realized gain versus frequency are reported in Fig. .7 (tags and reader's antenna are aligned) for two considered degree of hydration: $h_y \approx 0$ (by measuring the tag immediately after the casting) and $h_y \approx 1$ (by performing the same measurement after one month of drying).

Measurements and simulations show good agreement, mainly at the reference European frequency 868MHz, where differences are less than 1dB. The estimated read range, for the case of 3.2W EIRP radiated by the reader, is about 80cm in case of fresh concrete ($h_y \approx 0$) and reaches over 2m in case of dry concrete ($h_y \approx 1$).

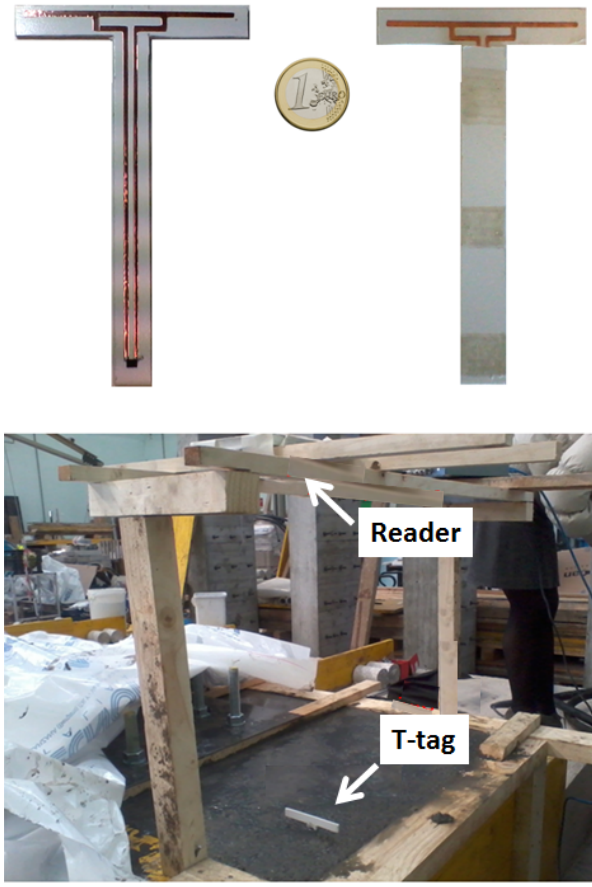

Figure .6.: Top) Prototypes of the T-tag and bottom) measurement set-up for communication performance characterization. Measurements were performed along the direction linking the tag to the reader.

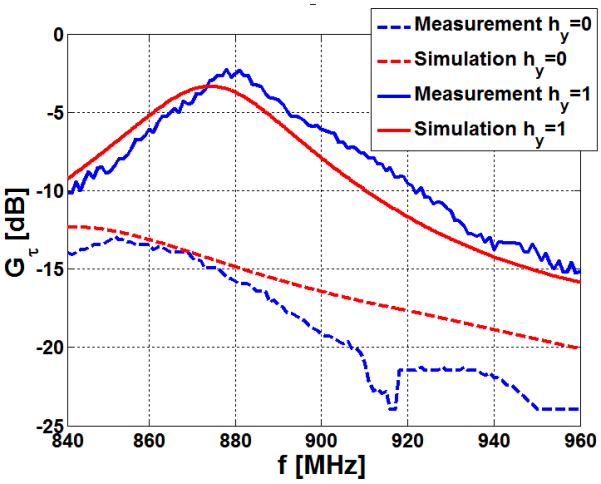

Figure .7.: Simulated and measured realized gains versus frequency in case of T-tag immersed in concrete and for two degrees of hydration.

Temperature Sensing

The temperature sensing capabilities of the T-tag were finally tested during the controlled heating of a cylindrical specimen of fresh concrete (diameter: 15cm; height: 30cm) placed inside an industrial oven (Fig. .8top). The T-tag was inserted into the concrete so that the RFID chip EM4325 was at 12cm depth. A K-type thermocouple was moreover placed in the same position to provide a reference measurement. Data acquisition from the thermocouple, was controlled by MGCplus of HBM, a modular system for laboratory and test benches, while the T-tag was wirelessly interrogated by the CAEN-Quark UHF reader [90], capable to establish the non-standard protocol for temperature acquisition and reading.

Immediately after casting, the specimen was exposed for 2 hours to ambient temperature and hence heated by a oven set to 50°C for approximately 3 hours. The reader's antenna was placed outside the oven, at 20 cm from the oven glass cover. Finally, the oven was turned off to analyze the cooling process. Fig. .8 bottom shows the measured temperatures of the RFID sensor and thermocouple. It is clearly visible how the temperature measured by the T-tag and the thermocouple exactly follow a same profile, with a maximum difference of less than 0.5°C all along the process, confirming the full reliability of the passive radio-sensor for concrete temperature monitoring applications.

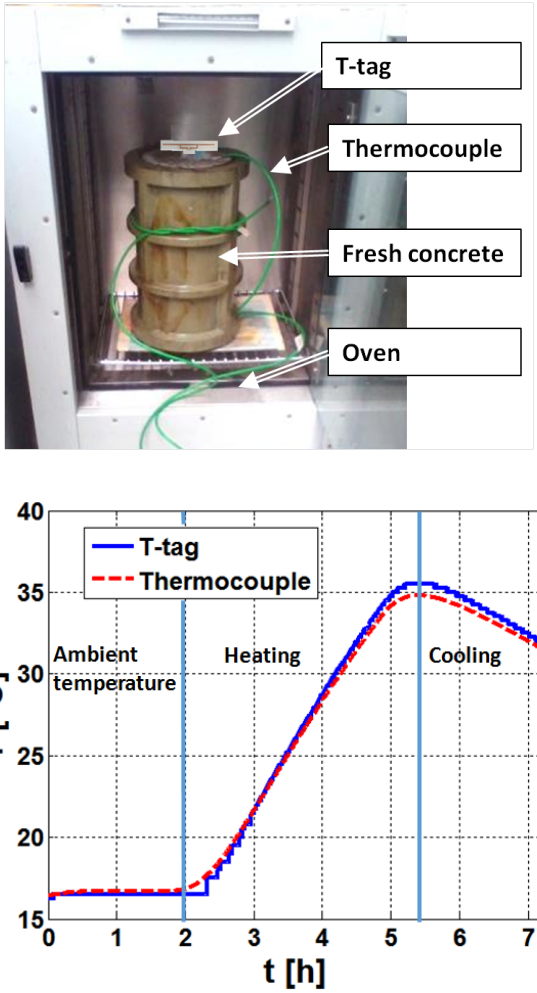

Figure .8.: Top) measurement set-up for temperature sensing inside concrete; bottom) temperature curves inside concrete measured by the T-tag and the thermocouple, during the heating/cooling process.

Conclusions

The proposed passive RFID sensor for thermal measurements inside the concrete has been obtained by a multi-physic modelling and design procedure fully accounting for the change of the electromagnetic properties of the concrete during hydration. The achieved sensor preserves reasonable communication performance suitable for short-range remote sensing all along the drying process and it is able to detect temperature variations inside concrete with a resolution of 0.25°C. From temperature measurements it is possible to derive fundamental parameters such as the degree of hydration and the mechanical properties. Current limits of the proposed tag concern the modest reading distance for fresh concrete (80cm) and the upper limit of temperature measured in passive mode (64°C). Improvements of the sensor are currently under research, by considering more reliable substrate materials to minimize production costs and maximize the resistance, and by experimenting new layouts with shielded transmission lines that are fully insensitive to changes in dielectric properties of the concrete.

Appendix B: Authors' Contribution

The Journals' article list [P-1]- [P-10] can be found in the "List of Pubblications and Awards" Section.

- [P-1] S. Manzari is the main contributor of the work. She designed the antennas, studied and analyzed the performance by simulations, measurements and system analysis. She wrote the article in collaboration with the second author C. Occhiuzzi. The co-authors helped in supervising the project and improving the text.
- [P-2] S. Manzari is the main contributor of the work. She designed, fabricated and measured the prototypes. She wrote the article. Co-authors helped in the supervision of the project.
- [P-3] A. A. Babar and S. Manzari are the main contributors of the work. The antenna is designed and fabricated by A. A. Babar, whereas, S. Manzari developed and characterized the substrates. A. A. Babar and S. Manzari collaborated in performing the measurements, experiments, analysis of the results, and co-authoring the text.
- [P-4] S. Manzari is the main contributor of the work. She implemented all the simulations, manually fabricated the RFID humidity sensor tags and carried out all the measurements and analysis contained in the article, regarding the RFID tag as antenna and sensor both. She implemented a procedure to characterize a sensitive polymer at radiofrequency during humidity exposure. Other coauthors' contribution regarded the supervision of the scientific work, the design of the antenna used as a sensor, the selection and integration of a moisture-sensitive polymer, the contribution in co-authoring and improving the text.

- [P-5] S. Manzari and S. Pettinari are the main contributors of the work. S. Pettinari designed the wearable tag during his master thesis under the supervision of S. Manzari. S. Manzari actively collaborated in the simulation analysis, the prototypes fabrication, the measurements and the analysis of the results. S. Manzari wrote the text.
- [P-6] S. Manzari is the main contributor of the work. She implemented all the simulations, manually fabricated the RFID humidity sensor tags and carried out all the measurements contained in the article. She performed the data analysis in comparison with the proposed models She implemented a procedure to characterize a sensitive lumped element at radiofrequency during a specific process to be monitored, such as humidity exposure. She wrote the text. Second author's contribution regarded the supervision of the scientific work and text improvement.
- [P-7] S. Manzari co-authored the text of this review article. She wrote the parts regarding the wetarable antennas and the chemical/temperature RFID sensors.
- [P-8] S. Manzari is the main contributor of the work. She performed all the simulations, fabricated the prototypes and tested them during different gas exposures. Co-authors helped in selecting different sensitive materials, preparing the chemical depositions on the tag and the measurements set-up, and supervising the work.
- [P-9] C. Occhiuzzi is the main contributor of the work. Author S. Manzari contributed by fabricating and measuring the hardware part of the Nightcare system, i.e. the wearable tags and the reader antenna. She wrote in the paper the corresponding text part.
- [P-10] M. C. Caccami is the main contributor of the work. She developed during Master thesis all the mathematical models for phase sensing and performed the measurements and data analysis. S. Manzari fabricated the prototypes, supervised the thesis work and co-authored the text.

Bibliography

[1] L. Atzori, A. Iera, and G. Morabito, "The internet of things: A survey," *Computer Networks*, vol. 54, no. 15, pp. 2787 – 2805, 2010. [Online]. Available: http://www.sciencedirect.com/science/article/pii/S1389128610001568

[2] J. Gubbi, R. Buyya, S. Marusic, and M. Palaniswami, "Internet of things (iot): A vision, architectural elements, and future directions," *Future Generation Computer Systems*, vol. 29, no. 7, pp. 1645 – 1660, 2013, including Special sections: Cyberenabled Distributed Computing for Ubiquitous Cloud and Network Services amp Cloud Computing and Scientific Applications Big Data, Scalable Analytics, and Beyond. [Online]. Available: http://www.sciencedirect.com/science/article/pii/S0167739X13000241

[3] A. Dohr, R. Modre-Opsrian, M. Drobics, D. Hayn, and G. Schreier, "The internet of things for ambient assisted living," in *Information Technology: New Generations (ITNG), 2010 Seventh International Conference on*, April 2010, pp. 804–809.

[4] S. Kelly, N. Suryadevara, and S. Mukhopadhyay, "Towards the implementation of iot for environmental condition monitoring in homes," *Sensors Journal, IEEE*, vol. 13, no. 10, pp. 3846–3853, Oct 2013.

[5] [Online]. Available: RFIDjournalhttp://www.rfidjournal.com/

[6] D. M. Dobkin, *The RF in RFID: passive UHF RFID in Practice*. Amsterdam: Elsevier.

[7] Y. Cheung, K. Choy, C. Lau, and Y. Leung, "The impact of rfid technology on the formulation of logistics strategy," in *Management of Engineering Technology, 2008. PICMET 2008. Portland International Conference on*, July 2008, pp. 1673–1680.

[8] G. Marrocco, "Pervasive electromagnetics: sensing paradigms by passive rfid technology," *Wireless Communications, IEEE*, vol. 17, no. 6, pp. 10 –17, december 2010.

[9] C. . Occhiuzzi, S. Caizzone, and G. Marrocco, "Wireless sensing of things by passive rfid technology," *IEEE Antennas and Propagat. Magazine*, vol. 55, no. 6, pp. 14,34, Dec. 2013.

[10] D. Puccinelli and M. Haenggi, "Wireless sensor networks: applications and challenges of ubiquitous sensing," *Circuits and Systems Magazine, IEEE*, vol. 5, no. 3, pp. 19–31, 2005.

[11] V. Gungor, B. Lu, and G. Hancke, "Opportunities and challenges of wireless sensor networks in smart grid," *Industrial Electronics, IEEE Transactions on*, vol. 57, no. 10, pp. 3557–3564, Oct 2010.

[12] C. D. Natale, A. Macagnano, E. Martinelli, R. Paolesse, G. D'Arcangelo, C. Roscioni, A. Finazzi-Agro, and A. D'Amico, "Lung cancer identification by the analysis of breath by means of an array of non-selective gas sensors," *Biosensors and Bioelectronics*, vol. 18, no. 10, pp. 1209 – 1218, 2003. [Online]. Available: http://www.sciencedirect.com/science/article/pii/S0956566303000861

[13] D. Briand, F. Molina-Lopez, A. Quintero, G. Mattana, and N. de Rooij, "Printed sensors on smart rfid labels for logistics," in *New Circuits and Systems Conference (NEWCAS), 2012 IEEE 10th International*, June 2012, pp. 449–452.

[14] C. Occhiuzzi, A. Rida, G. Marrocco, and M. Tentzeris, "Rfid passive gas sensor integrating carbon nanotubes," *Microwave Theory and Techniques, IEEE Transactions on*, vol. 59, no. 10, pp. 2674–2684, Oct 2011.

[15] J. Siden, J. Gao, and B. Neubauer, "Microwave conference, 2009. apmc 2009. asia pacific," Dec 2009, pp. 2375–2378.

[16] J. Virtanen, L. Ukkonen, T. Bjorninen, A. Elsherbeni, and L. Sydanheimo, "Inkjet-printed humidity sensor for passive uhf rfid systems," *Instrumentation and Measurement, IEEE Transactions on*, vol. 60, no. 8, pp. 2768–2777, Aug 2011.

[17] R. Nair, E. Perret, S. Tedjini, and T. Baron, "A group-delay-based chipless rfid humidity tag sensor using sili-

con nanowires," *Antennas and Wireless Propagation Letters, IEEE*, vol. 12, pp. 729–732, 2013.

[18] E. Amin, M. Bhuiyan, N. Karmakar, and B. Winther-Jensen, "Development of a low cost printable chipless rfid humidity sensor," *Sensors Journal, IEEE*, vol. 14, no. 1, pp. 140–149, Jan 2014.

[19] L. K. Fiddes and N. Yan, "{RFID} tags for wireless electrochemical detection of volatile chemicals," *Sensors and Actuators B: Chemical*, vol. 186, no. 0, pp. 817 – 823, 2013. [Online]. Available: http://www.sciencedirect.com/science/article/pii/S0925400513005704

[20] R. Bhattacharyya, C. Floerkemeier, and S. Sarma, "Rfid tag antenna based temperature sensing," in *RFID, 2010 IEEE International Conference on*, April 2010, pp. 8–15.

[21] R. Bhattacharyya, C. Di Leo, C. Floerkemeier, S. Sarma, and L. Anand, "Rfid tag antenna based temperature sensing using shape memory polymer actuation," in *Sensors, 2010 IEEE*, Nov 2010, pp. 2363–2368.

[22] S. Caizzone, C. Occhiuzzi, and G. Marrocco, "Multi-chip rfid antenna integrating shape-memory alloys for detection of thermal thresholds," *Antennas and Propagation, IEEE Transactions on*, vol. 59, no. 7, pp. 2488–2494, July 2011.

[23] J. Virtanen, Y. F., L. Ukkonen, A. Elsherbeni, A. A. Babar, and L. Sydanheimo, "Dual port temperature sensor tag for passive uhf rfid systems," *Sensor Review,*, vol. 34, no. 2, pp. 154–169, 2012.

[24] F. Yang, Q. Qiao, J. Virtanen, A. Z. Elsherbeni, L. Ukkonen, and L. Sydanheimo, "Reconfigurable sensing antenna: A slotted patch design with temperature sensation," *Antennas and Wireless Propagation Letters, IEEE*, vol. 11, pp. 632–635, 2012.

[25] [Online]. Available: EM4325,www.emmicroelectronic.com

[26] [Online]. Available: IDSSL900A,http://www.impinj.com/

[27] P. Nikitin and K. V. S. Rao, "Antennas and propagation in uhf rfid systems," in *RFID, 2008 IEEE International Conference on*, April 2008, pp. 277–288.

[28] A. Babar, A. Elsherbeni, L. Sydanheimo, and L. Ukkonen, "Rfid tags for challenging environments: Flexible high-dielectric materials and ink-jet printing technology for compact platform tolerant rfid tags," *Microwave Magazine, IEEE*, vol. 14, no. 5, pp. 26–35, July 2013.

[29] G. Marrocco, "The art of uhf rfid antenna design: impedance-matching and size-reduction techniques," *Antennas and Propagation Magazine, IEEE*, vol. 50, no. 1, pp. 66 –79, feb. 2008.

[30] T. Bjorninen, L. Sydanheimo, L. Ukkonen, and Y. Rahmat-Samii, "Advances in antenna designs for uhf rfid tags mountable on conductive items," *Antennas and Propagation Magazine, IEEE*, vol. 56, no. 1, pp. 79–103, Feb 2014.

[31] S. Amendola, R. Lodato, S. Manzari, C. Occhiuzzi, and G. Marrocco, "Rfid technology for iot-based personal healthcare in smart spaces," *Internet of Things Journal, IEEE*, vol. 1, no. 2, pp. 144–152, April 2014.

[32] C.-H. Huang and K.-W. Cheng, "Rfid technology combined with iot application in medical nursing system," *Bulletin of Networking, Computing, Systems, and Software*, vol. 3, no. 1, 2014. [Online]. Available: http://bncss.org/index.php/bncss/article/view/31

[33] P. Nikitin and K. Rao, "Theory and measurement of backscattering from rfid tags," *Antennas and Propagation Magazine, IEEE*, vol. 48, no. 6, pp. 212 –218, dec. 2006.

[34] S. Manzari, C. Occhiuzzi, and G. Marrocco, "Feasibility of body-centric systems using passive textile rfid tags," *Antennas and Propagation Magazine, IEEE*, vol. 54, no. 4, pp. 49–62, Aug 2012.

[35] P. Nikitin, R. Martinez, S. Ramamurthy, H. Leland, G. Spiess, and K. V. S. Rao, "Phase based spatial identification of uhf rfid tags," in *RFID, 2010 IEEE International Conference on*, April 2010, pp. 102–109.

[36] L. Yang, R. Zhang, D. Staiculescu, C. Wong, and M. Tentzeris, "A novel conformal rfid-enabled module utilizing inkjet-printed antennas and carbon nanotubes for gas-detection applications," *Antennas and Wireless Propagation Letters, IEEE*, vol. 8, pp. 653 –656, 2009.

[37] T. Le, T. Thai, V. Lakafosis, M. Tentzeris, Z. Lin, Y. Fang, K. Sandhage, and C. Wong, "Graphene enhanced wireless sensors," in *Sensors, 2012 IEEE*, Oct 2012, pp. 1–4.

[38] G. Marrocco, "Rfid grids: Part i:electromagnetic theory," *Antennas and Propagation, IEEE Transactions on*, vol. 59, no. 3, pp. 1019 –1026, march 2011.

[39] S. Caizzone and G. Marrocco, "Rfid grids: Part ii: Experimentations," *Antennas and Propagation, IEEE Transactions on*, vol. 59, no. 8, pp. 2896 –2904, aug. 2011.

[40] A. D'Amico and C. Di Natale, "A contribution on some basic definitions of sensors properties," *Sensors Journal, IEEE*, vol. 1, no. 3, pp. 183–190, Oct 2001.

[41] C. Occhiuzzi, G. Contri, and G. Marrocco, "Design of implanted rfid tags for passive sensing of human body: the stentag," *Antennas and Propagation, IEEE Transactions on*, vol. to appear, 2012.

[42] S. Capdevila, L. Jofre, J.-C. Bolomey, and J. Romeu, "Rfid multiprobe impedance-based sensors," *Instrumentation and Measurement, IEEE Transactions on*, vol. 59, no. 12, pp. 3093–3101, Dec 2010.

[43] R. Krigslund, S. Dosen, P. Popovski, J. Dideriksen, G. Pedersen, and D. Farina, "A novel technology for motion capture using passive uhf rfid tags," *Biomedical Engineering, IEEE Transactions on*, vol. 60, no. 5, pp. 1453–1457, May 2013.

[44] C. Occhiuzzi, C. Paggi, and G. Marrocco, "Passive rfid strain-sensor based on meander-line antennas," *Antennas and Propagation, IEEE Transactions on*, vol. 59, no. 12, pp. 4836–4840, Dec 2011.

[45] [Online]. Available: NXPUcodeI2Cwww.nxp.com

[46] W. R. Turner, D. S. Brown, and D. V. Harrison, "Properties of paraffin waxes," *Industrial Engineering Chemistry*, vol. 47, no. 6, pp. 1219–1226, 1955. [Online]. Available: http://pubs.acs.org/doi/abs/10.1021/ie50546a049

[47] [Online]. Available: AnsoftHFSS,http://www.ansoft.com/products/hf/hfss/

[48] [Online]. Available: ParaplastTissueEmbeddingMediumdatasheet, http://www.2spi.com/catalog/msds/msds02847.html

[49] [Online]. Available: AlienHiggs2,www.alientechnology.com/docs/products/DS_H2.pdf

[50] [Online]. Available: TagformanceVoyantic, RFIDmeasurementssolutions,http://www.voyantic.com

[51] J. Virtanen, T. Bjorninen, L. Ukkonen, and L. Sydanheimo, "Passive uhf inkjet-printed narrow-line rfid tags," *Antennas and Wireless Propagation Letters, IEEE*, vol. 9, pp. 440–443, 2010.

[52] C. Occhiuzzi, S. Cippitelli, and G. Marrocco, "Modeling, design and experimentation of wearable rfid sensor tag," *Antennas and Propagation, IEEE Transactions on*, vol. 58, no. 8, pp. 2490 –2498, aug. 2010.

[53] G. Marrocco and F. Amato, "Self-sensing passive rfid: From theory to tag design and experimentation," in *Microwave Conference, 2009. EuMC 2009. European*, 29 2009-oct. 1 2009, pp. 001 –004.

[54] [Online]. Available: CSTmicrowavestudio,http://www.cst.com

[55] [Online]. Available: ThingMagicM5readerwww.thingmagic.com/embedded-rfid-readers/mercury5e/1-embedded-rfid-readers/3-mercury5e

[56] [Online]. Available: ImpinjMonza4,www.emmicroelectronic.com

[57] C. Floerkemeier, M. Langheinrich, E. Fleisch, F. Mattern, and S. Sarma, *The Internet of Things, Sensor Applications in the Supply Chain: The Example of Quality-Based Issuing of Perishables*, May 2009.

[58] H. Patel, N. Rao, and A. Saha, "Heat exposure effects among firefighters," *Indian Journal of Occupational and Environmental Medicine*, vol. 10, no. 3, pp. 121–123, 2006. [Online]. Available: http://www.ijoem.com/article.asp?issn=0019-5278;year=2006;volume=10;issue=3;spage=121;epage=123;aulast=Patel;t=6

[59] J.-M. Picdi and B. Rmili, "An ultra low power rfid sensor platform for launchers applications," in *Wireless for Space and Ex-*

treme Environments (WiSEE), 2013 IEEE International Conference on, Nov 2013, pp. 1–5.

[60] M. Freund and G. Mózes, *Paraffin Products: Properties, Technologies, Applications*, ser. Analytical Chemistry Symposia Series. Akad. Kiadó, 1982. [Online]. Available: http://books.google.it/books?id=iEIiAQAAMAAJ

[61] [Online]. Available: AgilentTechnologies, 85070EDielectricProbeKit,http://www.agilent.com

[62] P. Nikitin, K. V. S. Rao, S. Lam, V. Pillai, R. Martinez, and H. Heinrich, "Power reflection coefficient analysis for complex impedances in rfid tag design," *Microwave Theory and Techniques, IEEE Transactions on*, vol. 53, no. 9, pp. 2721–2725, Sept 2005.

[63] C. R. 18. S. Manzari, S. Caizzone and G. Marrocco, "Feasibility of wireless temperature sensing by passive uhf-rfid tags in ground satellite test beds," in *IEEE International Conference on Wireless for Space and Extreme Environments 2014*, october 2014.

[64] [Online]. Available: http://www.avx.com/docs/Catalogs/nb12-21.pdf

[65] [Online]. Available: Feko,www.feko.info

[66] U. Lange, N. V. Roznyatovskaya, and V. M. Mirsky, "Conducting polymers in chemical sensors and arrays," *Analytica chimica acta*, vol. 614, no. 1, pp. 1–26, 2008.

[67] H. Bai and G. Shi, "Gas sensors based on conducting polymers," *Sensors*, vol. 7, no. 3, pp. 267–307, 2007.

[68] Y. Wang and J. T. Yeow, "A review of carbon nanotubes-based gas sensors," *Journal of Sensors*, vol. 2009, 2009.

[69] T. Blythe and D. Bloor, *Electrical Properties of Polymers*. Amsterdam: Cambridge University Press.

[70] H. S. A. BS, "Moisture and wound healing," *Journal des Plaies et Cicatrisation*, vol. 9, pp. 7–11, Oct 2005.

[71] Y. Amin, Y. Feng, Q. Chen, L.-R. Zheng, and H. Tenhunen, "Rfid antenna humidity sensor co-design for usn applications," *IEICE Electronics Express*, vol. 10, no. 4, pp. 20 130 003–20 130 003, 2013.

[72] W. U. M. K. A.Elschner, S.Kirchmeyer, *PEDOT: Principles and Applications of an Intrinsically Conductive Polymer*. CRC Press, 2010.

[73] T. Kinkeldei, C. Zysset, K. Cherenack, and G. Troster, "A textile integrated sensor system for monitoring humidity and temperature," in *Solid State Sensors, Actuators and Microsystems Conference TRANSDUCERS, 2011 16th International*, June 2011, pp. 1156–1159.

[74] J. Reboun, A. Hamacek, T. Dzugan, and M. Kroupa, "Sensorial characteristics of conductive polymers," in *Electronics Technology, 2009. ISSE 2009. 32nd International Spring Seminar on*, May 2009, pp. 1–5.

[75] E. Martinelli, M. Stabile, A. Catini, R. Paolesse, A. DAmico, and C. D. Natale, "An array of capacitive sensors based on a commercial fingerprint detectors," *Sensors and Actuators B: Chemical*, vol. 130, no. 1, pp. 264 – 268, 2008, proceedings of the Eleventh International Meeting on Chemical Sensors IMCS-11 {IMCS} 2006 {IMCS} 11. [Online]. Available: http://www.sciencedirect.com/science/article/pii/S0925400507006132

[76] N. Wiziack, A. Catini, M. Santonico, A. DAmico, R. Paolesse, L. Paterno, F. Fonseca, and C. D. Natale, "A sensor array based on mass and capacitance transducers for the detection of adulterated gasolines," *Sensors and Actuators B: Chemical*, vol. 140, no. 2, pp. 508 – 513, 2009. [Online]. Available: http://www.sciencedirect.com/science/article/pii/S0925400509004675

[77] M. F. Kolosnjaj J, Szwarc H, "Toxicity studies of carbon nanotubes," *Adv Exp Med Biol. Advances in Experimental Medicine and Biology*, vol. 9, no. 620, pp. 181–204, Oct 2005.

[78] [Online]. Available: CleviosPH500http://clevios.com

[79] M. J. J. Kamil, "Flexible temperature sensor integrated with rfid tag," in *XIII International PhD Workshop OWD*, October 2011.

[80] N. Kirsch, N. Vacirca, E. Plowman, T. Kurzweg, A. Fontecchio, and K. Dandekar, "Optically transparent conductive

polymer rfid meandering dipole antenna," in *RFID, 2009 IEEE International Conference on*, april 2009, pp. 278 –282.

[81] N. Kirsch, N. Vacirca, T. Kurzweg, A. Fontecchio, and K. Dandekar, "Performance of transparent conductive polymer antennas in a mimo ad-hoc network," in *Wireless and Mobile Computing, Networking and Communications (WiMob), 2010 IEEE 6th International Conference on*, oct. 2010, pp. 9 –14.

[82] [Online]. Available: ThingMagicM6readerhttp://www.thingmagic.com/fixed-rfid-readers/mercury6

[83] S. Manzari, C. Occhiuzzi, S. Nawale, A. Catini, C. Di Natale, and G. Marrocco, "Humidity sensing by polymer-loaded uhf rfid antennas," *Sensors Journal, IEEE*, vol. 12, no. 9, pp. 2851–2858, Sept 2012.

[84] S. Manzari and G. Marrocco, "Modeling and applications of a chemical-loaded uhf rfid sensing antenna with tuning capability," *Antennas and Propagation, IEEE Transactions on*, vol. 62, no. 1, pp. 94–101, Jan 2014.

[85] L. J. K. L. JP, "A summary review of wireless sensors and sensor networks for structural health monitoring," *Shock Vibr. Dig.*, vol. 38, pp. 91–128, March 2006.

[86] C. K. Leung and T. Pheeraphan, "Microwave curing of portland cement concrete: experimental results and feasibility for practical applications," *Construction and Building Materials*, vol. 9, no. 2, pp. 67 – 73, 1995. [Online]. Available: http://www.sciencedirect.com/science/article/pii/095006189400001I

[87] K. Shams and M. Ali, "Dielectric properties of concrete and their influence on radar testing," *NDT E International*, vol. 34, no. 6, pp. 419 – 425, 2001.

[88] G. Klysz, J. Balayssac, and X. FerriÃšres, "Evaluation of dielectric properties of concrete by a numerical fdtd model of a gpr coupled antenna parametric study," *NDT E International*, vol. 41, no. 8, pp. 621 – 631, 2008. [Online]. Available: http://www.sciencedirect.com/science/article/pii/S0963869508000352

[89] A. V. Beek and M. Hilhorst, "Dielectric measurements to characterize the microstructural changes of young

concrete," *NDT E International*, vol. 1, 1999. [Online]. Available: http://www.sciencedirect.com/science/article/pii/S0963869501000093

[90] [Online]. Available: CAENQuarkRFIDreader,http://www.caenrfid.it/en/CaenProd.jsp?parent=59&idmod=750

List of Pubblications

Journals

1. S. Manzari, C. Occhiuzzi, G. Marrocco, "Feasibility of Body-centric Passive RFID Systems by Using Textile tags", *Antennas and Propagation Magazine, IEEE.*, Vol. 54, No.4, 2012, pp. 49-62.
2. S. Manzari, A. Ali Babar, L. Ukkonen, A. Z. Elsherbeni, G. Marrocco, L. Sydänheimo, "Performance Analysis of Pure Paraffin Wax as RFID Tag Substrate", *Microwave and Optical Technology Letters*, February 2012, Vol. 54, 2, pp. 442-446.
3. A. Ali Babar, S. Manzari, A. Z. Elsherbeni, L. Sydänheimo, L. Ukkonen, "Passive UHF RFID tag for Heat Sensing Applications", Antennas and Propagation, IEEE Transactions on, Vol. 60, No.9,2012 pp. 4056-4064.
4. S.Manzari, C. Occhiuzzi, S. Nawale, A. Catini, C. Di Natale, G. Marrocco, "Humidity Sensing by Polymer-loaded UHF RFID Antennas", *Sensors Journal, IEEE,* Vol. 12, N. 9,2012, pp. 2851-2858.
5. S. Manzari, S. Pettinari, G. Marrocco, "Miniaturized Wearable UHF-RFID Tag with Tuning Capability", *Electronics Letters*, Vol. 48, No. 21, 2013 pp. 1325-1326.
6. S. Manzari, G Marrocco, "Modeling and Applications of a Chemical-Loaded UHF RFID Sensing Antenna with Tuning Capability" *IEEE Transactions on* , vol.62, no.1, pp.94-101, Jan. 2014.
7. S. Amendola, R. Lodato, S. Manzari, C. Occhiuzzi, G. Marrocco, "RFID Technology for IoT based Personal Healthcare in Smart Spaces", *IEEE Internet of Things Journal* , vol.1, no.2, pp.144-152, April 2014.

8. Manzari, S.; Catini, A; Pomarico, G.; Di Natale, C.; Marrocco, G., "Development of an UHF RFID Chemical Sensor Array for Battery-Less Ambient Sensing," *Sensors Journal, IEEE* , vol.14, no.10, pp.3616,3623, Oct. 2014.
9. C. Occhiuzzi, C. Vallese, S. Amendola, S. Manzari, G. Marrocco, "NIGHT-Care: a passive RFID system for remote monitoring and control of overnight living environment", *Procedia Computer Science, Volume 32, 2014, Pages 190-197.*
10. M. C. Caccami, S. Manzari and G. Marrocco, " Phase-oriented Sensing by means of Loaded UHF RFID Tags", *submitted to IEEE Transactions on Antennas and Propagation*, 2014 .

Books

1. R. Lodato, S. Manzari, C. Occhiuzzi and G. Marrocco, "Flexible and Conformable Antennas for Bodycentric Radiofrequency Identification", chapter in *Advancement in Wearable and Flexible Antennas*, WIT Press.
2. C. Occhiuzzi, C. Vallese, S. Amendola, S. Manzari, G. Marrocco, "RFID Ambient Intelligence System for the Remote Monitoring and Control of Sleep Quality", chapter in *Wearable Electronic Sensors: for safe and healthy living.*

Conferences

1. S. Manzari, C. Occhiuzzi, G. Marrocco, "Experimental Characterization of Bodycentric Passive RFID Systems", *IEEE International Symposium on Antennas and Propagation APS/URSI 2011.*
2. S. Manzari, C. Occhiuzzi, G. Marrocco, "Reading Range of Wearable Textile RFID Tags in Real Configurations", *5th European Conference on Antennas and Propagation (EUCAP)*,2011, Rome.
3. S. Manzari, C. Occhiuzzi, G. Marrocco, "Body-centric RFID Systems", *4th International Symposium on Applied Sciences in Biomedical and Communication Technologies ISABEL 2011*, Barcelona.

4. A. Ali Babar, S. Manzari, A. Z. Elsherbeni, L. Sydänheimo, G. Marrocco, L. Ukkonen, "Exploiting the Characteristics of Paraffin as a Substrate for UHF RFID and Antenna Applications", 2012 *IEEE International Symposium on Antennas and Propagation and USNC-URSI*, Chicago.
5. S.Manzari, C. Occhiuzzi, S. Nawale, A. Catini, C. Di Natale, G. Marrocco, "UHF RFID Humidity Sensor Tag Based on Hygroscopic Polymeric Load", *6th European Conference on Antennas and Propagation (EUCAP)*,2012, Prague.
6. S.Manzari, C. Occhiuzzi, S. Nawale, A. Catini, C. Di Natale, G. Marrocco, "Polymer-Doped UHF RFID Tag for Wireless-Sensing of Humidity", *IEEE 6th annual Conference on RFID 2012*, Orlando.
7. S.Manzari, C. Occhiuzzi, S. Nawale, A. Catini, C. Di Natale, G. Marrocco, "Chemical Loaded Antenna for Humidity Detection", *RINEM 2012,* Rome.
8. S. Manzari, S. Pettinari, G. Marrocco, "Miniaturized and Tunable Wearable RFID Tag for Body-Centric Applications", *3rd IEEE International Conference on RFID-Technology and Applications 2012 (RFID-TA)*, 2012, Nice.
9. S.Manzari, A. Catini, C. Di Natale, G. Marrocco, "Ambient Sensing by Chemical-loaded UHF-RFIDs", *in proceedings of 7th European Conference on Antennas and Propagation (EUCAP)*,2013, Gothenburg.
10. Manzari, S., Catini, A., Paolesse, R., Marrocco, G., & Di Natale, C. "Chemical-Loaded Passive UHF-RFID Array for Ambient Sensing" *Paper presented at Symposium on Olfaction & Electronic Nose*, Deagu South Korea.
11. S. Manzari, A. Catini, G. Marrocco, C. Di Natale, "Chemically Sensitive Passive UHF-RFID Array" *IMCS conference*, Buenos Aires, 2014.
12. S. Manzari, A. Catini, G. Marrocco, C. Di Natale , "Chemical sensors based on passive UHF-RFID arrays", secondo convegno nazionale sensori, Rome, february 2014.
13. M. C. Caccami, S. Manzari and G. Marrocco, " Phase-oriented Chemical Sensing by Passive UHF-RFID", *URSI General Assembly and Scientific Symposium* (Bejing) august 2014.

14. C. Occhiuzzi, C. Vallese, S. Amendola, S. Manzari, G. Marrocco, Multi-channel Processing of RFID Backscattering for Monitoring of Overnight Living, *General Assembly and Scientific Symposium* (Bejing) august 2014.
15. S. Manzari, A. Catini, C. Di Natale, G. Marrocco, "Experimental Analysis of Selectivity and Dynamic Ranges of Passive UHF-RFID Chemical Sensors", *EuMW European Microwave Week*, Rome, october 2014.
16. C. Occhiuzzi, C. Vallese, S. Amendola, S. Manzari, G. Marrocco, "NIGHT-Care: a passive RFID system for remote monitoring and control of overnight living environment", *ANT/SEIT 2014*, pp.190-197.
17. S. Manzari, T. Musa, M.Randazzo, Z. Rinaldi, A. Meda and G. Marrocco, "A Passive Temperature Radio-Sensor for Concrete Maturation Monitoring", *5rd IEEE International Conference on RFID-Technology and Applications 2014* (RFID-TA), 2014, Tampere .
18. S. Manzari, S. Caizzone, C. Rubini and G. Marrocco, "Feasibility of Wireless Temperature Sensing by Passive UHF-RFID Tags in Ground Satellite Test Beds", *IEEE International Conference on Wireless for Space and Extreme Environments* 2014.

Awards

1. 2012: Winner of the "**Best Student Paper Award**" at RFID-TA conference held in Nice (France)
2. 2012: IEEE **MTT-S/AP-S 2012 prize** of central-south Italy
3. 2014: Third position in the "**Best Student Paper Award**" at RFID-TA conference held in Tampere (Finland)
4. 2014: Winner of the "**Student Competition**" at EuMW conference held in Rome (Italy)

Acknowledgments

I am using this opportunity to express my gratitude to everyone who supported me throughout the course of this PhD project. I would like to thank all the Engineers that during the last three years worked with me or helped with valuable discussions: A. Ali Babar, Alexandro Catini, Cecilia Occhiuzzi, Stefano Pettinari, Tullio Musa, Martina Randazzo, Maria Cristina Caccami, Stefano Caizzone, Sara Amendola, Rossella Lodato and Cinzia Rubini. Their contribution to the contents and results contained in this Thesis is extremely precious, and I really appreciated their collaboration and friendship.

I would also like to thank all the professors who helped and guided me during my research: Prof. Corrado di Natale, Prof. Fernando Bardati, Prof. Piero Tognolatti, Prof. Meda, Prof. Leena Ukkonen and Prof. Lauri Sydhaneimo. I am sincerely grateful to them for sharing their illuminating views on a number of issues related to my research.

Many thanks to my thesis reviewers, Johan Sidén and Smaïl Tedjini, for the valuable suggestions they have given in their evaluation of my Thesis and for the positive words they spent on my research.

I am extremely thankful to my Advisor Prof. Gaetano Marrocco, for supporting me with great professionalism and humanity, for his inspiring guidance, invaluably constructive criticism and friendly advices during the whole PhD. He has really instilled the love for research in me.

Last but not least, thanks to my family for supporting me always, if I can define myself as a very lucky person, it's just because of them.